INFLUENCE OF NEUROARCHITECTURE ON INFUSATE DISTRIBUTION: APPLICATIONS FOR A NOVEL EPILEPSY THERAPY

By

SVETLANA KANTOROVICH

A DISSERTATION PRESENTED TO THE GRADUATE SCHOOL
OF THE UNIVERSITY OF FLORIDA IN PARTIAL FULFILLMENT
OF THE REQUIREMENTS FOR THE DEGREE OF
DOCTOR OF PHILOSOPHY

UNIVERSITY OF FLORIDA

2012

To my parents, James and Adele; sister, Yelana; and brother, Vladimir

ACKNOWLEDGMENTS

I have many people to thank for who and where I am today. First and foremost, I would like to thank the chair and members of my committee who have shaped the scientist I have become. My advisor, Dr. Paul Carney, generously provided me with scientific freedom to pursue my interests and concomitantly bestowed incredible opportunities for translational research. I would also like to express my gratitude to Drs. Malisa Sarntinoranont, William Ogle, Jake Streit, and Michael King for serving on my committee and being exceptional mentors. Special thanks to Dr. King for being a consistent source of reliable information, patience, and advice, and to Dr. Thomas Mareci for meticulous analysis and critique of my experiments and publications.

I am very thankful for all the wonderful members of my laboratory, past and present. Thank you Rabia for teaching me everything I know in the world, especially the serious things. Thank you Mansi for laying down smooth tracks to follow and staying for the next generation. Thank you Stephen for being my recording guru and a source of great wisdom. Thank you eMalick for your intellectual curiosity, without which we would have never become collaborators and good friends. Thank you Garrett for becoming a MRI genius so that our experiments were completed without a hitch. I am grateful I had the opportunity to work with and learn from you. Thank you Phil and Aaron for your friendship and support, and many thanks to Frank, Shiva, Eric, Matt, Dave, and Junli for providing an exciting and encouraging lab environment.

Finally, I wish to thank my family and friends. I have been blessed with the best parents, James and Adele Kantorovich, who have never wavered in their support or confidence in my abilities. Without the sacrifices they have made, I would never be where I am today. I'd like to thank my brother, Vladimir, a role model whose footsteps I

have been following, and my twin sister, Yelana, an interactive designer who is the reason my presentation slides always look professionally amazing. Last but not least, thank you Jeannette for being the best friend I could ask for, and Wade for sticking with me from day one. I could never have done it without you.

TABLE OF CONTENTS

LIST OF TABLES

LIST OF FIGURES

LIST OF ABBREVIATIONS

AAV	Adeno-associated virus
AED	Anti-epileptic drug
AP	Anterior-posterior anatomical direction
BBB	Blood-brain-barrier
CA	Cornu ammonis subfield of the hippocampus
CC	Corpus callosum
CD-68	Cluster of Differentiation 68
CED	Convection-enhanced delivery
CNS	Central nervous system
CSF	Cerebrospinal fluid
DAB	3,3'-diaminobenzidine
DG	Dentate gyrus
DV	Dorsal-ventral anatomical direction
ECS	Extracellular space
EEG	Electroencephalography
FJC	Flouro Jade C
GABA	γ-aminobutyric acid
Gd-albumin	human serum albumin labeled with gadolinium chelated by diethylene triamine pentaacetic acid, macromolecular magnetic resonance imaging contrast agent
Gd-DTPA	gadolinium chelated by diethylene triamine pentacetic acid, low molecular weight magnetic resonance imaging contrast agent
GFP	Green fluorescent protein
GFAP	Glial fibrillary acidic protein
HF	Hippocampal fissure

ICV	Intracerebroventricular
ILAE	International League Against Epilepsy
IP	Intraperitoneal
mTLE	mesial temporal lobe epilepsy
ML	Medial-lateral anatomical direction
MR	Magnetic Resonance
MRI	Magnetic Resonance Imaging
PEEK	Polyaryletheretherketone
SE	Status epilepticus
SNR	Signal-to-noise ratio
SSLSE	Self-sustained limbic status epilepticus
T	Tesla
T1	Longitudinal-relaxation time constant
T2	Transverse-relaxation time constant
TLE	Temporal lobe epilepsy
VI	Velum interpositum

Abstract of Dissertation Presented to the Graduate School
of the University of Florida in Partial Fulfillment of the
Requirements for the Degree of Doctor of Philosophy

INFLUENCE OF NEUROARCHITECTURE ON INFUSATE DISTRIBUTION: APPLICATIONS FOR A NOVEL EPILEPSY THERAPY

By

Svetlana Kantorovich

May 2012

Chair: Paul R. Carney
Major: Medical Sciences - Neuroscience

Temporal Lobe Epilepsy (TLE) is the most common partial-onset epilepsy and often refractory to antiepileptic drugs. Despite pharmacological advances in epilepsy treatment, seizures cannot be controlled in many patients because current drugs do not target causes of the disorder. Convection-enhanced delivery (CED), a local drug delivery technique, has the potential to deliver novel therapeutics while avoiding systemic toxicity and blood-brain-barrier limitations. However, the efficacy of CED depends on appropriate tissue targeting, which requires a deeper understanding of the effect of neuroarchitecture on interstitial transport. To investigate the influence of microanatomy on CED, the volume and pattern of infusate distribution was examined after varying the site of infusion, integrity of structure, and compound infused. Gd-albumin, a magnetic resonance (MR) contrast agent, was infused into two sites in normal rat hippocampi. Infusions were repeated in animals injured by an episode of status epilepticus (SE), a prolonged seizure known to cause neuronal damage and edema in the hippocampus and associated structures. Infusions in injured animals were implemented 24 hours post-SE, as prophylactic treatment has the potential to reduce structural damage, diminish associated cognitive impairment, or prevent

epileptogenesis. Infusions were also implemented at 60 days post-SE, during chronic TLE. High-resolution T1- and T2-relaxation-weighted MR images were acquired at 11.1 Tesla *in vivo* to visualize Gd-albumin distribution and morphological changes, respectively. Histological analysis was performed to validate infusions and characterize injury at higher resolution. Finally, information gained from infusion studies with Gd-albumin was used to guide proof-of-principle studies with neural stem cells and viral vectors. Infusions in normal hippocampi spread along preferential paths parallel to fiber directions and within fissures, with limited penetration across densely-packed cell layers. Infusions in injured hippocampi followed similar patterns, but resulted in significantly larger distribution volumes that correlated with increased injury severity. Therapeutic carrier systems exhibited comparable spatial characteristics to Gd-albumin infusions, but were also influenced by cell interactions. These studies show anisotropic hippocampal architecture plays a leading role in the distribution of infusate by CED. This information can be applied to improve targeting guidelines, incorporated into injury-specific computation models, and considered in treatment strategies involving novel therapeutic agents.

CHAPTER 1
BACKGROUND

Motivation

Epilepsy is a chronic neurological disorder that affects about 1% of people in the United States, with approximately 50 million people affected worldwide (Browne and Holmes, 2001). There are over 40 types of epilepsies, diverse in etiology but similarly characterized by the recurrence of spontaneous seizures. Seizures are transient episodes of abnormal, excessive, or synchronous neuronal activity in a focal area or throughout the brain (Sander, 1993). Unfortunately, despite being one of the world's oldest recognized conditions, treatments for epilepsy lag behind developments of other neurological disorders. This is especially true for temporal lobe epilepsy (TLE), in which one-third of patients are resistant to available antiepileptic drugs (AEDs). As temporal lobe epilepsy is the most common form of epilepsy in the adult population, this leaves hundreds of thousands of patients with uncontrolled seizures. Therefore, the objective of the research presented in this dissertation was to develop and optimize a novel therapeutic strategy for the prevention and treatment of focal epilepsy using convention-enhanced delivery (CED). CED is a local drug-delivery technique that uses positive pressure to deliver infusate directly into parenchymal interstitial space. This mechanism of delivery is applicable to a wide variety of potential treatments because it does not require passage through the blood-brain-barrier (BBB). The introduction of inhibitory neuropeptides, viral agents, or stem cell therapy is impossible using currently available delivery options. Using CED, these agents can be delivered in a targeted manner over clinically relevant volumes.

CED has the potential to overcome many obstacles in drug delivery, but detailed knowledge about the influence of biophysical properties of the brain on delivery into complex regions is lacking. In addition to the extensive work being done to understand the influence of infusion parameters and cannula design, a thorough understanding of interstitial flow in both normal and injured areas is necessary to provide direction for safe and effective delivery. This body of work addresses these concerns through the characterization of direct intracranial delivery in normal animals (Chapter 2) and in an animal model of epilepsy (Chapter 3). Chapter 4 discusses applications of this strategy in specific therapeutic modalities. Finally, Chapter 5 summarizes findings and proposes future conduits for the progression of this work.

Epilepsy

Epilepsy is one of the world's oldest recognized neurological disorders. The term is reserved for "a condition characterized by two of more recurrent epileptic seizures over a period longer than 24 hours, unprovoked by any immediate identified cause" (Commission on Epidemiology and Prognosis of the International League Against Epilepsy, 1993). It has also been referred to as "the epilepsies", due to the many manifestations of the disorder across geographical, racial, or social boundaries. This section will introduce the various syndromes, describe the etiology, pathophysiology, common treatments, and discuss animal models used to study the disorder.

Classification of the Epilepsies

The epilepsies are classified based on etiology, semiology, origin of seizures, and epilepsy syndromes. Two systems of classification of epilepsies are in use today. The first, developed by the International League Against Epilepsy (ILAE) , is based on seizure semiology (Commission on Classification and Terminology of the International

League Against Epilepsy, 1981). This scheme divides seizures into three broad types based on EEG observations: 1) partial (focal) seizures that involve one area of the brain, 2) generalized seizures that involve the whole brain, and 3) unclassifiable seizures, which may be generalized and partial, continuous, multifocal, or generalized to only one hemisphere. These broad types are further subdivided by the appearance of additional clinical observations, such as specific motor signs or loss of consciousness. This classification scheme is detailed in Figure1-1A. The ILEA 1981 system is easy to implement, but doesn't provide information about the severity, cause, or prognosis of the disease. Thus, another system of classification based on epilepsy syndromes was developed by the ILAE eight years later (Commission on Classification and Terminology of the International League Against Epilepsy, 1989). Similar to the first system, the epilepsies are divided broadly into four groups: 1) localization-related seizures that involve distinct parts of the brain, 2) generalized seizures that involve both sides of the brain, 3) undetermined seizures that may be localized or generalized, and 4) special syndromes. These groups are then further divided by etiology, i.e. whether the cause is unknown (idiopathic), identifiable (symptomatic) or hidden (cryptogenic). This classification is shown in Figure 1-1B. The ILEA 1989 system is helpful for diagnostic purposes and is used as a complement to the 1981 system. For example, TLE is classified as a symptomatic localization-related syndrome. People suffering from TLE may experience simple partial seizures, complex partial seizures, or secondarily generalized tonic-clonic seizures.

Temporal Lobe Epilepsy

The focus of this dissertation is on TLE, the most common form of epilepsy in adults (Engel, 2001a), and among the most frequent types of intractable epilepsy

(Engel, 2001b). TLE refers to spontaneous recurrent seizures originating in the limbic system. There are two main types of TLE: 1) mesial TLE (mTLE), in which seizures begin in the hippocampus, parahippocampal gyrus, or amygdala, and 2) lateral TLE, in which seizures arise from the neocortex. mTLE, the more common form, is poorly controlled with pharmacological intervention and hence most likely to benefit from alternative therapeutic strategies.

Limbic system circuitry

Given that TLE affects the limbic system, it is necessary to introduce the limbic system circuitry (Amaral and Lavenex, 2007) that underlies pathological features of the disorder. Limbic areas commonly affected in TLE include the hippocampal formation, parahippocampal gyrus, thalamus, and septum. The hippocampal formation consists of the dentate gyrus, Cornu Ammonis (CA) fields CA1, CA2, and CA3, subiculum, presubiculum, parasubiculum, and entorhinal cortex. These regions are cytoarchitectonically distinct, but linked by largely unidirectional neuronal pathways to form functional circuits.

The dentate gyrus (DG) is a trilaminate region that receives direct input from the entorhinal cortex via the perforant path. It has a relatively cell-free molecular layer, a granule cell layer, and a polymorphic cell layer (hilus) containing mossy cells and interneurons. The molecular and granule cell layers form a sideways U shape in which the blade superior to the CA3 cell layer is referred to as the suprapyramidal blade and the blade inferior to the CA3 cell layer is referred to as the infrapyramidal blade. Granule cells, the principal excitatory cells of the DG, synapse bilaterally on mossy cells in the polymorphic layer and ipsilaterally on CA3 pyramidal cells.

The CA1, CA2, and CA3 regions are known specifically as the hippocampus proper. Inputs and outputs to the hippocampal proper are organized within distinct layers, or strata.

- The pyramidal cell layer contains principle cells.
- Stratum oriens contains basal dendrites, interneurons, and some CA3 axons.
- Stratum radiatum contains apical dendrites, some CA3 axons, and several classes of interneurons.
- Stratum lacunosum-moleculare contains entorhinal cortex fibers, afferents from subcortical regions, and interneurons. This layer abuts the hippocampal fissure, a cell-free region continuous with ventricular space that is lined by pia mater and filled with cerebrospinal fluid (CSF) and blood vessels (Humphrey, 1967)
- Stratum lucidum is a thin acellular layer in the CA3 containing mossy fibers.
- The alveus is a fiber-containing layer composed of axons from the pyramidal cells in the subiculum and hippocampus. It eventually merges with the fimbria, which goes on to become the fornix.

Information from mossy fibers in the DG advances to the CA3, and is then carried from the CA3 to the apical and basal dendrites of the CA1 via Shaffer collaterals. The CA3 also has a massive associational network which includes projections to the CA3 and CA2, and commissural connections to the contralateral CA3, CA2, and CA1. The CA1 has very limited associational projections and only weak commissural projections.

The CA1 projects axons to the deep layers of the entorhinal cortex and to the deep portion of the subicular molecular layer. The subiculum is a main output of the hippocampus; it sends projections to the deep layers of entorhinal cortex, perirhinal cortex, amygdaloid complex, endopiriform nucleus, diencephalon (nucleus reuniens, paraventricular nucleus, paratenial nucleus), neocortex (prelimbic cortex, infralimbic cortex, retrosplenial cortex, orbitofrontal cortex), basal forebrain (septal nucleus, nucleus accumbens), mammillary nuclei, and brain stem. It does not give rise to

commissural connections, but has a substantial association projection that extends temporally from the cells of origin. The subiculum also projects to the presubiculum and parasubiculum, which distributes processed information to a series of cortical and subcortical structures.

There many extrinsic connections with the hippocampus and other limbic regions. Most external input comes from the entorhinal cortex and is known as the perforant path. Neurons of layer II of the entorhinal cortex project axons to the DG and CA3, while layer III of the entorhinal cortex projects to the CA1 and the subiculum. CA1 also receives input from the amygdaloid complex, perirhinal and postrhinal cortices, nucleus reunions of the thalamus, and the septum. The CA3 receives connections from the amygdaloid complex as well, and has reciprocal bilateral connections with the lateral septum.

Etiology and pathophysiology of TLE

The precise cause of TLE is unknown in most cases, but it is typically seen after an initial precipitating injury such as status epilepticus (SE), brain injury, tumors, meningitis, encephalitis, and febrile seizures during childhood (French et al., 1993; Mathern et al., 1996; Pitkanen and Sutula, 2002; Lewis, 2005).

The hallmark pathology of TLE is hippocampal sclerosis (Blumcke et al., 2002; de Lanerolle and Lee, 2005), although cases without those changes exist as well. Histological evaluation of biopsy specimens from chronic epilepsy reveal hippocampal atrophy and scarring with varying degrees of regional neuronal loss and gliosis. Classic hippocampal sclerosis consists of selective loss of pyramidal cells in the CA1 and hilus (de Lanerolle et al., 2003), but neurodegeneration has also been described in the CA2 and CA3 as well (Bruton, 1988). Recurrent connectivity within the dentate gyrus has

been proposed as a major epileptogenic mechanism (Mathern et al., 1995a) due to several observations in hippocampal sclerosis. Loss of interneuronal subtypes (Mathern et al., 1995b) and excitatory mossy cells (Blumcke et al., 2000) have been noted, with abnormal hippocampal neurogenesis, dispersion of the dentate granule cell layer, and mossy fiber sprouting (Thom et al., 2005). Cytological alterations, including enlargement of neurofilaments, abnormal dendritic nodular swellings, ramification of end folial neurons, have also been reported, though these features may represent adaptive rather than primary abnormalities (Blumcke et al., 1999). In addition to the hippocampus and dentate gyrus, pathological changes have commonly been reported in the human amygdala (Hudson et al., 1993), entorhinal cortex (Du et al., 1993), and thalamus (Margerison and Corsellis, 1966; Bruton, 1988).

It remains uncertain whether neuropathological findings represent a substrate for TLE development or are a consequence of repeated seizures. In other words, the question of whether “seizures beget seizures” has been a point of contention for over a century (Gowers, 1881). Animal models have been used to address this issue and have shown that recurrent seizures can produce hippocampal damage (for review, see (Ben-Ari et al., 2008)). Clinical evidence is inconclusive (Hauser and Lee, 2002) because there are epilepsy syndromes that are progressive, and there are syndromes that remit regardless of the number of seizures experienced. However, in human TLE, the remission of seizures after the surgical removal of a damaged focus (Wiebe et al., 2001) suggests this damage is only one feature of a disease process that includes other predispositions.

Current Treatments for Epilepsy

The most common treatment of epilepsy is pharmacotherapy. There are a number of anti-epileptic drugs (AEDs) available for the management of epileptic seizures that are delivered through the use of pills or intravenous injections. These may function by decreasing the excitation of neurons by blocking sodium or calcium channels, or by enhancing their inhibition with the potentiation of inhibitory neurotransmitters, like γ-aminobutyric acid (GABA). The most commonly used older AEDs for TLE are phenytoin, carbamazepine, primidone, valproate, and phenobarbital. Newer drugs, such as gabapentin, topiramate, lamotrigine, levetiracetam, pregabalin, tiagabine, lacosamide, and zonisamide have also been incorporated into the clinic. Unfortunately, these medications are only effective for about two-thirds of patients (Brodie and Dichter, 1996) and often come with a number of side effects (Baker et al., 1997).

Some intractable epilepsy cases are remediable with surgical resection of the epileptic focus. Not all individuals are candidates for surgery however, and among those who are, nearly 20% will refuse to accept the risks of a major surgical procedure (Berg et al., 2003). Moreover, although epilepsy surgery is often considered the only causal treatment of epilepsy, in most patients anti-epileptic drug treatment must be continued after surgery to achieve seizure control (Loscher and Schmidt, 2002). In fact, the probability of achieving a one year remission from surgery is only about 57%. This suggests that in many patients undergoing epilepsy surgery, the focal tissue contributing to intractability is removed, rather than the complex epileptogenic network underlying the epileptic process.

The ketogenic diet is a less common treatment that was advocated after 1921, when it was noted that ketosis and acidosis induced by a high fat/low carbohydrate diet had anticonvulsant effects (Geyelin, 1921). This diet consists of very large amounts of fat (minimum 1g per kg per day of protein) with a typical fat-to-carbohydrate ration of 4:1 or 3:1. While those who respond to the diet show dramatic improvement, its use is primarily for generalized epilepsies associated with diffuse brain abnormalities. Less success is seen in patients with complex partial seizures or epileptiform discharges in the temporal region (Beniczky et al., 2010). Ketone bodies appear throughout the brain, so this treatment is not considered targeted and is difficult to maintain. Furthermore, there are some potential concerns regarding its effects on growth in children (Rubenstein, 2008) and the effect of an almost all fat diet on cardiac status.

Patients may also have the option of receiving electrical stimulation as a potential treatment for intractable epilepsy. The most common form of stimulation treatment is the vagus nerve stimulator, although there is increasing interest in deep brain stimulation and direct regional stimulation of epileptic regions (Theodore and Fisher, 2004). The stimulation of the vagus nerve causes an increase in inhibition and a decrease in excitability, therefore raising the threshold for seizure (Vonck et al., 2001). The mechanism of action is unclear, but it does not require craniotomy, and efficacy is comparable to adjunctive antiepileptic drugs (DeGiorgio et al., 2000; Sirven et al., 2000). Similarly, stimulation of the anterior thalamic nucleus has been shown to be important in generalized seizures (Mirski and Ferrendelli, 1986). Mirski et al. showed they could inhibit the anterior thalamic nucleus with high frequency (100 Hz) stimulation. Timed electrical stimulation in response to measured preictal brain dynamical changes

has also shown to prevent seizures (Nair S, 2005). Despite these encouraging results, difficulties and risks persist. The vagus nerve stimulator could result in complications such as left-vocal-cord paralysis, lower facial weakness, sternocleidomastoid spasm, and transient bradycardia or asystole (Charous et al., 2001).

The above-mentioned limited therapeutic options leave a large number of patients untreated. Despite pharmacological, surgical, and electrical advances in the treatment of epilepsy, seizures cannot be controlled in many patients because current therapies target the symptoms of the disease (seizures) once it is already fully developed. It is important to note that there are currently no protocols for preventative treatments, although mounting evidence suggests prophylactic treatment after an initial insult may result in a positive modifying effect on the development of epilepsy (for review see [4, 5]). Early treatment has the potential to reduce structural damage, diminish associated behavioral and cognitive impairment, or prevent epileptogenesis. This subject is addressed in more detail in Chapter 3.

Animal Models of Epilepsy

Many different animal models of epilepsy have been described for various purposes. In general, there are genetic animal models and models in which seizures are induced in normal animals. Induced seizures may be created with electrical or chemical application, and can result in the development of spontaneous (chronic) or on-demand (acute) seizures. Both electrical and chemical acute seizure models, such as the maximal electroshock seizure (MES) and pentylenetetrazole (PTZ) models (White et al., 1995), and are commonly used for AED discovery because they are easy to use and time-efficient. MES and PTZ models induce seizures in healthy rodents. Alternatively, electrical kindling is an on-demand seizure model in which the repeated application of

electrical stimuli induces permanent susceptibility to seizures. Kindling models are generally used to characterize the anticonvulsant potential of a compound screened with the initial screening tests (Loscher, 2011).

Chronic, or post-SE, animal models are typically used to evaluate epilepsy prevention or disease-modification because the epileptic condition results as a consequence of injury followed by a latent period. Chemical SE models, such as kainate (Hellier et al., 1998) and pilocarpine (Cavalheiro, 1995), are routinely used, but have high mortality rates and considerable inter-animal variability. The self-sustaining limbic SE model (Nitsch and Klatzo, 1983; van Vliet et al., 2007), on the other hand, is often considered to have the greatest parallels with human TLE (Schmidt and Loscher, 2009). This is an electrically-induced SE model that replicates essential characteristics of epilepsy as it occurs in humans (Lothman et al., 1990), including comparable electrophysiological correlates, pathological changes in the limbic system, and histological changes in the hippocampus (Falconer, 1974; Babb, 1987; Bertram et al., 1990; Goodman, 1998; Marchi et al., 2010). This animal model is used in the studies described within this work because it most closely approximates structural changes. Importantly, a fraction of these animals also exhibit pharmacoresistance to current AEDs (Loscher, 1997). Although more labor intensive, appropriate models of refractory epilepsy should also be incorporated into the development of novel epilepsy therapies.

Comparative Neuroanatomy of the Rat and Human Hippocampal Formation

The description of the limbic system circuitry in this chapter has dealt primarily with the rat hippocampal formation because much of the neuroanatomical information available has been gained from studies of the rat, and the work described in this dissertation involves the rat hippocampus. There are, however, a number of differences

in morphologic variations from species to species (Amaral and Lavenex, 2007). For example, the CA1 and entorhinal cortex are disproportionately larger in primates than rodents. The volume of the dentate gyrus and hippocampus is 100 times larger in humans than in rats (3300 mm^3 versus 32 mm^3). There are 15 times more dentate granule cells in humans compared to rats, and the human CA1 has 35 times more pyramidal cells than the rat CA1. Additionally, although a common topography in the entorhinal-hippocampal projection seems to be present in rat and human, there is also more extensive interchange of information between the hippocampal formation and the neocortex. The full extent of the differences between these species cannot yet be accurately gauged; there very well may be substantial variation in the cellular morphology, connectivity, and chemical neuroanatomy across species. Fortunately, the characteristic architecture of the hippocampal formation presents little variation with phylogenetic development. Both the rat and human hippocampus have a basic morphology of an elongated, curved, and rod-like structure. Densely-packed cell layers are obvious in rats and humans, with progressive lamination from dentate gyrus to entorhinal cortex. Many models for temporal lobe epilepsy have been advanced based on cell degeneration and fiber sprouting in the rat hippocampus that have been verified in humans as well. The hippocampal formation is also in a similar location, close to olfactory structures, in all mammals. Due to the similarities in dense cell layers, hippocampal fissures, and hippocampal lamination, the rat hippocampus still presents a good model for spread of infusate within the human hippocampus, especially if these features are capable of significantly influencing distribution.

Drug Delivery

As mentioned in “Current Treatments for Epilepsy”, AEDs prescribed today must enter the brain by crossing over from the blood. Theoretically, the transvacular route, composed of 100 billion capillaries separated by only 40 μm^2 (Pardridge, 2003b), has the potential to distribute drugs throughout the brain. In reality, this method is limited by the proclivity for systemic toxicity and notably, the blood-brain-barrier (BBB).

The BBB is a specialized interface between circulating blood and the brain responsible for maintaining CNS homeostasis and limiting entry of substances that can alter neuronal function (Bradbury, 1985; Goldstein and Betz, 1986). It consists of tight junctions between endothelial cells that are supported and reinforced with the glia limitans. The tight junctions result in a very high resistance between cells that limits para-cellular transport (Figure 1-2A), while enzymes present inside the endothelial cells degrade most solutes travelling trans-cellularly (Figure 1-2B). With the exception of small (<1000 Daltons) hydrophobic molecules that can freely diffuse through the membrane, the BBB is extremely efficient at restricting passage of substances from the bloodstream. Treatment responsiveness of pharmacoresistant partial (focal) epilepsy is dependent on clinically-relevant drug concentrations at the focus. Hence, this neuroprotective role of the BBB presents a major challenge for the delivery of medication, especially non-lipophilic therapeutic agents that have been shown to be effective in experimental systems. The challenge to circumvent the BBB for drug delivery has been met with methods developed to disrupt the BBB, pass through the BBB, or deliver substances behind the BBB. These drug delivery strategies are described in the rest of this section.

Disruption of the BBB

Systemic administration of drugs with concomitant BBB disruption has been a strategy pursued to increase parenchymal drug concentrations. These include infusion of solvents (dimethyl sulfoxide or ethanol) and metals, X-irradiation, induction of pathological conditions, or administration of antineoplastic agents. These techniques are usually toxic and not clinically useful. Intracarotid injection of an inert hypertonic solution such as mannitol or arabinose has been employed to increase the permeability of the BBB temporarily. Osmotic dehydration of the endothelial cells enlarges pore size between tight junctions to allow drugs to enter the brain (Rapoport, 2000), and it is short-lasting and spontaneously reversible (Siegal et al., 2000). This method has been used to deliver chemotherapeutic drugs for treating brain tumors (Doolittle et al., 2002; Haluska and Anthony, 2004). Other factors have also been transported into the CNS with the use of mannitol: manganese for neuroimaging (Fa et al., 2011), neurotrophic factors for experimental stroke treatment (Yasuhara et al., 2010), and a rabies virus glycoprotein-labeled nanocarrier (Hwang et al., 2011). Despite favorable results obtained in some patients with brain tumors, this method is probably not the right treatment for epilepsy. One study found seizures occurred 7% of the time during hyperosmotic BBB opening in cancer patients who were previously seizure-free (Haluska and Anthony, 2004). Another study documented seizures began directly following BBB opening in 25% of the procedures delivering mannitol with chemotherapy (Marchi et al., 2007). The increase of seizure risk is most likely because this procedure indiscriminately opens the BBB to any circulating toxins or endogenous serum components that can disturb the homeostasis of extracellular ions (Friedman, 2011).

Therefore, there is considerable risk of infection or passage of unwanted molecules/proteins in addition to the targeted drug.

Passage Through the BBB

Drug design

Another strategy for drug delivery is to sneak drugs into the brain through the BBB. BBB penetration is favored by low molecular weight, lack of ionization at physiological pH, and lipophilicity (Pardridge, 1988). Small lipophilic molecules can diffuse passively across the BBB (Figure 1-2B). Creating hydrophobic analogues of small hydrophilic drugs is a strategy employed to transport compounds into the brain. However, this strategy has been met with disappointment. The price of increasing lipophilicity for better permeability is decreased plasma solubility, leading to increased binding to plasma proteins and lower concentrations of drug available (Misra et al., 2003). A potential solution to this problem is to create prodrugs, pharmacologically inactive compounds that are converted to their active form with a chemical modification once inside the BBB. Esterification or amidation of hydroxyl-, amino-, or carboxylic acid-containing drugs are added to enhance lipid solubility, then hydrolysis of the modifying group will releases the active compound once in the CNS (Huttunen et al., 2011). Prodrugs have been created for valproic acid (Trojnar et al., 2004; Peura et al., 2011), phenytoin (Fechner et al., 2008; Rautio et al., 2008), and gabapentin (Cundy et al., 2004; Rautio et al., 2008). Although a clever solution, this strategy, too, suffers from important limitations. Increased lipophilicity increases uptake into other tissues, which may exacerbate toxicity at non-target sites. Additionally, increased lipophilicity enhances efflux processes, resulting in poor tissue retention and short biological action. Finally, hydrolysis of the prodrug may lead to unwanted metabolites that contribute to

the toxicity of the compound. (Bodor and Kaminski, 1987; Lambert, 2000). Recently, prodrugs have been developed to include multi-step activation and other moieties to enhance target specificity and prevent unwanted metabolic conversions (Huttunen et al., 2011). With improvement, the prodrug approach may prove to be a feasible way to transport drugs into the CNS.

Mediated transport

There are several transport systems involved in the movement of macromolecules across the BBB that may be exploited for drug delivery. For example, the brain requires essential small and large hydrophilic molecules for normal functioning and survival that cannot passively diffuse across the BBB. These substances are recognized by specific transporters on endothelial cells and transported into the brain (Figure 1-2). Carrier-mediated transport pathways (Figure 1-2C) consist of membrane transporter proteins expressed at the luminal and basolateral endothelial membrane that allow certain small, hydrophilic circulating nutrients or peptides to pass through the endothelial cell. These pathways include:

- Hexose transport system for glucose and mannose
- Neutral amino acid transport system
- Acidic amino acid transport system for glutamate and aspartate
- Basic amino acid transport system for arginine and lysine
- b-amino acid transport system for b-alanine and taurine
- Monocarboxilic acid transport system for lactate and short-chain fatty acids
- Choline transport system for choline and thiamine
- Amine transport system for mepyramine
- Nucleoside transport system for purine bases such as adenine and guanine
- Peptide transport system for small peptides such as enkephalins

Drugs can be modified to increase their affinity for a specific carrier system to increase their BBB penetration through an endogenous approach. The drug Levodopa, an exogenous precursor of dopamine, is transported this way. Levadopa has a high affinity

for the large neutral amino acids system, and is decarboxylated to dopamine once inside the BBB.

Another mediated transport system, receptor-mediated transcytosis (Figure 1-2D), allows the transfer of other essential molecules, such as hormones and lipoproteins, into the brain. A protein or antibody that is transported this way under normal conditions may be conjugated to the drug of interest to facilitate its transport through the BBB. Various enzymes, growth factors and neurotrophic factors have been delivered to the brain by targeting the transferrin receptor (Zhang and Pardridge, 2005), a transporter for an essential protein needed for iron delivery to cells, the human insulin receptor (Coloma et al., 2000; Pardridge, 2003a), and the low-density lipoprotein receptor related proteins (Spencer and Verma, 2007; Demeule et al., 2008; Karkan et al., 2008). Alternatively, drugs can also be encapsulated by a delivery system recognized by specific receptor involved in membrane transport. Polymer nanoparticles and liposomes have been the delivery system most studied, but dendrimers, micelles, carbon nanotubes, emulsions, solid lipid nanoparticles, and nanostructured lipid carriers have are also being developed (Hughes, 2005). These carriers can be targeted to a specific receptor or delivered to the brain via adsorptive mediated transcytosis (Fig 1-2E), the vesicular endocytosis of charged substances (Agyare et al., 2008).

It is important to note that the kinetics, structural binding requirements, and in-vivo activity post modification must be considered when using BBB transporter proteins. Certain drugs do not retain their pharmaceutical function following transformations, and dissociation from receptors may be challenging if there is high binding affinity (Gabathuler, 2010). Furthermore, an essential point to note is that peripheral organs

express these proteins as well; therefore, systemic toxicity remains a concern for all of these strategies.

Passage Behind the BBB

As described so far in this section, there have been many advances in drug design that show potential in treating CNS diseases. However, the risk factors associated with the successes to date have prompted researchers to pursue another class of strategies that do not rely on the cardiovascular system. Drug manipulation is not necessary because the following methods are geared toward circumventing the BBB altogether. The result is higher concentrations within the CNS without the risk of systemic side effects. However, any type of intracerebral drug delivery involves navigation through the extracellular space (ECS), which makes up 15-25% of the CNS tissue volume (Sykova, 1997a). The ECS can slow or facilitate the movement of various substances in the CNS, and is thus an important factor in drug distribution. The next section describes the ECS in more detail and is followed by a description of several approaches for drug delivery directly into the CNS.

Extracellular space

The ECS is a system of interconnected channels that is occupied by interstitial fluid and extracellular matrix components. Extracellular matrix components include glycosaminoglycans (e.g. hyaluronate), glycoproteins, and proteoglycans, which provide structural support, regulate intercellular communication, and bind proteins. Various extracellular matrix adhesion molecules have also been described, such as fibronectin, tanescin, and laminin (Thomas and Steindler, 1995). Interstitial fluid is essentially the same as CSF, but local ionic changes occur as a result of neuronal activity. Interstitial fluid also contains metabolites (glucose, O2, CO2, HCO3-), free radical scavengers,

amino acids, catecholamines, neurotransmitters, DNA, RNA, peptides, lipids, hormones, growth factors, cytokines, chemokines, and various enzymes. The membranes, macromolecules, and charged particles in the ECS, together with neuronal and glial cell processes, all affect the size and shape of ECS channels. Irregular geometry of these channels can slow or facilitate the movement of various substances in the CNS, including the transport of exogenous drugs.

The macroscopic properties of the ECS are described by volume fraction and tortuosity. The volume fraction is the quotient of the volume of the ECS and the total tissue volume. The volume fraction in a normal isotropic region of the brain is estimated to be 0.2, i.e., the ECS makes up approximately 20% of brain tissue (Van Harreveld, 1972; Fenstermacher and Kaye, 1988). Tortuosity is another ECS parameter that quantifies how much the diffusion of molecules is hindered in tissue compared to free medium. Tortuosity in homogenous and isotropic brain regions is about 1.6, but larger molecules (with relative molecular mass above 10kDa) generally exhibit larger tortuosity (Nicholson and Sykova, 1998). Heterogeneity in tortuosity is often tested by measuring diffusion along three orthogonal axes. A difference in tortuosity along different axes indicates anisotropy.

Within the hippocampus, both volume fraction and tortuosity have shown considerable regional variation, implying the ECS is not a fixed volume, but varies among the hippocampal subfields. These parameters exhibit lower values in CA1 as compared to CA3 and dentate gyrus, specifically in stratum pyramidale as compared to other strata (McBain et al., 1990; Perez-Pinzon et al., 1995). Within stratum radiatum, isotropic tortuosity is present along medio-lateral and antero-posterior directions, but is

increased along the dorso-ventral axis depending on the distance from stratum pyramidale (Mazel et al., 1998; Hrabetova, 2005). Local differences in ECS parameters may be a result of varying distances between cellular membranes, diffusion barriers in the extracellular matrix, or differential sizes of cell bodies or processes in each region (McBain et al., 1990). For instance, the pyramidal cell layer is more tightly packed in CA1 than CA3; CA3 cells (300-700 μm^2) are larger than those in CA1 (~193 µm2); and the massive associational network which is so apparent in CA3 is largely missing in CA1 (Amaral and Lavenex, 2007). The decrease in CA1 volume fraction may be due to overall homogenously smaller intercellular channels or it may reflect heterogenous channels that are on average smaller. The latter is supported by measurements taken of gaps between cells, which range from 38-64 nm in width, with uneven distentions in some regions as compared to others (Brightman, 1965; Van Harreveld et al., 1965; Bondareff and Pysh, 1968; Cragg, 1979). However, histological fixation in older morphological studies may have resulted in artificial narrowing in some regions (Hrabetova and Nicholson, 2007).

While the shape and size of cells and their processes create obstacles that diffusing molecules have to circumnavigate, it is not clear how these and other elements in the brain increase or decrease ECS parameters. Changes in volume fraction and extracellular tortuosity are often independent. Osmotic or ischemic insults result in reduction of the volume fraction and a rise in tortuosity, presumably due to cellular swelling (Sykova et al., 1994; Perez-Pinzon et al., 1995; Hrabetova and Nicholson, 2000). Inflammatory and demyelinating diseases result in an increase in volume fraction and a decrease in tortuosity, perhaps due to an increase in blood-brain barrier

permeability (Simonova et al., 1996). However, during astrogliosis, a persistant increase in tortuosity without a decrease in volume fraction has been found (Sykova et al., 1999a). The converse has also been observed. Seizure activity, which induces large increases in extracellular potassium (Dietzel et al., 1980; Dietzel et al., 1989), results in subsequent water movement into surrounding cells and thus a reduction in extracellular volume fraction, but not necessarily a change in tortuosity (McBain et al., 1990).

There remain many unknowns regarding what elements change ECS parameter and how these parameters affect spread and clearance mechanisms of the brain. Moreover, although pathological insults have been associated with changes in ECS and extracellular matrix, the ability of ECS to bind, slow, or facilitate the migration of substances remains an open question. However, the heterogeneity of ECS architecture does affect intercellular communication, nutrient and metabolite trafficking (McBain et al., 1990; Sykova, 1997b; Nicholson and Sykova, 1998; Sykova and Nicholson, 2008), and potentially, as is described in the rest of Chapter 1, drug delivery in the brain.

Intracerebroventricular/intrathecal delivery

In intracerebroventricular (ICV) administration, drug is introduced directly into the cerebrospinal fluid (CSF). Theoretically, when drugs are infused directly into the CSF, not only is systemic toxicity reduced, but the drugs have longer half-lives due to decreased protein binding and enzymatic activity relative to drugs in plasma. High local concentrations of drug have been administered into the CSF with the Ommaya reservoir, a plastic reservoir implanted subcutaneously in the scalp and connected to the ventricles within the brain via an outlet catheter (Ommaya, 1963). Pumps have similarly been used to elevate drug concentrations in the CSF (Bakhshi and North, 1995). In 2006, continuous ICV infusions of valproic acid were compared to bolus ICV

injections and intraperitoneal (IP) injections in a rat kindling model of epilepsy (Serralta et al., 2006). The ICV bolus injection resulted in the highest concentrations of VPA in the brain, but all three methods were able to control generalized and focal seizures. The ICV infusion was the only one to achieve anticonvulsant effects with minimal toxicity. In 2007, Oommen et al. researched the effectiveness on a osmotic pump delivering gabapentin on flurothyl induced seizures in rats and found delivery delayed onset of generalized tonic-clonic seizures (Oommen et al., 2007). Despite these favorable results, ICV delivery is still plagued by diffusion. Solutes within CSF must diffuse into brain parenchyma, a slow process in which concentration decreases logarithmically with each millimeter of brain tissue (Blasberg et al., 1975). The ECS of the brain is extremely tortuous, so drug diffusing from ventricles into this space is very slow and inversely proportional to the molecular weight of the drug (Pardridge, 1997). Although some molecules have been effectively distributed through intracerebroventricular (ICV) injection (Barcia and Gallego, 2009), in general, drug distribution from CSF into parenchyma is log orders slower than CSF clearance (and clearance of drugs infused into CSF) from the brain (Pardridge, 2005, 2007). ICV injection has been useful in cases where high drug concentrations in the CSF or immediately adjacent parenchyma are desired (Harbaugh et al., 1988).

Intracerebral delivery

The most direct way of administering drug to a specific area in the brain is to deliver it directly to the brain interstitium. Like ICV injections, this method can yield high concentrations and minimal systemic exposure without the limitation the BBB poses to size or chemical properties of therapeutic agents. Additionally, direct targeting of the

seizure focus is more desirable due to the drop of drug concentration from the distance of the implant or injection site (Saltzman and Olbricht, 2002).

Implantable polymers. Implantation of biocompatible sustained-release polymers is a strategy employed to bypass the BBB. A drug can be loaded into these polymers and diffuse into the surrounding tissue at a controllable rate. For non biodegradable polymers such as ethylene vinyl acetate copolymer (EVAc), the rate of drug diffusion into surrounding tissue is dependent on the loaded agent. For biodegradable polymers, such as the polylactic-co-glycolicacid (PLGA) family, the release of drug is dependent on the diffusivity of the macromolecule and the degradation rate of the polymer (Luo et al., 1999). This method has been shown to release drugs successfully, but it still relies on diffusive transport, which yields a concentration profile drop-off and is dependent on molecular size.

Convection-enhanced delivery. Convection-enhanced delivery (CED) is an approach developed to overcome the obstacles in diffusion-dependent central nervous system (CNS) delivery methods. CED was first described by Bobo et al. (1994) as a local drug-delivery technique that uses a small hydrostatic positive-pressure gradient to deliver infusate directly into parenchymal interstitial space. Because CED relies on bulk flow, it can overcome slow diffusivity and result in a more widespread distribution volume as compared with diffusion-based approaches. When transport is dominated by diffusion, a large concentration gradient develops from the site of infusion to the margins of the distribution volume as drug molecules move passively from regions of high to low concentration. In contrast, CED provides a uniform concentration throughout the region with a sharp drop-off in concentration at the borders (Rogawski, 2009).

Dispersion of agents is powered by gradients of pressure in addition to gradients of concentration. As a result, convection-driven flow overcomes slow diffusivity and can result in a larger volume of distribution as compared with other diffusion-based drug delivery methods (for review, see (Raghavan et al., 2006)). Furthermore, CED is generally independent of molecular size (Bobo et al., 1994; Sampson et al., 2011) as long as macromolecules are within the ECS width of CNS tissues (38-64 nm, (Thorne and Nicholson, 2006)). Previous studies have demonstrated intracranial CED into either white or gray matter can be used to distribute small or large molecular weight molecules in a homogenous, targeted, and safe manner (Bobo et al., 1994; Chen et al., 1999).

Underlying the success of CED as a therapeutic drug delivery system is a good understanding of the principles governing delivery and flow of macromolecules within the CNS. There are several known factors affecting the final distribution of infusate in the brain. Firstly, infusion pump parameters, such as flow rate and duration of infusion, will affect the inflow of the solution. Because infusate is delivered into the ECS, transport is dominated by convection and controlled through the flow rate, duration, and pressure of the infusion (Raghavan et al., 2006). Secondly, certain infusate properties have a significant impact on distribution. These properties include viscosity (Jagannathan et al., 2008), surface properties, (Chen et al., 2005), particle charge (Saito et al., 2006), and particle coating (MacKay et al., 2005). Backflow of the infusate along the infusion cannula can also affect distribution. Backflow may be a result of tissue disruption along the catheter track, allowing the infusate to flow into low-resistance spaces (Guarnieri et al., 2005), or the pressure from the infusion may push the tissues away from the catheter, defined as intrinsic backflow (Morrison et al., 1999).

Backflow is an important issue to take into account because it can result in the spread of infusate into unintended regions and diminish the dose needed within the target tissues (Figure 1-3). This problem is addressed by using thinner catheters (Lonser et al., 2002), step-design catheters (Krauze et al., 2005), and guidelines for catheter placement in humans (Raghavan et al., 2006) and animals (Kim et al., 2009; Astary et al., 2010). These guidelines will be further addressed in Chapter 2.

CED for epilepsy. CED has already been proposed as a novel therapeutic therapy to treat epilepsy (Rogawski, 2009) and continues to show promise. AEDs currently prescribed and developed are limited to orally-active or BBB-permeable agents. CED is applicable to a wide variety of potential anti-epileptic drugs since it does not require passage through the BBB. CED can be used deliver anticonvulsant or neuroprotective peptides and other high molecular weight molecules that have already shown promise as epilepsy treatments experimentally (McLaughlin et al., 2000; Haberman et al., 2003; Richichi et al., 2004). An example of CED delivery of novel therapeutic agents can be seen in Figure 1-4.

While CED for epilepsy remains experimental, several studies have already shown the feasibility of undertaking it for epilepsy treatment (Stein et al., 2000; Heiss et al., 2005; Gasior et al., 2007). CED has also been used clinically in malignant glioma (Voges et al., 2003), growth factor (Gill et al., 2003), and gene therapy vector (Marks et al., 2008) delivery studies. With the high drug concentrations that can be achieved at specific sites, CED has a wide range of applications in the field and treatment of epilepsy. However, the efficacy of the procedure at this stage remains poorly determined partly due to the heterogeneity of drug distribution and the effect of edema

on interstitial transport. More detailed knowledge about the anatomical and biophysical features of the brain is necessary for optimization of delivery into complex or injured brain regions. This topic is the focus of Chapter 2 and Chapter 3.

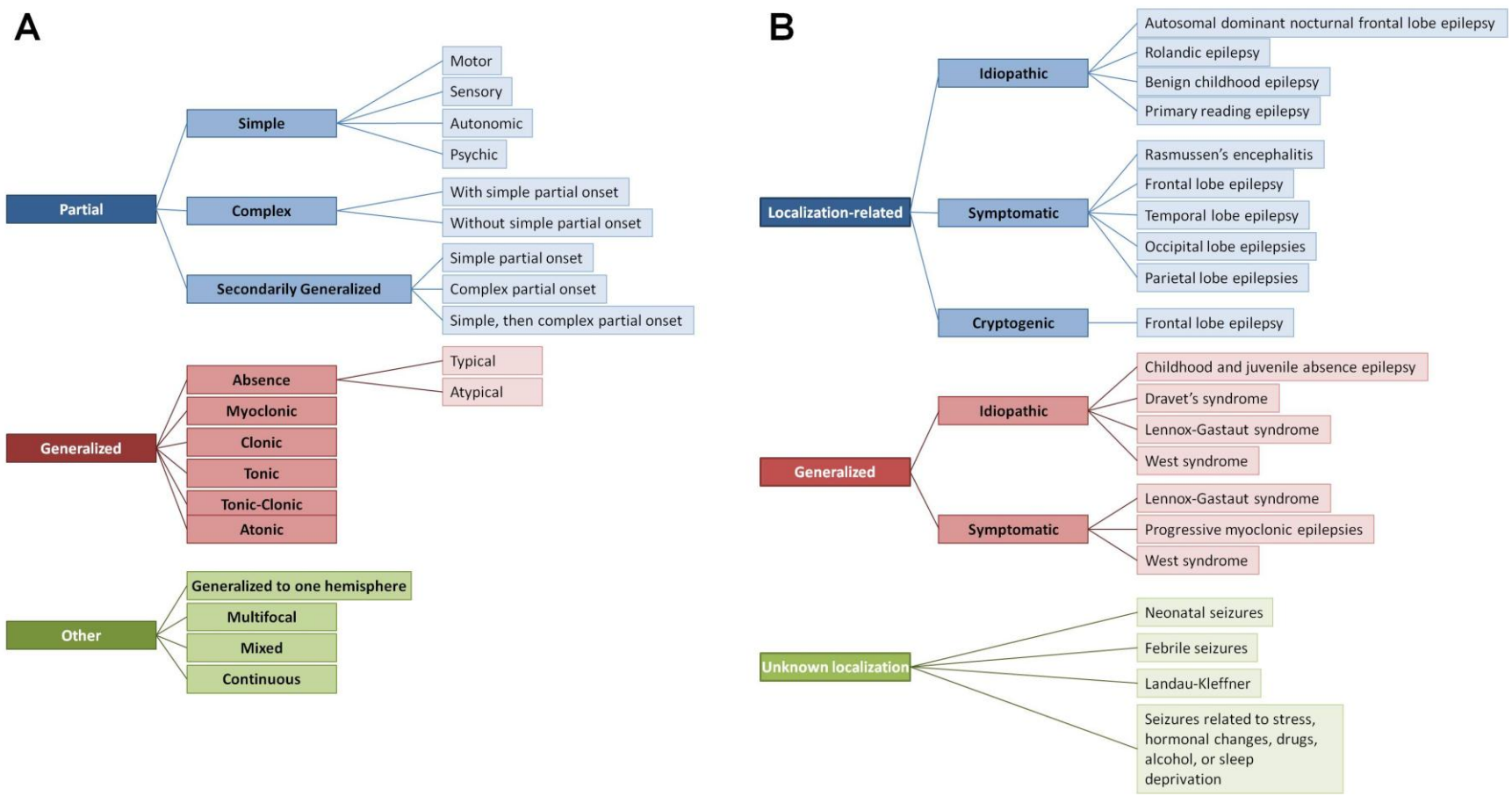

Figure 1-1. The epilepsies are classified based on etiology, semiology, origin of seizures, and epilepsy syndromes. Two systems of classification of epilepsies are in use today. A) The International League Against Epilepsy (ILAE) developed the first system based on seizure semiology in 1981. B) ILAE developed the second system based on epilepsy syndromes in 1989.

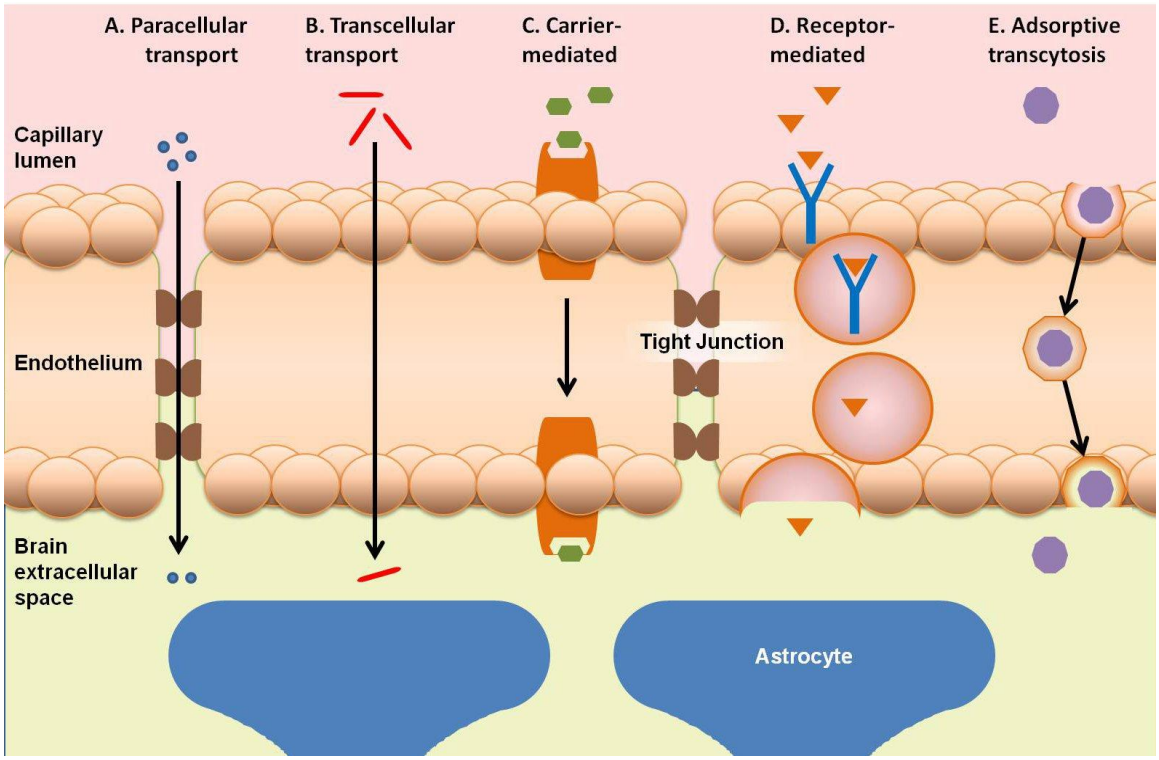

Figure 1-2. Schematic of the various routes of molecular transport across the BBB. These pathways can be exploited to transport biochemically-altered drugs from the systemic circulation into the brain. A) Small water-soluble agents travel through tight junctions connecting endothelial cells. B) Small, lipophilic molecules diffuse through endothelial cell membranes. C) Carrier-mediated transport systems are available for specific molecules such as amino acids, peptides, nucelosides, glucose, etc. D) Receptors are expressed for the transport of transferrin, insulin, lipoproteins, and other molecules that are actively transported across the BBB. E) Adsorptive transcytosis involves nonspecific binding of charged ligands, such as albumin, to membrane surface charges followed by endocytosis.

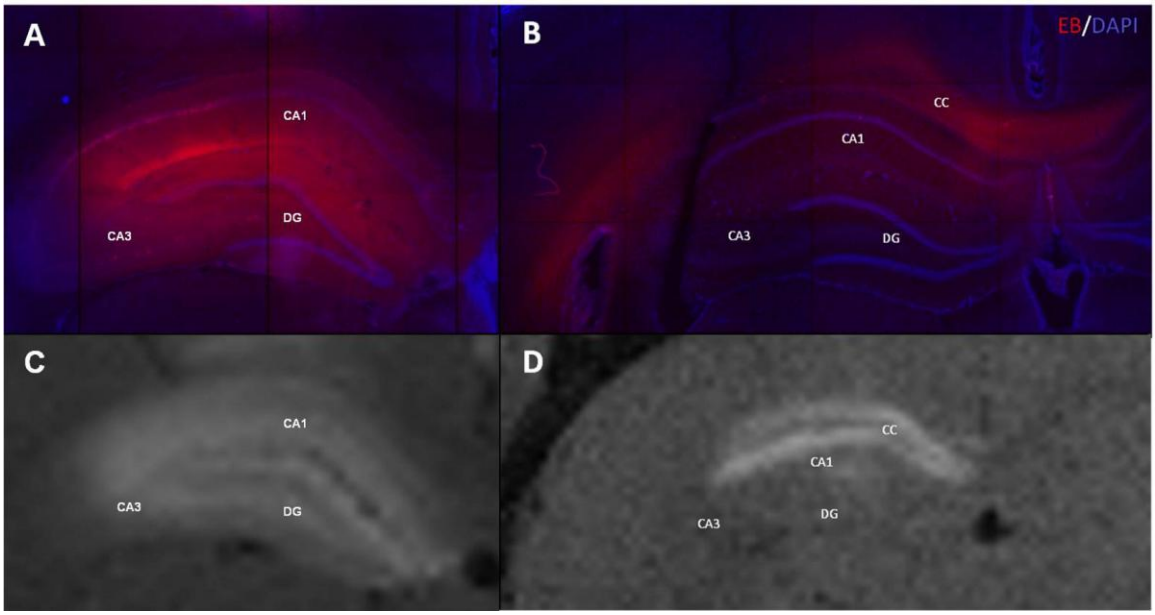

Figure 1-3. Final CED distribution with and without backflow of an MR contrast agent tagged with a fluorescent tracer in the rodent septal hippocampus. A,C) During successful CED, the tracer (A, red fluorescence) and contrast agent (C) travel along the contours of the hippocampal laminar structure. B,D) When backflow occurs, much of the infusate travels away from the targeted site into white matter tracks, or other low resistance pathways. EB = Evans blue dye; DAPI = 4',6-diamidino-2-phenylindole nuclear counterstain; DG = dentate granule cells; CA3 = Cornu Ammonis hippocampal subfield 3; CA1 = Cornu Ammonis hippocampal subfield 1; CC = corpus callosum.

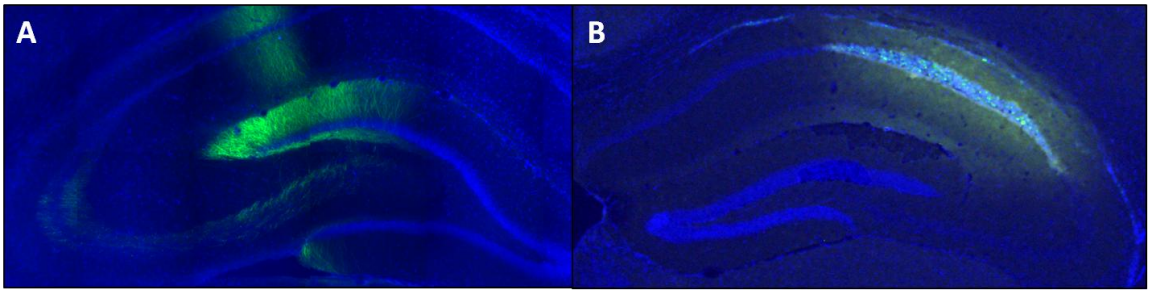

Figure 1-4. Lentivirus and neural stem cells targeted to the septal hippocampus via CED. A) Lentiviral transduction of CAMKII-ChR2/YFP in CA1 pyramidal cells and dentate granule cells. B) Engraftment of neural stem cells expressing GFP in the CA1 subfield of the septal hippocampus. Counterstained with DAPI, 4',6-diamidino-2-phenylindole nuclear counterstain.

CHAPTER 2
CONVECTION-ENHANCED DELIVERY IN THE NORMAL RAT HIPPOCAMPUS

Introduction

Current CED research focuses on evaluating the efficacy of drug carriers, optimizing infusion parameters and infusion hardware (e.g. flow rate and duration, cannula design), and understanding the influence of the underlying tissue structure on the final distribution of the infused agent in the CNS (Raghavan et al., 2006; Sampson et al., 2007b; Jagannathan et al., 2008; Song and Lonser, 2008). With sufficient understanding of the controlling influences, CED might be used to target local delivery of therapeutics into complex regions of the brain with heterogeneous and intricate neuroanatomy. One such structure is the hippocampus, which is comprised of densely packed layers of neurons (gray matter), and their axonal projections (white matter) in a tightly-rolled, banana-shaped structure. In addition, the hippocampus includes perivascular spaces and pial surfaces that line the ventricular compartments continuous with hippocampal fissures. The hippocampus is vulnerable to damage as a result of trauma (Tate and Bigler, 2000) and is the central component of rare conditions such as limbic encephalitis (Corsellis et al., 1968) and dementia with isolated hippocampal sclerosis (Dickson et al., 1994). Hippocampal involvement is critical to the manifestation of TLE (Bertram, 2009), and has been recognized in co-morbidities of epilepsy, such as schizophrenia (Maier et al., 1995; Nelson et al., 1998) and Alzheimer's disease

---

Parts of this chapter are reprinted with permission from Elsevier from Astary GW, Kantorovich S, Carney PR, Mareci TH, Sarntinoranont M (2010) Regional convection-enhanced delivery of gadolinium-labeled albumin in the rat hippocampus in vivo. J Neurosci Methods 187:129-137.

This work was made possible by the collaboration with Dr. Garrett Astary. Dr. Astary helped with the infusions and distribution analysis, and performed the MR imaging and image segmentation described in this chapter.

(deToledo-Morrell et al., 2007; Ohm, 2007; Duyckaerts et al., 2009). If the CED distribution of a therapeutic agent within the hippocampus can be predicted, this may enable the application of CED to the treatment of TLE and other hippocampal disorders. However, accurate prediction of distribution profiles in the hippocampus requires an understanding of how the underlying tissue architecture influences transport of a delivered agent.

With the use of contrast agents, magnetic resonance (MR) imaging provides a means of non-invasively monitoring distribution profiles of agents delivered by CED and can provide insight into the influence of anatomy on tracer distributions. Typically, gadolinium-based contrast agents are used, which contain a paramagnetic center that interacts with surrounding water to reduce the longitudinal and transverse relaxation times (Lauffer et al., 1987). In a relaxation-weighted image, the reduced longitudinal relaxation times (T1) result in a higher signal in regions of tissue exposed to the contrast agent, provided transverse relaxation times (T2) are not substantially reduced. MR can also be used to monitor CED by observing an increase in water signal seen in T2-weighted images (Heiss et al., 2005). Gadolinium-based contrast agents have been co-infused with therapeutic agents to track their distribution in real-time. Co-infusion of glucocerebrosidase and diethylene triamene penta-acetic acid chelated gadolinium (Gd-DTPA) into the region of the right facial and abducens nuclei was used to treat a patient with Gaucher's disease and allowed researchers to monitor the distribution of the agent as well as observe the agent cross a pial surface to enter the third ventricle (Song and Lonser, 2008). Other studies have also been performed to investigate the effect of pial surfaces on final distribution volumes of small molecular weight (Gd-DTPA) and large

molecular weight (Gd-DTPA-bound albumin (Gd-albumin)) tracers infused into the primate brainstem (Jagannathan et al., 2008). As a free ion, gadolinium is highly toxic but is regarded as safe when administered as a chelated compound. Gd-DTPA has been used in animal and human CNS studies, without showing signs of toxicity (Song and Lonser, 2008; Ding et al., 2009); however, it has been shown to have an adverse affect on patients with pre-existing kidney disease (Abujudeh et al., 2009). Liposomal drug carriers containing Gd have also been synthesized to provide a more direct method of monitoring the distribution of these therapeutic agent carriers (Krauze et al., 2008; Fiandaca et al., 2009). MR has been used to monitor the distribution of these delivery vehicles as well as evaluate the performance of backflow-resistant cannulae (Fiandaca et al., 2009). MR has also been used to evaluate the effect of infusate viscosity on final distribution volumes in rat brain striatal tumors (Mardor et al., 2009). However, no previous studies have implemented high-resolution MR to investigate CED for delivering an agent into a structure as complex as the hippocampus.

In addition to MR, histology has also been used to evaluate tracer distribution of agents infused into the CNS. Light microscopy was used to detect the presence of Evans blue dye infused into the striatum of a mouse brain via an implantable microfluidic device designed for chronic CED (Foley et al., 2009). Fluorescence microscopy has been used to observe the distribution of polyethylene glycol-coated liposomal doxorubicin infused into the rat brain parenchyma with an intracranial tumor (Kikuchi et al., 2008). Not only can histology provide higher-resolution visualization of distribution at the cellular level, but histological staining protocols can verify particular structural details that may influence distribution.

This chapter describes the effect of tissue structure on infusate distributions after CED and limited diffusion in the hippocampus of normal animals. Final distribution patterns of the MR contrast agent, Gd-albumin, labeled with Evans blue dye, infused into the left-side septal and right-side temporal hippocampus of a rat were evaluated with two currently available imaging modalities: (1) in vivo imaging of contrast agent distribution using high resolution MR imaging and (2) fluorescence microscopy of the distribution of Evans blue in histological slices. Gd-albumin is an ideal model for macromolecular flow through the interstitial space due to low reactivity, convection-dominated transport, and ease of labeling with contrast agent. MR provided a means of non-invasively monitoring distribution profiles of contrast agents delivered by CED in vivo, while optical microscopy yielded higher resolution of finer structural detail. Black-gold staining was used to label myelinated white matter structures, and Cresyl violet staining was used to visualize cell bodies. The results of this study demonstrate the influence of infusion site and normal hippocampal structure on CED delivery.

Methods

Animal Preparation and Surgical Procedures

Experiments were performed on 2.5-month old male Sprague-Dawley rats (n = 7) using protocols and procedures approved by the University of Florida Institutional Animal Care and Use Committee. Anesthesia was initiated with xylazine (10 mg/kg, SQ) and isoflurane (4%) in 1 L/min oxygen, then animals were placed in a stereotaxic Kopf apparatus, and inhalation anesthesia (1.5% in 1.5 L/min oxygen) was delivered via a nose mask. The skull was exposed by a mid-sagittal incision that began between the eyes and extended caudally to the level of the ears to expose bregma and lambdoidal sutures. One hole was drilled into the skull above the left-side septal hippocampus and

a second hole was drilled above the right-side temporal hippocampus. Then 5.0 µL of Gd-DTPA-albumin (10 mg/mL in PBS solution; MW ~ 87 kDa,; ~35 Gd-DTPA molecules per albumin molecule; R. Brasch Laboratory, University of California, San Francisco, CA), tagged with Evans Blue dye was infused into the septal dentate gyrus of the hippocampus [-3.7mm AP, -2.2mm ML, -3.4mm DV] and another 5 µL into the temporal CA1 subregion of the hippocampus [-5.0mm AP, 4.9mm ML, - 5.0mm DV] at a rate of 0.3 µL/min. Over concerns that the Gd-albumin may be aggregating, high performance liquid chromatography (HPLC) was used to evaluate the macromolecular constituents of the infusate solution. HPLC resulted in a single elutant peak suggesting the Gd-albumin was not aggregating and the covalent bonds attaching the Gd-DTPA molecules to albumin were intact.

The infusion system consisted of a 100 µL gas-tight syringe (Hamilton, Reno, NV) driven by a syringe pump (Cole-Parmer, Vernon Hills, IL) connected to polyaryletheretherketone (PEEK) tubing (ID = 0.381 mm, OD = 0.794 mm, length ~ 0.5 m, Upchurch Scientific, Oak Harbor, WA). The PEEK tubing was coupled to a silica cannula (ID = 50 µm, OD = 147 µm, Polymicro Technologies, Phoenix, AZ) via a microfluidic connector. Immediately following the infusion surgery (~30 min), animals were transported to the 11.1 Tesla (T) magnet for MR imaging.

At the end of the experiment, animals under inhalation anesthesia (1.5% in 1.5 L/min oxygen) were given xylazine (10 mg/kg, SQ) and ketamine (80 mg/kg, IP). Upon ensuring deep anesthesia, the chest activity was opened to expose the heart, and a needle connected to an infusion pump was inserted into the left ventricle. 200-300 mL of 0.9% saline solution was circulated by the heart, followed by 200-300 mL of 4%

formaldehyde solution. The brain was then extracted from the skull following decapitation and stored in 4% formaldehyde solution overnight.

MR Imaging and Image Segmentation

MR experiments were performed using a Bruker Avance imaging console (Bruker NMR Instruments, Billeria, MA) connected to a Magnex Scientific 11.1 T horizontal bore magnet system (Varian, Inc., Magnex Scientific Products, Walnut Creek California). A custom-made 130 degree arc, 3.5 cm rectangular linear-field surface coil constructed on a 4 cm diameter half-cylinder was used for linear transmission and detection of MR signal. Two sets of high-resolution T1-weighted images, with slices oriented in the coronal and sagittal directions, were acquired using a spin-echo sequence with a 2 cm × 2 cm field-of-view in a matrix of 160 × 160, recovery time of 1000 ms, echo time of 10 ms and 20 slices, slice thickness 500 μm. Coronally-oriented and sagittally-oriented data were acquired with 8 averages and 6 averages respectively.

Final distribution volumes of Gd-albumin were calculated by performing semi-automatic image segmentation on the high-resolution T1-weighted coronal images using the ITK-SNAP open-source medical image segmentation tool ((Yushkevich et al., 2006); http://www.itksnap.org/). Septal and temporal hippocampus infusion volumes were segmented separately with the following specific threshold criteria. Voxels were included in the infusion volume if their signal intensity was at least 6 standard deviations higher than the signal intensity in the corresponding region contralateral to the site of infusion. Final distribution volumes in the septal and temporal hippocampus were calculated by counting the number of voxels included in each segmented region and multiplying by the volume of a single voxel.

Histology

Black Gold was used to stain myelin in mounted sections. Black-Gold II powder (Histo-Chem Inc., Jefferson, AR) was resuspended in saline solution (0.9% NaCl) to a final concentration of 0.3%. The solution was heated to 60°C, and rehydrated tissue sections were incubated for 12-18 minutes, until desired intensity was achieved. The sections were then rinsed in double distilled water for 2 minutes, followed by sodium thiosulfate solution (1%) for 3 minutes. Finally, sections were rinsed three times with double distilled water for 5 minutes per rinse.

Cresyl violet staining was performed to stain cell bodies in mounted sections. Slides were incubated in Cresyl violet solution for 2-3 minutes until desired intensity was achieved. Slides were then dehydrated using a series of gradated alcohols (75%, 95%, 100%) for 5 minutes each. The dehydrated sections were then cleared in xylene for 2 minutes and cover-slipped with mounting media.

Microscopy

Following mounting and staining, slides were examined on an Olympus BH-2 brightfield and epifluorescence microscope (Olympus America Inc., Center Valley, PA) with a Hitachi KP-D581 color digital video camera (Hitachi Medical Systems America, Inc., Twinsburg, OH) interfaced with an Integral Technologies frame grabber (Pelco, Clovis, Ca) in a desktop computer. Motorized stage and focus (Prior Scientific, Rockland, MA), and image acquisition were controlled through ImagePro Plus (Media Cybernetics, Silver Springs, MD). Anatomical structures were mapped to coronal sections of the Paxinos and Watson rat brain atlas (Paxinos, 1998).

Results

Infusion Site

Infusions (n=14) were targeted into the dentate gyrus of the left-side septal hippocampus (n=7) and into the right-side CA1 of the temporal hippocampus (n=7). Actual infusion sites were confirmed with MR and histology. Damage due to insertion of the cannula was minimal with some bleeding at the site of the cannula tip (Figure 2-1A) and at the interface between the corpus callosum and alveus of the hippocampus (Figure 2-1B), as visualized with histology. Contrast agent infused into the septal hippocampus was observed to have only limited penetration into the ipsilateral temporal hippocampus (Figure 2-2A,C). Similarly, contrast agent infused into the temporal hippocampus showed severely limited penetration into the ipsilateral septal hippocampus (Figure 2-2B,D) with small amounts observed in the fimbria.

Infusion sites were clearly identifiable in all subjects in the septal hippocampus and 6 of the 7 subjects in the temporal hippocampus. In the septal hippocampus infusions, 6 of 7 infusion sites were located in stratum radiatum of the CA1 subfield of the hippocampus. One infusion site was located in the polymorphic layer of the dentate gyrus. In 4 of 7 temporal hippocampus infusion subjects, the infusion site was located in stratum radiatum of the CA1 subfield of the hippocampus. In 2 of the subjects, the infusion site was determined to be in stratum oriens of the CA1 subfield of the hippocampus.

Gd-albumin Distribution in the Septal Hippocampus

The profile of the contrast agent distribution into the septal hippocampus was easily distinguishable from surrounding tissue. Exposed regions displayed a hyperintense signal with respect to surrounding regions in T1-weighted images (Figure

2-3). MR images showed that the contrast agent entered the CA1, CA3 and dentate gyrus subfields of the hippocampus in all animals (Figure 2-3) and suggest that contrast agent penetrated poorly into the dense dentate gyrus granule cell layer and CA1 pyramidal cell layer. These regions remain hypointense with respect to the surrounding subfields and are clearly distinguishable in coronal images (arrowheads in Figure 2- 3). The contrast agent was seen to cross the midline of the brain in 3 of the 7 subjects. In two of these subjects, the contrast agent crossed the midline of the brain by entering the corpus callosum and traveling medially to the side of the brain contralateral to the infusion site. In one subject, the contrast agent also entered the septal hippocampal commissure and was visible in a small portion of the CA1 subfield of the contralateral hippocampus. Contrast agent penetration into the fimbria subfield of the hippocampus was not seen in any of the subjects suggesting the densely packed cell layer CA1 and CA3 subfields served as a barrier to transport into this region (Figure 2- 3).

Gd-albumin Distribution in the Temporal Hippocampus

The contrast agent penetrated the CA1 and CA2 subfields of the temporal hippocampus in all subjects. In 5 of 7 subjects, contrast agent was seen in the dentate gyrus, CA1, CA2, and CA3 subfields of the hippocampus (Figure 2-4B,C,E-F). However in two of the subjects, penetration of the contrast agent into CA1 and CA2 was limited and primarily located in the alveus of the hippocampus (Figure 2-4G,H), most likely due to the lateral location of the infusion site (see above “Infusion Site” results section). The contrast agent did not appear to enter the granule cell layer and hippocampal fissure, since these regions were hypointense relative to the neighboring dentate gyrus. Contrast agent was also observed at the interface between the corpus callosum and the cortex in these subjects.

Backflow

Severe backflow, resulting in a significant amount of contrast agent entering the cortex, was seen in 3 of the 7 septal infusions (Figure 2-3C,E,F). Mild backflow resulted in minor exposure of the cortex to contrast agent in 2 of the 7 subjects (Figure 2-3D,H). In 3 of the 7 subjects, backflow allowed the contrast agent to enter the corpus callosum and travel in both the medial and lateral directions along this white matter fibrous structure (Figure 2-3B,C,F).

Severe backflow in temporal infusions resulted in significant amounts of the contrast agent entering the cortex in 3 of the 7 subjects (Figure 2-4B,C,E). Minor backflow was observed in 3 of the 7 subjects (Figure 2-4D,F,G) and no backflow was seen in 1 subject (Figure 2-4H). In cases of minor backflow, contrast agent did not enter the cortex and remained in the hippocampus, usually penetrating the alveus of the hippocampus.

Image Segmentation

The three dimensional contrast agent distributions were visualized with a semi-automated segmentation of the contrast agent enhanced regions. Because MR imaging was conducted approximately 30 minutes after CED, the observed distribution profiles include the effects of CED as well as post-CED diffusion. Distribution volumes, including the effects of CED and diffusion, were calculated from the segmentations for each data set and included back flow volumes. For the septal hippocampus infusion, the mean and standard deviation of the calculated distribution volume was 23.4 ± 1.8 μL. For the temporal hippocampus infusion, the mean and standard deviation of the calculated distribution volume was 36.4 ± 5.1 μL. The temporal hippocampus distribution volume was greater than the septal hippocampus distribution volume ($p \leq 0.0003$, power of test

= 0.99). The contribution of diffusion after the end of CED to the measured distribution volumes was estimated using an analytical solution of one-dimensional diffusion from a sphere. The radius of the sphere was determined such that the volume of the sphere would be equal to distribution volumes of the contrast agent in the septal and temporal hippocampus. The diffusion coefficient of albumin in rat cortical slices, D = 1.63 × 10-7 cm^2/s (Tao and Nicholson, 1996), was used in this estimation. Based on these results we estimate that diffusion after the end of CED may increase distribution volumes up to 40%. This diffusional spread is equivalent to the contrast agent traveling 2-3 voxels (0.250-0.375 mm) during the time-delay between CED and MR imaging (for comparison, the average anterior-posterior spread of the tracer was measured to be 5.4 mm for septal infusions and 4.75 mm for temporal infusions).

Histological Analysis

Evans blue fluorescence confirmed the distributions seen in MR imaging. Dense cell layers that appeared hypointense in MR images likewise did not fluoresce in histological images (arrowheads, Figure 2-5 and 2-6), indicating little or no penetration of the infusate. However, infusate was seen to distribute around the dense cell layers then penetrate the dentate gyrus and CA1-CA3 subregions in all septal infusions and 5 of 7 temporal infusions, which is consistent with MR results. Preferential distribution was dependent upon location of the cannula tip. When the cannula tip was located in the interface between the CA1 and hippocampal fissure (asterisks, Figures 2-5 and 2-6), fluorescence was greatest in the molecular layer of the dentate gyrus and CA1 immediately adjacent to the hippocampal fissure. In one subject (Figure 2-3D), the cannula tip was in the polymorphic layer of the dentate gyrus, which resulted in a larger volume of contrast agent accumulated internal to the dentate gyrus granule cell layer.

In 2 of 7 temporal infusion subjects, Evans blue was observed to be predominately distributed within the alveus of the hippocampus (closed arrows, Figure 2-6C) and corpus callosum (open arrows, Figure 2-6C), as was seen in MR (Figure 2- 4G,H). These distributions were observed in sections displaying cannula tracts and those with no visible tissue damage. Due to a more lateral infusion site in these two subjects, infusate traveled along the axis of the white matter fiber tract and was limited mediolaterally by the pyramidal cell layer and the cortex adjacent to the fiber tracts (Figure 2-6C). One temporal infusion showed Evans blue in the perivascular space (Figure 2-6A).

Discussion

This study compared the distribution profiles of Gd-albumin in the septal and temporal hippocampus after CED and limited diffusion in normal animals. Distribution of the contrast agent was visualized with high resolution MRI; shape and volume analysis was performed with segmentation; and validation was completed with histology, which also provided finer resolution to further elucidate the role of tissue structures on final distribution patterns. Images from histology and fluorescence microscopy were compared to MR images acquired *in vivo* to confirm the distribution of the infusate in hippocampal subregions. Results demonstrate that the distribution profile and shape of the infusions are dependent upon infusion site and underlying neuroanatomical and cytoarchitectonic structure.

Distribution Profile and Shape

The infusion site was a critical factor influencing distribution of the contrast agent. The temporal infusions distributed throughout the posterior dorsoventral hippocampus, while the septal infusion distributed throughout the anterior end to the septal pole of the

hippocampus. In addition, infusion into the septal target site resulted in a smaller distribution area compared to the temporal site and an apparent disconnect was noted between septal and temporal hippocampal infusion sites.

Infusion site variability within the septal and temporal hippocampus also influenced the distribution profile of the infused agent. For the septal hippocampus infusions, variability (~1 mm) in the cannula placement within the medial-lateral/anterior-posterior plane had negligible effects on tracer distribution, as observed in both MR and fluorescence microscopy (Figure 2-3). Although occurring in only one animal, variability in the depth of the cannula tip seems to have the most impact on final tracer distribution (Figure 2-3D), which was most apparent in fluorescence imaging (data not shown). In this subject, the most intense fluorescence signal was seen interior to the granule cell layer of the dentate gyrus. In contrast, the most intense fluorescence signal was seen around the hippocampal fissure and CA1 subregion of the hippocampus for all other subjects. In the temporal hippocampus infusions, variability (~ 1 mm) in the depth of cannula penetration had little impact on final distributions; however, variability in the location of the cannula tip in the medial-lateral direction had a significant impact. This is seen in two subjects where infusions lateral to the targeted infusion site resulted in tracer distributing entirely within the alveus of the hippocampus and the corpus callosum (Figure 2-4G,H). Since the infusion sites were stereotaxically targeted using an atlas developed from a fixed rat brain, deviations between the fixed rat brain and in vivo rat brain, anatomical variability between rats, and experimental error may contribute to variability in the infusion site.

The dorsoventral disconnect may have several explanations. Since infusions were only conducted at one volume, it is possible that the volume used was not sufficiently large enough to distribute throughout the entire hippocampus. Alternatively, anatomical "sinks" (such as ventricles or the hippocampal fissure) may "capture" a larger volume of the infusate. The fissure is a cell-free region continuous with ventricular space that is lined by pia mater and filled with CSF and blood vessels (Humphrey, 1967). It could act as a mass sink for the contrast agent, especially since Gd-albumin is able to cross pial boundaries (Jagannathan et al., 2008). Indeed, hyperintense regions were observed in the MR imaging within and surrounding the hippocampal fissure (Figures 2-3 and 2-4), and this finding was confirmed with fluorescence imaging (Figures 2-5 and 2-6). Although this finding may be explained by targeting, a preferential distribution into the fissure is also seen in images where the cannula tip is not positioned in the fissure (Figure 2-6), indicating the contrast agent may be following the path of least resistance and collecting within the hippocampal fissure.

A third explanation for the dorsoventral disconnect may arise from the effect of differential axonal projections to, from, and between septal and temporal hippocampi. For example, different densities of projections have been found to the septal and temporal hippocampus from the entorhinal cortex (Krettek and Price, 1977; Dolorfo and Amaral, 1998), amygdala (Krettek and Price, 1977), ventral tegmental area, and locus coeruleus (Haring and Davis, 1985; Verney et al., 1985). Hilar (Fricke and Cowan, 1978) and CA3 projections (Ishizuka et al., 1990; Li et al., 1994) are also coded toward specific areas of the hippocampus. These axonal structural differences likely underlie

functional differences between the septal and temporal hippocampus (Moser et al., 1993; Jung et al., 1994; Esclassan et al., 2009) and may affect CED distribution.

This study demonstrates that neuroanatomical structure influences CED distribution of contrast agent at the molecular level. Although contrast agent entered all subfields of the hippocampus in each subject, limited penetration was observed in the granule cell layer in the dentate and pyramidal cell layer in the CA3 and CA1. These cell layers consist of densely-packed excitatory cells that appeared as hypointense regions in the MR images (arrowheads, Figures 2-3 and 2-4), and displayed weak or no response to fluorescence imaging (arrowheads, Figures 2-5 and 2-6). Hydraulic conductivity describes the ease with which a fluid can move through a porous medium. In the case of densely-packed cell layers, the hydraulic conductivity would be low and permeation of the infused agent into these regions would be limited. Furthermore, the pyramidal cell layer in the CA3 of the septal hippocampus appeared to prevent infusate from entering the fimbria (Figure 2-3), while the CA1 and CA2 pyramidal cells layers served as a boundary in the temporal hippocampus (Figure 2-4). It is likely that the contrast agent traveled around these structural boundaries, along the trisynaptic circuit (Andersen et al., 1969) of the hippocampus. The trisynaptic circuit is comprised of axonal fibers connecting several subregions of the hippocampus. Preferential directions of water diffusion have been found to correspond to the average aligned fiber directions within a voxel (Basser and Jones, 2002). Hence, the hydraulic conductivity along the direction of these fibers would be lower than that perpendicular to the fiber direction leading to a preferential distribution along the trisynaptic circuit. However, further

studies with in vivo dynamic contrast-enhanced MRI (DCE-MRI) are necessary to confirm this hypothesis.

It should be noted that other factors may influence the distribution patterns of agents delivered by CED into the brain parenchyma. For example, choice in cannula design and flow rate can impact the severity of backflow while the total infusion volume will ultimately influence the distribution volume and exposure of structures to the agent. In this study, flow rate and infusion volume were fixed to 0.3 µL/min and 5 µL, respectively, for all subjects. Thus, we cannot comment on how these factors would influence distributions in the hippocampus based on our results. However, it is surmised that increasing the flow rate would contribute to backflow. Backflow would also be dependent on cannula design with generally smaller diameter cannula resulting in less backflow (Morrison et al., 1999). A step-design cannula has also been proposed that has been shown to eliminate backflow at flow rates up to 5 µL/min (Krauze et al., 2005). Although this study employed the use of a small diameter cannula and low flow rate, several cases of severe backflow were observed. This backflow could be due to tissue entering the cannula tip during insertion and obstructing flow. This tissue blockage would cause the pressure in the infusion system to rise until the blockage is cleared and then a volume of infusate would be injected into the tissue at a high flow rate. Further investigations evaluating the effects of flow rate, infusion volume and cannula design on hippocampal distribution volumes are warranted.

Analysis of Shape and Volume

Shapes segmented from the MR images matched well the shapes of the septal and temporal hippocampus, suggesting that the infusate distributed throughout each region. Certain anomalies, such as severe backflow or contrast agent entering the

corpus callosum, were also easily identified in the 3D segmentations. The 3D segmentations also allowed quantitative comparisons between the septal and temporal hippocampus infusion volumes. Assuming a brain tissue porosity of 0.2 (Mazel et al., 1998; Sykova and Nicholson, 2008) the expected distributed volume would be 25 µL. The septal hippocampus distribution volume calculated in this study was similar to this value; however, the volume distribution calculated in the temporal hippocampus was significantly higher than the distribution volume calculated in the septal hippocampus. This suggests that the temporal hippocampus may have a lower porosity than the septal hippocampus, or factors other than porosity may be influencing final distribution volumes. One potential factor is the proximity of the septal hippocampus infusions to the hippocampal fissure. Because the hippocampal fissure penetrates a larger portion of the septal hippocampus than the temporal hippocampus, a larger region of the septal hippocampus is in proximity to this mass sink. Another potential explanation for the observed difference in distribution volumes is the more compact shape of the septal hippocampus. Although it would be expected that the contrast agent would distribute throughout the septal hippocampus and then enter the temporal hippocampus, the dense pyramidal cell layer may serve as a barrier to this transport and may confine the distribution of the contrast agent to the septal hippocampus. The observed distribution profiles include the effects of CED and diffusion during the time delay between the final infusion and MR imaging. We estimate that the effect of diffusion may increase the measured distribution volumes by up to 40% which is equivalent to the contrast agent traveling 2-3 MR imaging voxels by diffusion during the time delay. It is important to recognize this post-infusion transport; however, the analysis of influence of hippocampal

tissue architecture on CED distributions and method of image segmentation for determining final distribution volumes are still valid since both convective and diffusive extracellular transport are influenced by tissue boundaries and preferential transport routes.

To avoid observer bias, the segmentation of contrast agent distribution within the infused structures was conducted using a semi-automatic routine employing the selection of a lower-limit threshold that was set high to assure accurate segmentation. All voxels above the threshold within the infused regions of the brain were included in the segmented volumes. This lower-limit threshold was not based on a percentage of the maximum signal observed in the MR images. The absolute value of the signal in the presence of the contrast agent depends on the contrast agent relaxivity and the baseline T1 values within that particular tissue (Caravan et al., 1999; Burtea et al., 2008). Thus, establishing a threshold based solely on a percentage of the maximum observed signal is not adequate for the quantitative determination of contrast agent distribution. To establish the threshold value, the average signal was measured in the contralateral, unexposed structure. The threshold value was then set to six times the standard deviation above this average signal. By setting the lower-limit threshold to 6 times the standard deviation above the average signal observed in contralateral structures, the threshold excludes over 99% of voxels that have a measured signal greater than the baseline value due to solely a fluctuation in noise. A similar method has been employed to establish a lower signal enhancement limit when calculating the concentration profile of a contrast agent infused into an agarose gel (Chen et al., 2008). Since the segmented volume is sensitive to the thresholding criteria, lowering the

criteria would result in larger calculated infusion volumes; however, the difference between the septal and temporal hippocampus distribution profiles would probably not substantially change.

Conclusions

This is the first study to observe CED delivery of MR-detectable agents into the hippocampus. Injury was limited to damages induced directly by the cannula. The observed infusate distribution did not cover the entire hippocampus, but rather distributed according to known neuroanatomic features of the hippocampus with a detailed dependence on the infusion site. It is important to note that these results describe distributions in normally developed hippocampi. It is reasonable to expect variability of infusate distribution in CNS injury that results in structural pathology. Understanding extracellular transport in complex and/or edematous regions is paramount for targeted delivery of therapeutics. When structural rearrangements in injured hippocampi render other treatment options ineffective, targeted and predictable delivery of therapeutics via CED might provide a method for delivery. Moreover, use of MR imaging to observe distributions of therapeutic agents co-infused with contrast agents may allow targeted treatment in cases of variability in individual brain anatomy. The following chapter (Chapter 3) will describe studies examining infusate distribution within the injured hippocampus.

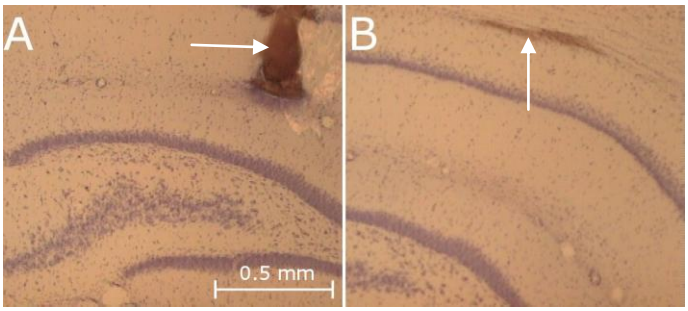

Figure 2-1. Damage induced by the infusion cannula in the septal hippocampus. A) Blood at the tip of the cannula. B) Blood within the alveus/corpus callosum boundary.

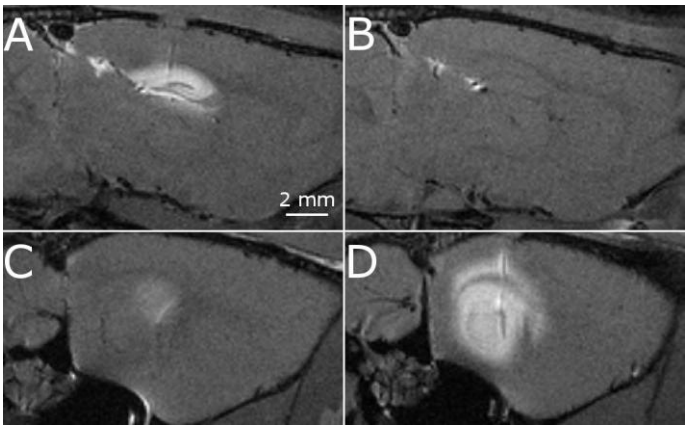

Figure 2-2. Sagittal images of a single rat demonstrating the apparent disconnect between the septal hippocampus (top row) and temporal hippocampus (bottom row). A) The disconnect is seen when the contrast agent is infused into the septal hippocampus (A and C) and temporal hippocampus (B and D).

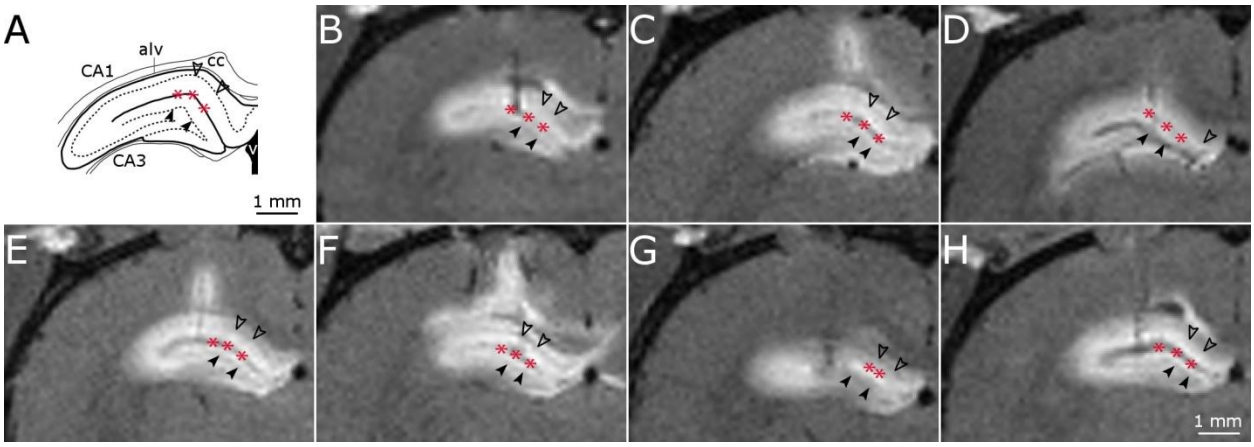

Figure 2-3. High-resolution T1-weighted MR images of septal hippocampus infusions. A) Schematic of key structures in the septal hippocampus adapted from (Paxinos, 1998). B-H) MR image coronal slice of infusion site for septal hippocampus infusions in 7 rats. Filled arrow heads, dentate gyrus granule cell layer; unfilled arrow heads, CA1 pyramidal cell layer; asterisk, hippocampal fissure.

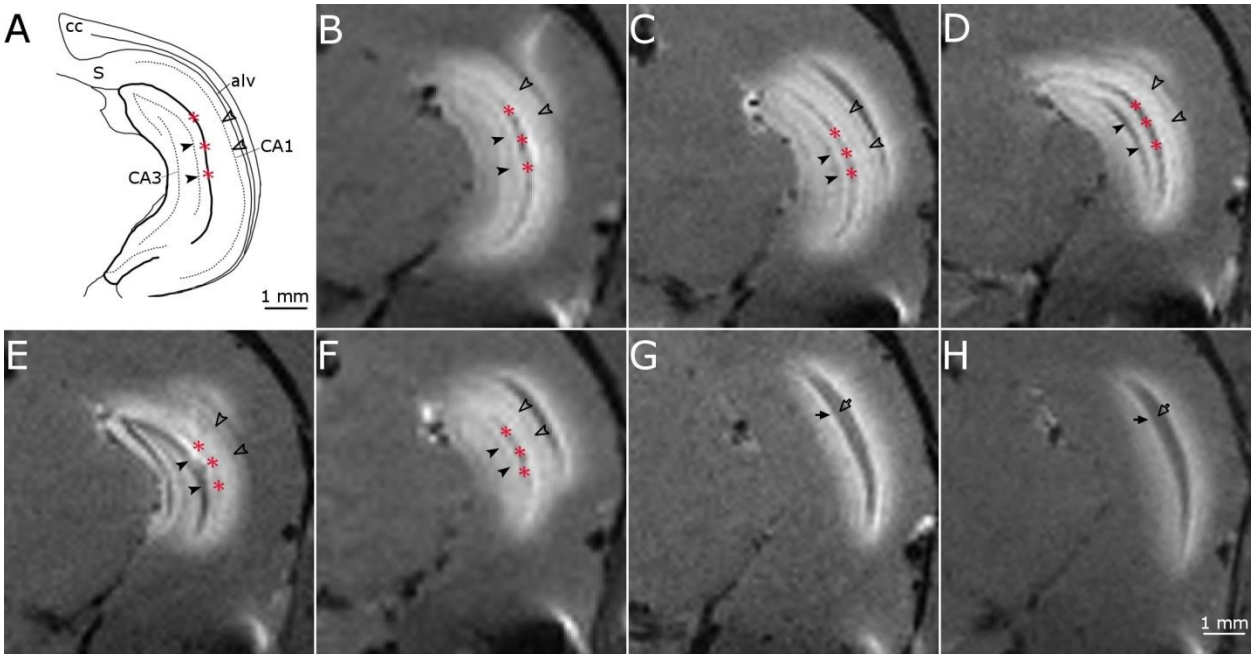

Figure 2-4. High-resolution T1-weighted MR images of temporal hippocampus infusions. A) Schematic of key structures in the temporal hippocampus adapted from (Paxinos, 1998). B-H) MR image coronal slice of temporal hippocampus infusions into 7 rats. Filled arrow heads, dentate gyrus granule cell layer; unfilled arrow heads, CA1 pyramidal cell layer; asterisk, hippocampal fissure, filled arrow, alveus; unfilled arrow, corpus callosum.

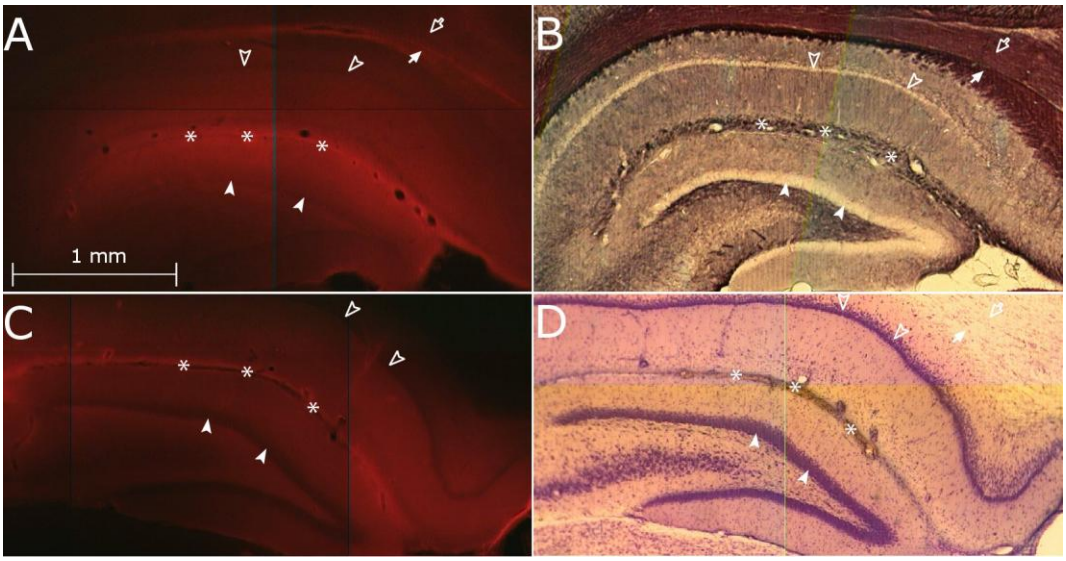

Figure 2-5. Histological images following infusate CED into the septal hippocampus showing Evans blue dye spreading throughout the septal hippocampus. A, C) Fluorescence images of 2 subjects showing limited penetration in the septal hippocampal dense granule cell layer (filled arrowhead) and pyramidal cell layer (unfilled arrowhead). Preferential distribution can be seen in the hippocampal fissure (asterisks) and alveus (filled arrow). B) Black-gold stained image in close proximity to (A) confirming alveus and dense cell layer approximations. D) Cresyl violet staining of a section in close proximity to (C) confirming dense cell layers.

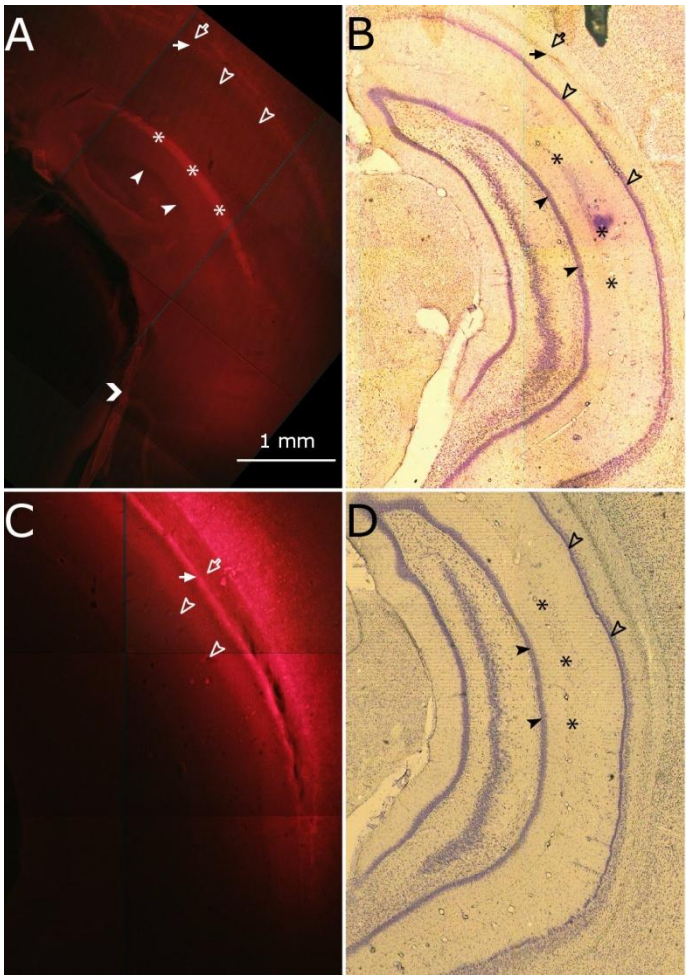

Figure 2-6. Histological images following infusate CED into the temporal hippocampus showing Evans blue dye spreading thoughout the temporal hippocampus. Arrowheads denote granule cell layer of the dentate gyrus and pyramidal cell layer of the CA1. A) A fluorescence image of Evans blue seen preferentially in the temporal hippocampal fissure (asterisks), alveus (filled arrow) and corpus callosum (unfilled arrow). B) Cresyl violet stained image of a section in close proximity to (A). C) Fluorescent image of Evans blue seen preferentially in the alveus and corpus callosum. Chevron shows Evans blue in the perivascular space. D) Cresyl violet stained image of a section in close proximity to (C).

CHAPTER 3
INFLUENCE OF LIMBIC SYSTEM INJURY ON INFUSATE DISTRIBUTIONS IN THE RODENT HIPPOCAMPUS

Introduction

The work shown in Chapter 2 established the local heterogeneity of neurostructural characteristics as a governing feature of CED. The dependence of interstitial flow on normal hippocampal structure suggests pathological changes within the hippocampus would introduce variability in the distributions, especially if myelin integrity or dense cell layers were affected. It is well documented that that SE (Meierkord et al., 1997; Kim et al., 2001; Fabene et al., 2003) and temporal lobe epilepsy (Babb, 1987; Kuzniecky et al., 1987; Bruton, 1988; Bernasconi et al., 2004; Parekh et al., 2010) result in structural changes within the limbic system, yet previous studies investigating the influences of pathology on hippocampal distributions are lacking. Therefore, in an effort to optimize targeted CED delivery into injured regions, this chapter describes the influence of microstructural changes in the hippocampus on the distribution of infusate in a pre-clinical SE-model of chronic limbic epilepsy. Limbic system injury was ranked using MR imaging and then corroborated at a cellular level using immunohistochemical and neurodegeneration markers. MR imaging was used to monitor and measure the distribution of Gd-albumin, and then distributions were compared to the results from control animal infusions described in Chapter 2.

Infusions were performed at acute and chronic points of TLE to illustrate the effect of different pathologies on infusate distributions in the hippocampus. Infusions

---

Excerpts from this chapter have been submitted for publication to Neurotherapeutics.

This work was completed with the help of Dr. Garrett Astary. Dr. Astary helped with the infusions, and performed the MR imaging and image segmentation described in this chapter.

performed 24 hours after an episode of self-sustaining limbic SE translate to a window for prophylactic treatment. Many treatment studies address only chronic time points in TLE, even though structural changes occur progressively from shortly after SE up to the appearance of spontaneous seizures (Parekh et al., 2010). Clinically, about 30% of epilepsies can be linked to an identifiable injury to the brain that triggers the development of the disorder (Manford et al., 1992; Hauser, 1997). Treatment after initial insults have the potential to reduce structural damage, diminish associated behavioral and cognitive impairment, or prevent epileptogenesis (for review see (Pitkanen, 2002a; Sutula, 2002)).

While there is mounting experimental evidence that preventative therapy can be beneficial in positive disease modification (Pitkanen, 2002b; Brandt et al., 2003; Nicoletti et al., 2008; Zafar et al., 2012), clinical evidence is controversial (Willmore, 2005). The failure of clinical trials has been attributed to the use of inappropriate treatment strategies (Pitkanen, 2002a) and pharmacokinetic issues, i.e. the lack of therapeutic levels in the brain after systemic administration (Brandt et al., 2003). The latter has been specifically raised in cases of inconsistent or absent monitoring of therapeutic levels in studies (Liu and Bhardwaj, 2007). This work addresses such concerns through employing CED, which, unlike systemic administration, ensures the application of a clinically relevant dosage and allows for provision of novel treatment strategies. Infusions were also performed at 60 days post-SE, once animals were spontaneously seizing. These infusions translate to the treatment of chronic TLE, and are specifically relevant for one third of patients with epilepsy who are resistant to current AEDs. CED

at this time point can be used to maximize the effectiveness of therapeutic agents by increasing drug concentration at the focus.

Both 24-hours and 60-day time points represent important treatment windows for epilepsy, but exhibit distinct pathologies. The findings from this study add injury-specific evaluations to the collection of principles influencing delivery of macromolecules within the CNS. Information from this study can be applied to improve targeting guidelines for CED, incorporated into computational CED transport models (Sarntinoranont et al., 2006; Kim et al., 2010), and considered in the planning of preventative delivery strategies of novel therapeutic agents.

Methods

Animals

Male Sprague-Dawley rats (Harlan Labs, Indianapolis, IN) weighing 225-250 g on arrival were allowed one week to acclimate to the 12-h light/dark cycle and given food and water ad libitum. All procedures were approved by the University of Florida Animal Care and Use Committee and conducted in accordance with the National Institutes of Health Guide for the Care and Use of Experimental Animals. A flow chart depicting the order of experiments can be seen in Figure 3-1.

Surgical Procedures

Anesthesia was initiated with xylazine (10 mg/kg, SQ) and 4% isoflurane in 1 L/min oxygen. Once animals were securely placed in a Kopf stereotaxic apparatus, anesthesia was maintained at 1.5% isoflurane in 0.4 L/min oxygen. The landmarks bregma and lambda were exposed by a mid-sagittal incision and three 50 μm diameter polyamide-coated tungsten microwire electrodes (Plastics One, Roanoke VA) were implanted for the induction of self-sustaining SE. Two electrodes were implanted into

the right temporal hippocampus [-5.3mm AP, 4.9mm ML, -5.0mm DV] for stimulating and recording, and one was implanted as a reference electrode into the corpus callosum [-3.3mm AP, 4.9mm ML, -2.4mm DV]. A cannula guide was also secured to the skull region above the left septal hippocampus [-3.7mm AP, -2.2mm ML] for the future infusion of contrast agent. Infusion was planned contralateral to electrodes to avoid the confound of electrode implantation on infusate distribution. Four nylon anchoring screws were placed in the skull to allow for maximum support of the headset, which was permanently secured with Cranioplast cement (Plastics One, Roanoke VA). All animals were given one week to recover from the implantation surgery before the stimulation procedure began.

Induction of Self-Sustaining Limbic Status Epilepticus (SE) by Hippocampal Electrical Stimulation

Approximating the evolution of structural changes that result in human epilepsy took precedence for the animal model chosen in this study because changes in cellular structure will undoubtedly affect migration in the interstitium. The self-sustaining SE model replicates essential characteristics of epilepsy as it occurs in humans (See Chapter 1), including the presence of a latent period. To create the model, one week post-electrode implantation, animals (n=28) were electrically stimulated to induce self-sustaining SE, a prolonged seizure lasting 30-90 minutes, as described in (Lothman et al., 1989). Stimulus trains (50 Hz of 1ms biphasic square wave pulses) were delivered for 10s on and 2s off for a total of 78 ± 16 minutes. A modified Racine scale (Racine, 1972; Borowicz et al., 2003) was used to grade the behavioral seizures as follows: grade 0 for no seizure response; grade 1 for immobility, eye closure, ear twitching, twitching of vibrissae, sniffing, facial clonus; grade 2 for head nodding associated with

more severe facial clonus; grade 3 for clonus of one forelimb; grade 3.5 for bilateral forelimb clonus without rearing; grade 4 for bilateral forelimb clonus with rearing; grade 5 for rearing and losing balance. Animals (n=19) that experienced Racine grade 4 or 5 seizures during the hippocampal stimulation and experienced electrographic seizure activity for at least 2 hours post stimulation were included in the study. Animals were continuously recorded with time-locked video-EEG until 24 hours or 60 days post-SE. These inclusion criteria were used to create a comparable injury across animals that would likely lead to the development of spontaneous seizures (Lothman et al., 1989; Bertram and Cornett, 1994; Bertram, 1997; Sanchez et al., 2006; Parekh et al., 2010).

MR Imaging

Twenty-four hours or 60 days post induction of SE, high-resolution T1 and T2-weighted MR imaging was performed to generate a reference for contrast enhancement images (T1) and to visualize morphological changes (T2). Immediately following infusion of Gd-albumin (see next section), high resolution T1-weighted imaging was repeated to visualize distribution profiles of the contrast agent. MR measurements were performed using a Bruker Avance imaging console (Bruker NMR Instruments, Billeria, MA) or Agilent Direct Drive imaging console (Agilent Technologies, Santa Clara, CA, USA) connected to a Magnex Scientific 11.1 T horizontal bore magnet system(Varian, Inc., Magnex Scientific Products, Walnut Creek, CA). A custom-made 130 degree arc, 3.5cm rectangular linear-field surface coil constructed on a 4cm diameter half-cylinder was used for linear transmission and detection of MR signal. High- resolution T1-weighted images, with slices oriented in the coronal direction, were acquired using a spin-echo sequence with a 2.5cm×2.5 cm field-of-view in a matrix of 200×200, recovery time of 1000 ms, echo time of 10ms, 8 averages, 30 slices, 500 µL slice thickness. T2-

weighted data were acquired using a fast spin echo sequence with 30 slices oriented in the coronal direction and a 2.5cm×2.5cm field-of view in a matrix of 208×208, recovery time of 3500ms, RARE factor of 8 and effective echo time of 45 ms.

T2-weighted images (30 coronal slices per brain) were examined and used to classify injury in animals. The high water content of edematous tissue results in prolonged T2 relaxation times and manifests as a hyperintense signal in T2-weighted images. Hyperintense signal was defined as injury in these images and then validated post-mortem (see Immunohistochemistry section). T2-weighted images were scored for injury as follows: 1 = unilateral piriform cortex and/or amygdala damage, 2 = score of 1 plus injury in the septal nuclei, 3 = a score of 2 plus injury in the middle thalamic nuclei, 4 = a score of 3 plus damage in the lateral thalamic nuclei, 5 = a score of 4 plus damage in the ventral subiculum, 6 = bilateral piriform cortex/amygdala damage, septal injury, and damage in the middle and lateral thalamic nuclei. An early indication of the development of spontaneous limbic seizures in this animal model is the presence of edema in the parahippocampal gyrus (Parekh et al., 2010). Because the purpose of this study was to examine injury before or after epileptogenisis, animals imaged at 24 hours post-SE that did not exhibit parahippocampal gyrus were excluded from subsequent analyses.

Infusion of Gd-albumin

Twenty-four hours (n=17) or 60 days (n=2) post induction of SE, animals were infused with 5.0 µL of Gd-albumin (10 mg/mL in PBS solution; MW∼87 kDa,∼35 Gd-DTPA molecules per albumin molecule; R. Brasch Laboratory, University of California, San Francisco, CA), tagged with Evans Blue dye (1 mg dye/50 mg Gd-albumin) into the septal dentate gyrus of the hippocampus [-3.7 AP, -2.2 ML, -3.4 DV]. The infusion was

performed through the previously implanted cannula guide using the same equipment and infusion parameters as described in Chapter 2. Results from experimental animals infused in this study were compared to results from control animals infused under similar conditions (see Chapter 2). The only difference between infusions performed in control animals and those performed in injured animals was a ~30 minute time delay between infusion and MR imaging in control animals. The contribution of diffusion after the end of CED in these animals was estimated in Chapter 2.

Immunohistochemistry

Following the last MR measurement, animals were transcardially perfused with 200 mL saline solution followed by 300 mL of 10% buffered formalin phosphate. Brains were extracted and stored in the formalin solution overnight at 4°C, then equilibrated in 30% sucrose solution for 72 hours. Brains were then sectioned coronally using a cryostat set at 50 µm. Every fifth section in succession was collected for staining with either Fluoro Jade C (FJC), Black Gold II, glial fibrillary acidic protein (GFAP), macrophage activation (CD-68), or Perl stain. GFAP, CD-68, and Perl-stained sections were counterstained with cresyl violet for visualization of cell-bodies.

FJC staining (Schmued et al., 2005) was used to visualize degenerating neurons with a modification by Lee et al (Lee et al., 2011). Mounted tissue sections were first immersed in 1% sodium hydroxide in 80% ethanol for 5 minutes. They were then rinsed for 20 minutes in 70% ethanol, followed by 2 minutes in distilled water, and then incubated in 0.02% potassium permanganate solution for 3 minutes. Slides were then rinsed for 2 minutes in distilled water and transferred for 15 minutes into a 0.0002% solution of Fluoro-Jade C (Histo-Chem Inc., Jefferson, AR) dissolved in a 0.1% acetic acid vehicle.Sections were stained for myelin using Black-Gold II (Schmued et al.,

2008). Mounted slides were incubated in a 0.3% Black-Gold II solution (Histo-Chem Inc., Jefferson, AR) at 60°C for 12-15 minutes, rinsed, then transferred to a 1% sodium thiosulfate solution for three minutes.

For assessment of micro- and astrogliosis, free-floating sections were incubated in 10mM citrate buffer, pH 9.0, for 25 minutes at 80°C for antigen retrieval. After a brief wash, they were stained for microglial activation and astrocytosis overnight using primary monoclonal antibodies against CD-68 (AbD Serotec; Raleigh, NC) or GFAP (G-A-5, Sigma Chemicals Co.; St. Louis, MO), respectively, at a concentration of 1:400. Sections were washed and incubated overnight in 1:10,000 biotinylated anti-mouse immunoglobulin G, reacted with a 1:1,000 Extravidin peroxidase solution for 2 hours, then visualized with 0.05% 3,3'-diaminobenzidine (DAB) in 0.0012% hydrogen peroxide in PBS.

Image Segmentation and Statistical Analysis

Final distribution volumes of Gd-albumin were analyzed by performing semi-automatic image segmentation on the T1-weighted coronal images using routines written in MATLAB® (The MathWorks® Inc., Natick, MA, USA) with the following specific threshold criteria. Voxels were included in the infusion volume if their signal intensity was higher than at least 6 standard deviations of the noise in the corresponding region contralateral to the site of infusion (control regions containing no Gd-albumin). The segmentation output of the MATLAB® routine was refined using the ITK-SNAP open-source medical image segmentation tool (Yushkevich et al., 2006). Dynamic and final distribution volumes in the septal and temporal hippocampus were calculated by counting the number of voxels included in each segmented region and multiplying by the volume of a single voxel.

Total hippocampal volumes were calculated by manually segmenting the T2 weighted pre-infusion images in ITK-SNAP. The borders of the hippocampus (e.g. corpus callosum, thalamus) were determined by white matter/gray matter contrast in the T2 weighted images, anatomical landmarks such as the velum interpositum and by referring to a rat brain atlas (Paxinos, 1998).

Distribution volumes of 24-hour animals were compared to injury ratings using Kendall's rank correlation. This non-parametric test is used for ordinal data and is generally considered to be equivalent to Spearman's rank correlation. The Kendall's tau correlation coefficient was chosen over Spearman's rho because tau is a better estimate of the corresponding population parameter and has more accurate p values in small sample sizes (Gibbons, 1993). Furthermore, Spearman's is difficult to interpret as a measure of the strength of a relationship and does not have a meaningful operational interpretation (Bland, 1995). The significance of differences in volume of distributions between control animals, 60 day animals, and injury classifications of 24 day animals was calculated by analysis of variance (ANOVA). Post hoc testing for individual classification differences was done with Newman-Keuls test. All tests were two-tailed; a $p<0.05$ was considered significant.

Results

SE-Induced Injury

Animals (n=19) were electrically stimulated in the temporal hippocampus to experience one episode of SE. T2-weighted images (Figure 3-2) were acquired 24 hours (n=17) or 60 days (n=2) post induction of SE to reveal edema within regions of the limbic circuitry. An early indication of the development of spontaneous limbic seizures in this animal model is the presence of edema in the parahippocampal gyrus

(Parekh et al., 2010). One animal did not exhibit edema in the parahippocampal gyrus and was not included in the subsequent injury analyses. Of the remaining 24-hour group, 3 of 16 animals exhibited edema in the bilateral parahippocampal gyrus (Figure 3-2P-R) and 13 of 16 animals exhibited unilateral edema (Figure 3-2C-O). Out of the 13 animals that exhibited unilateral edema, injury was ipsilateral to the stimulating electrode in 3 animals (Figure 3-2D,I,L), and contralateral in 10 animals (Figure 3-2C,E-H,J-K,N-O). Table 3-1 presents the T2 injury index classification of each animal at 24 hours post-SE. Of the 2 animals that were imaged 60 days post-SE (Figure 3-2S-T), only one revealed contralateral parahippocampus edema (Figure 3-2T) and enlarged ventricles in MR imaging. Neither of the animals exhibited edema in any other limbic structures.

Volumes of Distribution of Gd-albumin and Changes in Hippocampal Volume

Increasing classifications of injury were correlated with volumes of distribution of Gd-albumin in 24-hour animals (tau = 0.51, p=0.006), which averaged 21.2 ± 3.6 µL for animals classified as Class 1-2, 26.8 ± 5.4 µL for animals classified as 3-4, and 33.2 ± 6.0 µL for animals classified 5-6 (Figure 3-3). Distributions in animals with severe injury (Class 5 and above) were significantly increased as compared to previously measured control animals in Chapter 2 (p=0.018; average 23.4 µL ± 1.8 µL), and as compared to 60 day TLE animals (p=0.002, average 18.5 ± 2.1 µL). This increase may be underestimated, as distribution volume of control animals includes ~30 extra minutes of diffusion that occurred in the time delay between infusion and MR imaging. The contribution of diffusion was estimated in Chapter 2 to increase control distribution volumes up to 40% (2-3 voxels, 0.250-0.375 mm). Therefore, the relative increase of distribution volumes in injured animals may actually be larger. No significant differences

were found between animals presenting with ipsilateral versus contralateral parahippocampal injury.

Total hippocampal volumes of 24 hour animals pre-infusion were measured and compared to volumes of distribution post-infusion. These volumes were not significantly different between injury classes (Class 1-2:18.4 ± 1.0, Class 3-4:18.6 ± 1.6, Class 5-6:19.2 ± 1.7), indicating that in this study, the larger infusion volumes seen in injured animals cannot be solely explained by differences in hippocampal size.

Characteristics of Gd-albumin Distribution

While volumes of distribution correlated with magnitude of injury (Figure 3-3), the pattern of infusate spread was consistent between animals exhibiting various levels of injury and at different time points (Figure 3-4). All infusions showed clear demarcation within the hippocampus, with very minimal backflow only along the cannula tract in 9/19 (47%) animals. Six animals (32%) showed limited backflow within the corpus callosum overlying the hippocampal infusion site, and 4 animals (21%) exhibited no backflow at all. As described in control animals (see Chapter 2), spread of the contrast agent in experimental animals was seen in the dentate gyrus, CA3, CA2, CA1, and subiculum of the hippocampus. Additionally, both the dentate granule cell layer and pyramidal cell layers of CA3-CA1 and subiculum were clearly distinguishable from the surrounding hyperintense subfields, indicating poor contrast agent penetration. This was especially salient in the CA3 subregion in 8 animals (42%), where infusate coverage tapered at stratum pyramidale, not quite reaching stratum oriens (Figure 3-4B,F,G,K,L,R-T). In 4 animals (21%), infusate filled all layers of the CA3 subregion and also penetrated the fimbria (Figure 3-4I-J,M,P). As in controls, infusate did not extend to the contralateral hippocampus or any other subcortical structures in any animals; however, enhancement

was observed as hyperintensity in T1 images within extraventricular regions surrounding the septal and temporal hippocampus. Twelve animals (63%) exhibited leakage into the velum interpositum of the septal hippocampus, and 14 animals (74%) exhibited leakage into the midbrain cisterns of the temporal hippocampus, suggesting a portion of the contrast agent distribution was not accounted for within the hippocampal distribution volumes. Furthermore, 12 animals (63%) also exhibited leakage into the lateral ventricle ipsilateral to the infusion site.

Histology 24 Hours Post-SE

MR-visualized injury was validated and characterized using histological assessments of CNS injury. For animals infused 24 hours post-SE, injury was visualized in several limbic regions. Within the hippocampus proper (Figure 3- 5), neurodegeneration was observed via FJC staining in the CA3/CA2 subfield of all rats and in the hilus of rats with more severe injury (10/17 animals, Class 3-6). Positive FJC staining was not seen in the hippocampus of animals in injury Class 0-1 (compare Figure 3-5D,F). A minority (5/17) of animals in more severely injured classes (Class 4-6) also exhibited positive FJC staining in hippocampal subfield CA1. Activated microglia were detected by expression of CD68 (Figure 3-5G-I, arrows) in the CA3 of 10/17 rats encompassing injury Classes 2-6. Only a minority of animals exhibited activated microglia in the CA1 and hilus (5 rats in Classes 2-6 and 4/17 rats in Class 4-6, respectively). CD68-positive staining was not detected in animals of Class 0-1 (compare Figure 3-5G,I). GFAP staining was used to visualize the enlarged soma and processes typical of reactive astrocytes (Figure 3-5J-L, arrows). Hypertrophic astrocytes were seen in the hilus (Figure 3-5K, arrows) of the majority of rats (14/17 animals, Class 2-6) and

in the CA3 of 5 rats (Class 2-6). Activated astrocytes were only seen in the CA1 of 1 rat in Class 6, the most severe injury class.

All hyperintense regions identified in T2-weighted imaging were also immunostained for CNS injury markers. Hyperintensity observed in the parahippocampal gyrus (Figure 3-6) during in vivo T2-weighted imaging corresponded to fluid-filled cavities (Figure 3-6, asterisks), myelin degradation (Figure 3-6A-C), neuronal degeneration (Figure 3-6D-F), macrophage activation (Figure 3-6G-I), and astrogliosis (Figure 3-6J-L) 24 hours post-SE. Injury in the ventral subiculum (Figure 3-7), which resulted in a classification of Class 5 or above, resulted in considerable degeneration of myelin (compare Figure 3-7A,B) and neurons, as measured by FJC staining (compare Figure 3-7C,D) and cell layer integrity in cresyl violet staining (compare Figure 3-7E,F and G,H). Thalamic injury (Figure 3- 8) did not consist of notable myelin degradation (Figure 3-8A), but did encompass neuronal degeneration (Figure 3-8B, arrows) and microglia activation (Figure 3-8C, arrows). Activated astrocytes were seen in the medial habenular nucleus (Figure 3-8D, arrows).

No obvious difference was observed in the hippocampi of rats that exhibited ipsilateral versus contralateral edema in the parahippocampal gyrus. Animals in higher classes of injury (4 and above) exhibited increased activation of FJC, CD68, and GFAP in the CA1 subfield, and increased activation of CD68 in the hilus. All animals exhibited injury near the electrode stimulation site at the temporal hippocampus.

Histology 60 Days Post-SE

Histological analysis of 60-day animals revealed much less injury than acutely-injured animals. In one animal (Figure 3-9), no positive staining of neurodegeneration, microglia activation, or myelin degradation was seen in the hippocampus (red boxes),

thalamus (green boxes) or parahippocampus (blue boxes). Astrocytosis was visible in the hippocampus, but not in other regions. The other animal (Figure 3-10) exhibited slight microglia activation and substantial astrocyte activation in the hippocampus (red boxes) and thalamus (green boxes), but no neurodegeneration. Cavitation, astrocytosis, microgliosis, neurodegeneration, and myelin degradation were all seen in the parahippocampus of this animal (blue boxes).

Discussion

This study investigated the effect of injury at different time points on CED contrast-agent distribution profiles and volumes in the rat septal hippocampus. Distribution of Gd-albumin was visualized with high-resolution MR imaging, then volume analysis was performed with segmentation. Injury was rated based on edema visualized with T2-weighted MR images, and characterized with staining against neuronal degeneration, myelin degradation, astrocytosis, and macrophage activation.

The main finding in this study is that the volume of infusate distribution is increased in animals with more severe acute injury relative to mildly-injured animals, aged-matched controls, and chronically epileptic animals. In normal hippocampi, CED performed under similar infusion conditions resulted in distribution volumes roughly 5 times greater than the volume infused (see Chapter 2). This spread corresponds to an estimated brain tissue porosity of 0.2 (Mazel et al., 1998; Sykova and Nicholson, 2008), which assumes isotropic porous medium and no CSF leaks. The volumes of distribution in mildly injured animals at 24 hours (Class 1-4) in this study are similar to those measured in control animals (Class 0). However, volumes are significantly larger in animals that presented with a more severe CNS injury 24 hours post-SE, even with the presence of CSF leakage. This effect was not present after 60 days; implying injury may

confer measurable effects on distribution volumes via changes in the extracellular volume fraction.

Acute SE-Induced injury

Following brain injury, a cascade of pathological events evolves over minutes, days, and weeks. Severity of CNS injury was classified in T2-weighted MR images and identified with several histological stains. Although stimulation was always applied to the right hippocampus, injury was observed on both sides of the brain. At 24 hours post-SE, degeneration of neurons and myelin, in addition to activation of microglia and astrocytes was detected in the hippocampus, parahippocampal gyrus, thalamus, and septal nuclei. Injury in these areas is consistent with other histological reports at acute time points ranging from 8 to 48 hours. Damage has been reported in the piriform and amygdalar cortices after administration of pilocarpine (Wall et al., 2000; Nairismagi et al., 2006), kainate (Nakasu et al., 1995; Brandt et al., 2003), angular bundle stimulation (Gorter et al., 2003), and rostral forebrain stimulation (Handforth and Treiman, 1994). Damage has been reported in the CA1 and CA3 after administration of pilocarpine (Nicoletti et al., 2008), kainate (Brandt et al., 2003; Hsu et al., 2007), and rostral forebrain stimulation (Handforth and Treiman, 1994). Injury in the entorhinal cortex is commonly reported after angular bundle stimulation (Gorter et al., 2003), SSLSE, kainate, and pilocarpine models (Du et al., 1995). Midline thalamic nuclei were affected after rostral forebrain (Handforth and Treiman, 1994; Brandt et al., 2003) and angular bundle stimulation (Gorter et al., 2003). In addition, as in this study, the work by Brandt et al. (Brandt et al., 2003) and Gorter et al. (Gorter et al., 2003) report more extensive damage associated with lateral thalamic nuclei.

Injury and Final Infusate Distribution Volume

SE is a major risk factor for the development of chronic epilepsy in both humans (Sloviter, 1999) and animal models (Lothman et al., 1990; Cavalheiro, 1995; Hellier et al., 1998). Both acute and chronic time points present opportunities for treatment.

The pathological states observed in this and other studies at acute time points include morphological changes, such as neuronal death, glial cell loss or proliferation, glial swelling, production of damaging metabolites, inflammation, edema, demyelination, and loss of ionic, pH, and amino acid homeostasis. They may also be accompanied by substantial changes in ECS ionic composition (Sykova, 1983) and various changes in ECS diffusion parameters (Sykova, 1983; Sykova et al., 1994; Sykova, 1997a; Sykova et al., 1998; Sykova and Nicholson, 2008), suggesting reduction of the ECS. In fact, ECS volume shrinkage is likely a compensation mechanism for acute neuronal and glial swelling (Sykova, 1997a). The presence of cellular debris and inflammatory markers paired with ECS changes increases the tortuosity, or hindrance to diffusion, within the ECS. Geometrically, tortuosity is quantified as degree of curvature and complexity of the curve. Biologically, tortuosity is quantified as the ratio of the diffusivity in free space to that in the brain. Tortuosity in both applications changes with edema and neuropil remodeling. This has been documented in several models of brain injury, including cortical stab wounds (Vorisek et al., 2002), neural tissue grafts (Sykova et al., 1999b), and hypoxia (Sykova et al., 1994), where the ECS volume fraction in rat cortex was specifically measured to decrease by 80% and was accompanied by an increase in tortuosity. Hypertrophic astrocytes, which have been observed here and in many other studies, were postulated to be the cause. Hence, an acute insult resulting in cellular debris and/or the swelling of cells and fine glial processes would increase intercellular

tortuosity, affect the size of the intercellular channels, and change diffusional characteristics. Accordingly, the consequence of smaller intercellular channels would be a larger volume of Gd-albumin distribution in rats that experienced a greater degree of injury.

On the other hand, the microstructural injury present at chronic time points (weeks-years) has different characteristics and perhaps opposite effects on infusate distribution. A longitudinal study (Parekh et al., 2010) has shed light on the progressive changes occurring during epileptogenesis in the SE animal model. At acute phases, MR measurements (decreased average diffusivity (AD) and T2) in the hippocampi suggested the presence of cytotoxic edema and ongoing neurodegeneration that was confirmed with histology. At the onset of spontaneous seizures, MR measurements (increase in AD and T2) are indicative of vasogenic edema, and observed histologically as ongoing degeneration, and myelin degradation. Increased FA in the dentate gyrus suggested mossy fiber sprouting, which was confirmed with Timm's staining. Chronic thalamic damage was also seen that corresponded to microgliosis. Like the SE animal model, human mesial temporal lobe epilepsy is also commonly associated with hippocampal pathology with varying degrees of regional neuronal loss and gliosis. Additionally, pathological changes in the human amygdala (Hudson et al., 1993), entorhinal cortex (Du et al., 1993), and thalamus (Margerison and Corsellis, 1966; Bruton, 1988) have often been reported. Histological evaluation of biopsy specimens from chronic epilepsy reveal a majority of TLE patients have the hippocampal atrophy and scarring typical of Ammon's horn sclerosis, in addition to other abnormalities, such

as seizure-associated postnatal neurogenesis and mossy fiber sprouting (Thom et al., 2005).

Sclerotic hippocampi in chronic epilepsy have even been associated with increased ECS (Wieshmann et al., 1999), a development that may explain the change in distribution volumes compared to acutely-injured hippocampi. As opposed to acute damage, infusate spread in chronic TLE hippocampi was found to be decreased, perhaps due to enlarged interstitial spaces. While this study only observed two animals at chronic time points, histological analysis revealed less microglia activation and no neurodegeneration in the hippocampus. The more injured animal also exhibited enlarged ventricles, which may result in more drainage of the infusate and contribute to the decrease in infusate distribution volume.

Injury and Pattern of Infusate Distribution

The data in this study suggest acute SE-induced injury is significantly correlated with infusate distribution volumes. Interestingly, patterns of distribution within the septal hippocampus were consistent with those in control animals. Largely underestimated, the biophysical properties of the local tissue architecture at the infusion site are a critical consideration for planning the coverage of therapeutic agents in both normal and injured areas of the brain. Even in normal rat brains, measured tortuosity in vivo was found to be higher in regions including a dense cell layer, such as stratum pyramidale, as compared to stratum radiatum, which contains mostly fibers (Sykova et al., 1998). Isotropic, dense gray matter regions will affect CED distribution differently than directional white matter regions. Anisotropic regions such as axonal bundles often exhibit increased infusate transport along fiber directions (Vorisek and Sykova, 1997), while laminar structures such as the hippocampus may cause more widespread

dispersion. Additionally, ventricles and perivascular spaces can act as mass sinks in which infusate may pool or be directed towards subarachnoid spaces (Neuwelt, 2004; Astary et al., 2010). Gd-albumin access to fluid-filled spaces was observed in this study, where a majority of animals exhibited Gd-albumin leakage into the lateral ventricle, the velum interpositum, and the midbrain cisterns.

Other Factors Affecting Final Infusate Distribution

In this study, the severity of injury was significantly correlated with increases in measured distribution volumes. It is important to note that the volume differences between controls and injured animals may be underestimated because the observed distribution profiles in control animals include the effects of CED and diffusion during a ~30 minute time delay between the final infusion and MR imaging. The analysis of influence of hippocampal tissue architecture on CED distributions and method of image segmentation for determining final distribution volumes are still valid since both convective and diffusive extracellular transport are influenced by tissue boundaries and preferential transport routes.

There are also several other factors (discussed in more detail in the subsection “CED” of Chapter 1) that may add to the remaining variability in the final distribution of infusate (for review, see (Krauze et al., 2006)). Firstly, infusion pump parameters, such as flow rate and duration of infusion, will influence interstitial transport (Bobo et al., 1994). However, these factors were kept constant across animals, and thus were deemed to have a negligible effect on inter-subject variability. Secondly, distribution will vary based on properties of the infusate itself, including size, shape, viscosity, solubility, binding characteristics, concentration, and rate of efflux from the brain. Under certain infusion conditions, highly viscous solutes display greatly increased volumes of

distribution (Mardor et al., 2009) and water-soluble, non-transported compounds display slower efflux rates (Groothuis et al., 2007). Since the same compound was used for all experiments in this study, the physico-chemical properties of Gd-albumin do not explain the inter-subject variability. However, it should be noted that these properties pose a significant influence on the rates and routes of delivery and efflux of various solutes.

A third key factor that introduces variability in final distribution is backflow, which results in the spread of infusion into unintended regions. This issue can be addressed with preventive cannula designs (Morrison et al., 1999; Guarnieri et al., 2005; Ivanchenko and Ivanchenko, 2011), but remains an important variable in drug delivery studies. In this study, roughly half of the infusions exhibited very minimal backflow only along the cannula tract. About a quarter of the infusions resulted in no backflow, and another quarter had backflow along the overlying corpus callosum. When compared to infusions with no backflow, the distribution volumes of infusions exhibiting backflow were not significantly affected ($p=0.18$).

Finally, infusion site is a key factor in the final distribution of infusate due to the influence of normal local structural differences in CNS anatomy (see Chapter 2). Infusions in this study were targeted to the same stereotaxic coordinates in each animal, but there are small (≤ 1mm) differences in the exact cannula placement of each experiment due to inter-animal variability. The infusion site variability of the majority of animals in this study was very minimal; however, two Class 4 animals had infusion sites that were too lateral in the hippocampus. The resulting infusion coverage in these animals failed to cover the medial aspect of the CA1 subregion or the dorsal subiculum, resulting in artificially low distribution volumes that fell within the average of Class 1-2

animals. This type of infusion site variability can be avoided with careful MR-guided cannula insertion, but it underlines the effect of local tissue variability on the distribution of infusate.

Conclusions

This is the first study to observe CED delivery into the hippocampus of a pre-clinical rodent model of chronic epilepsy. This type of delivery bypasses systemic circulation and opens the possibility of therapy to a wide variety of potential compounds, since it does not require passage through the BBB or consideration of systemic safety. Several studies have described CED in normal hippocampi in different species, but understanding the influence of structural changes on extracellular transport in injured regions is critical for planning drug delivery studies. Historically, CNS injury has been associated with changes in the ECS, swelling of cellular elements, and overall increased tortuosity within the interstitial space. This was observed here as neuronal degeneration, myelin degradation, and macro- and microglia activation as an acute response to SE. Such changes can affect diffusion parameters and in this study, were found to be correlated with the final volume distribution of Gd-albumin. Recovery of acute changes at chronic time points resulted in significantly reduced infusion volumes as well. These results illustrate the importance of biophysical influences on CED and should be incorporated in the planning of future studies tracking therapeutic agents. Chapter 4 will describe two examples of CED of therapeutic carriers.

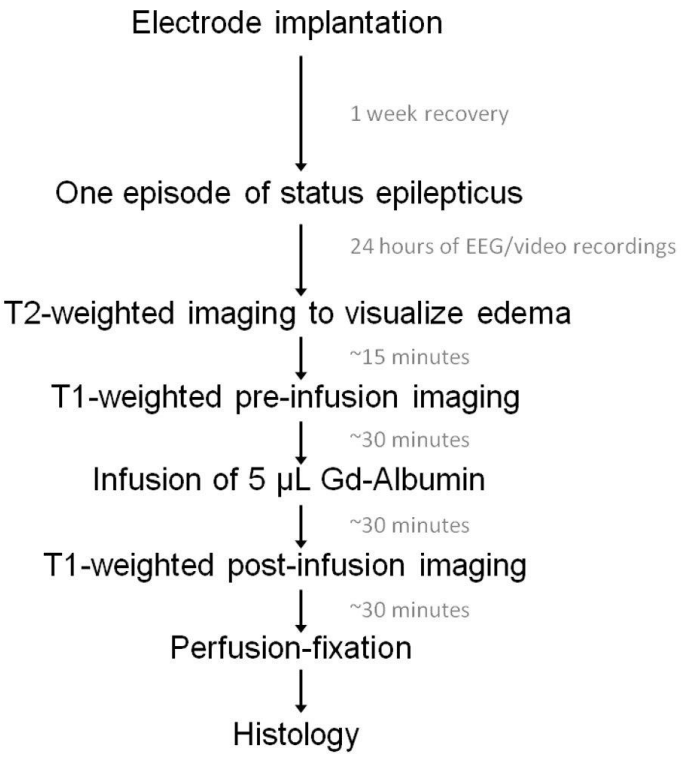

Figure 3-1. Experimental protocol flow chart

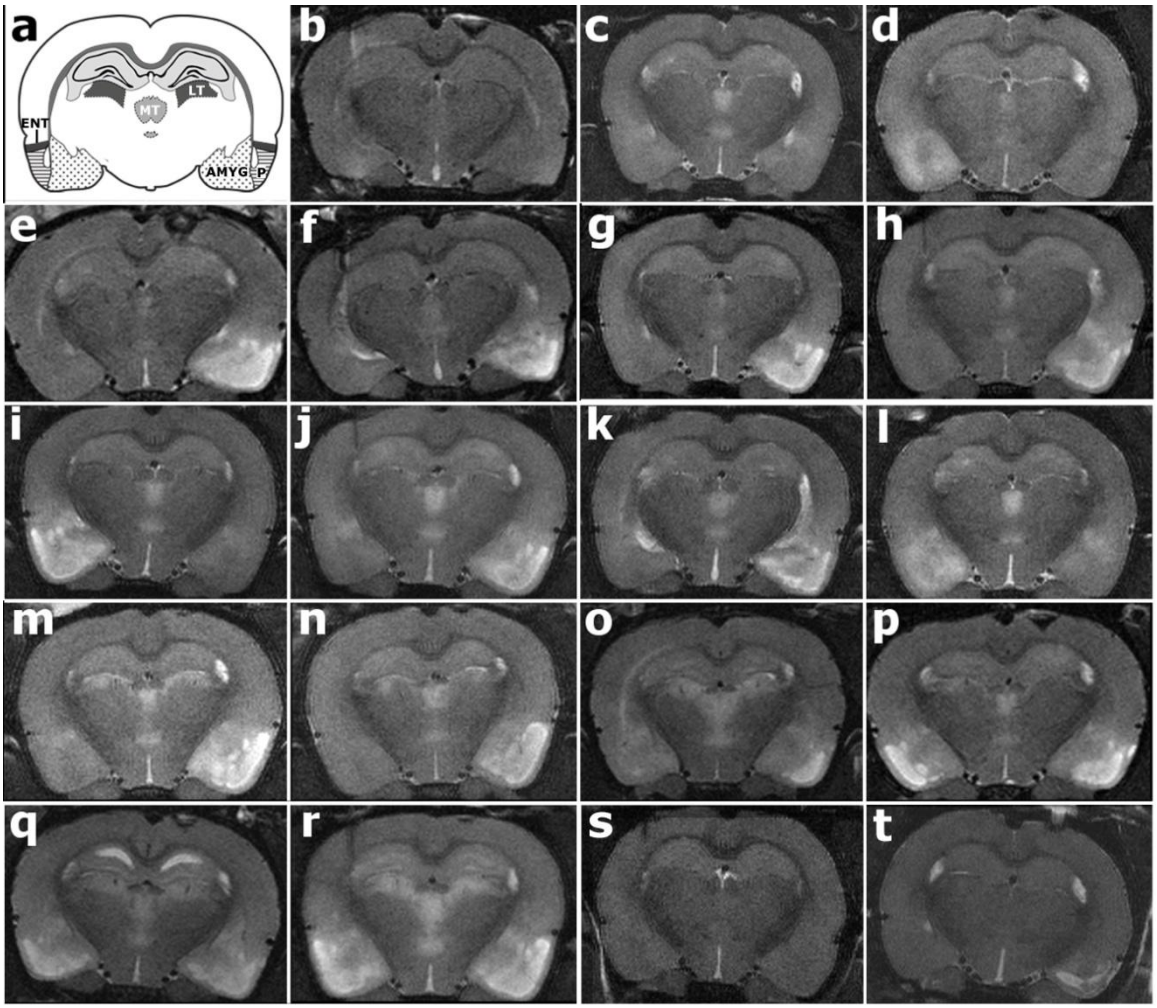

Figure 3-2. T2-weighted coronal images of 19 different rodent brains acquired post induction of SE reveal injury within regions of the limbic circuitry. Hyperintense regions signify areas of injury. A) Schematic of affected structures adapted from (Paxinos, 1998). B-R) MR images of injury induced in 17 different animals 24 hours post-SE. Structures most affected were the CA3 hippocampal subfield, ventral subiculum, piriform cortex (P), entorhinal cortex (ENT), amygdalar nuclei (AMYG), middle thalamic nuclei (MT), and laterodorsal/lateroposterior thalamic nuclei (LT). S-T) MR images of injury induced in two animals 60 days post-SE. Electrode implantation is on the left side of each image.

Table 3-1. Index of injury classification 24 hours post-SE epilepticus. Injured regions were identified using T2-weighted coronal images obtained *in vivo* prior to CED infusions.

Injury class	Injury description	Number of animals	Percentage of animals
Class1	Unilateral edema in the piriform cortex and amygdalar nuclei	2	12.5%
Class 2	Class 1 plus edema in septal nuclei	1	6.25%
Class 3	Class 2 plus edema in the middle thalamic nuclei	2	12.5%
Class 4	Class 3 plus edema in the laterodorsal/lateroposterior thalamic nuclei	5	31.25%
Class 5	Class 4 plus edema in the ventral subiculum	3	18.75%
Class 6	Class 5 plus bilateral edema in the piriform cortex and amygdalar nuclei	3	18.75%

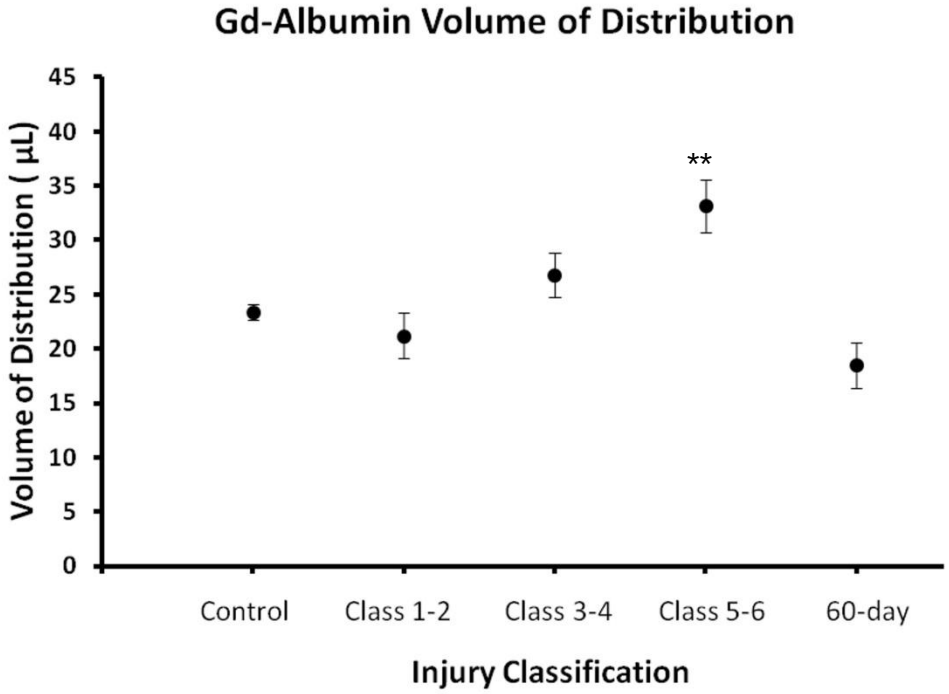

Figure 3-3. Increasing classifications of injury were correlated with volumes of distribution in 24-hour animals (tau = 0.51, p=0.006), which averaged 21.2 ± 3.6 µL for animals classified as Class 1-2, 26.8 ± 5.4 µL for animals classified as 3-4, and 33.2 ± 6.0 µL for animals classified 5-6. Distributions in animals Class 5 and above were significantly increased as compared to previously measured control animals (Class 0), which averaged 23.4 ± 1.8 µL (p=0.018, see Chapter 2)) and to animals infused 60 days post-SE (average 18.48 ± 2.1 µL, p=0.002).

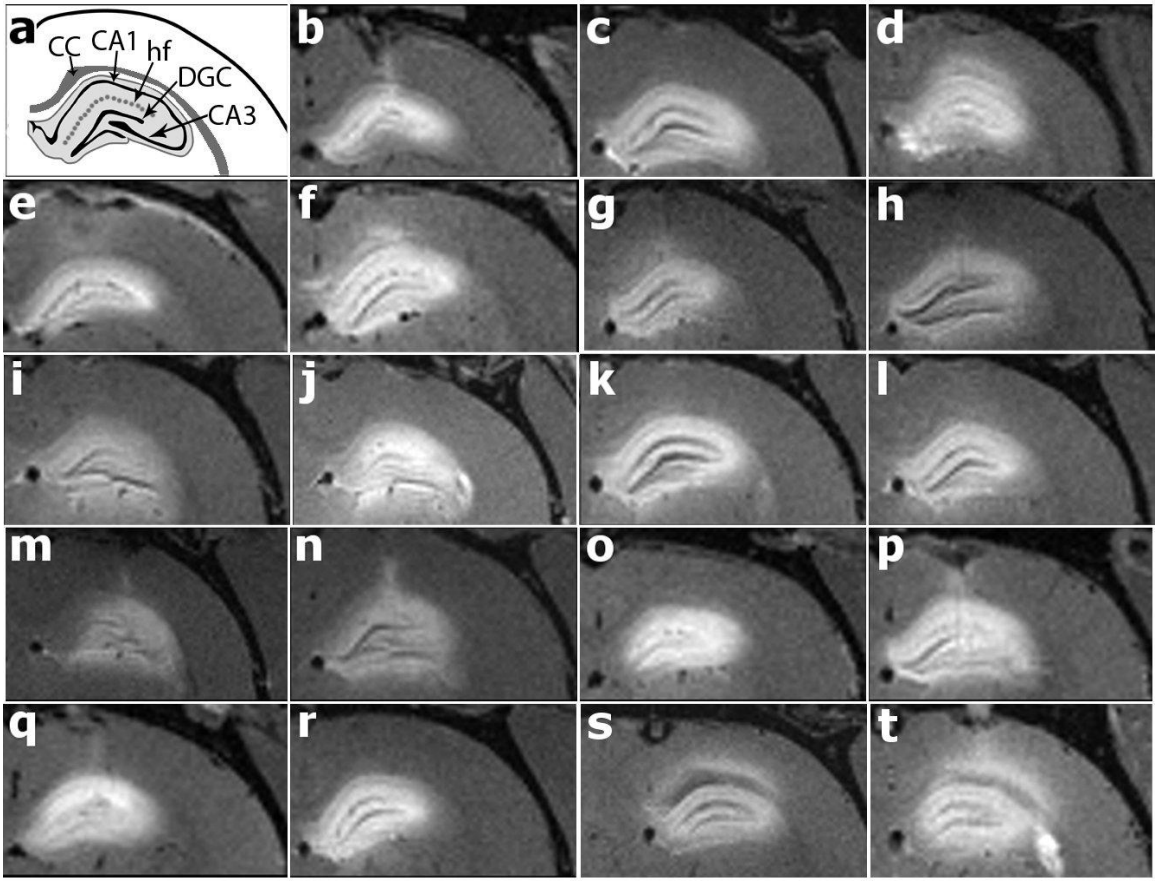

Figure 3-4. High resolution T1-weighted images of Gd-albumin infusions into the septal hippocampus of 19 different rodent brains post-SE. A) Schematic of key structures in the septal hippocampus adapted from (Paxinos, 1998). B-R) MR images of contrast agent distributions in the septal hippocampus 24 hours post-SE. S-T) Contrast agent distributions in the hippocampus of 2 animals 60 days post-SE. Hyperintense regions are voxels containing Gd-albumin. Distribution patterns contour along hippocampal circuitry with minimal backflow or exposure to extra-hippocampal regions. CC = Corpus callusom; CA1 = CA1 pyramidal cell layer; hf=hippocampal fissure; DGC = Dentate granule cell layer; CA3 = CA3 pyramidal cell layer.

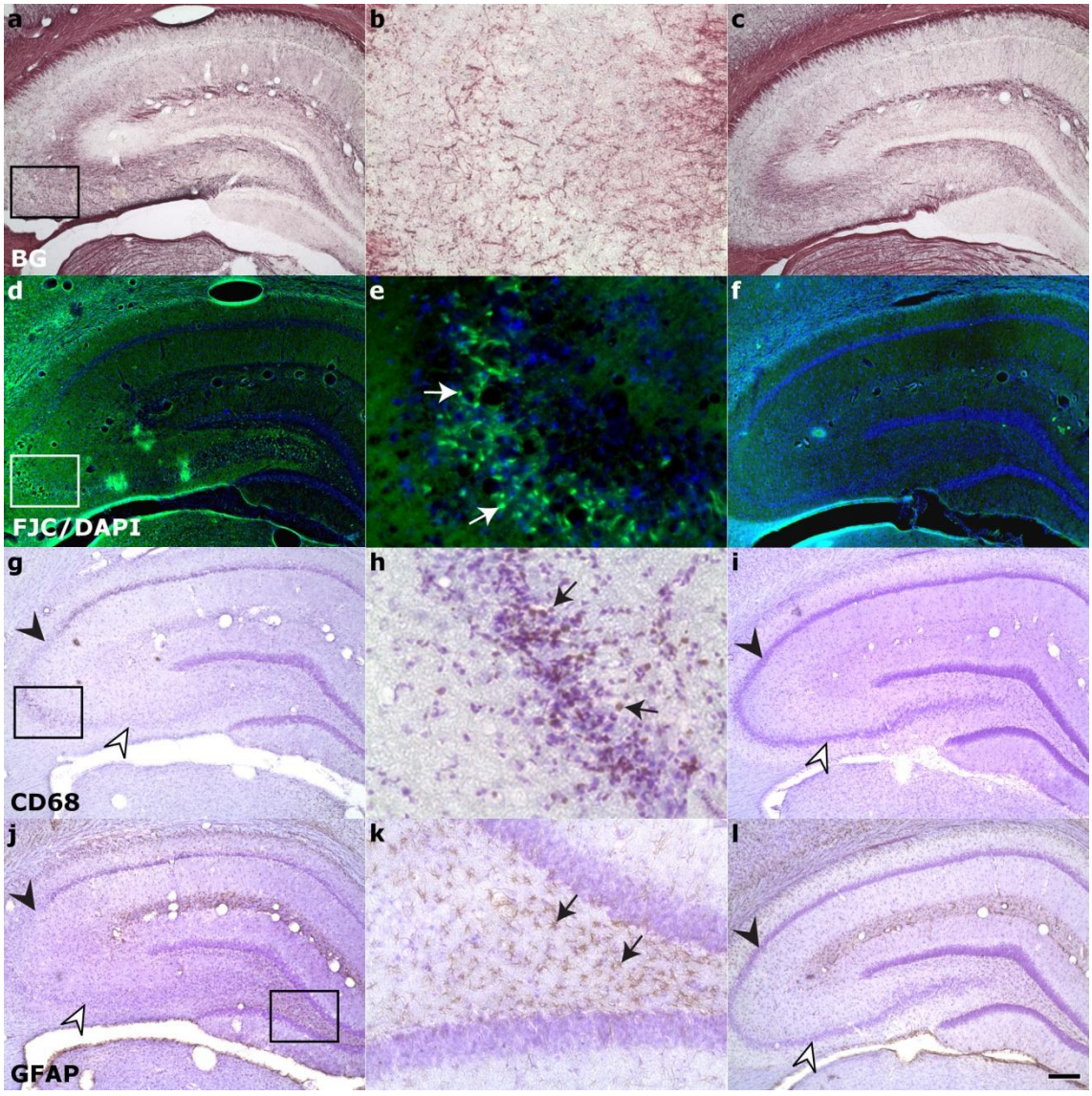

Figure 3-5. Characterization of hippocampal damage 24 hours post-SE. Representative stained sections of affected hippocampi (left column:low magnification, middle column:high magnification) are compared to unaffected hippocampi (right column) for A-C) myelin degradation, D-F) neuronal degeneration, G-I) macrophage activation, and J-L) astrocytosis. Higher magnification of boxed areas show ongoing neurodegeneration within CA3 (E, arrows) that corresponds with macrophage activation (H, arrows). Cell loss is corroborated through loss of cresyl violet staining in CA2 (closed arrowheads, compare G,I and J,L) and CA3 (open arrowheads, compare G,I and J,L). Astrocytosis was seen predominantly in the hilus (K, arrows), while myelin degradation was not appreciably different within the hippocampus (compare A,C). BG = Black-gold II; FJC/DAPI = Flouro-jade C with 4',6-diamidino-2-phenylindole nuclear counterstain; GFAP = Glial fibrillary acidic protein; CD68 = Cluster of Differentiation 68; CV = Cresyl violet. Scale bar is 50µm for b,e,h,k; 200µm for all other.

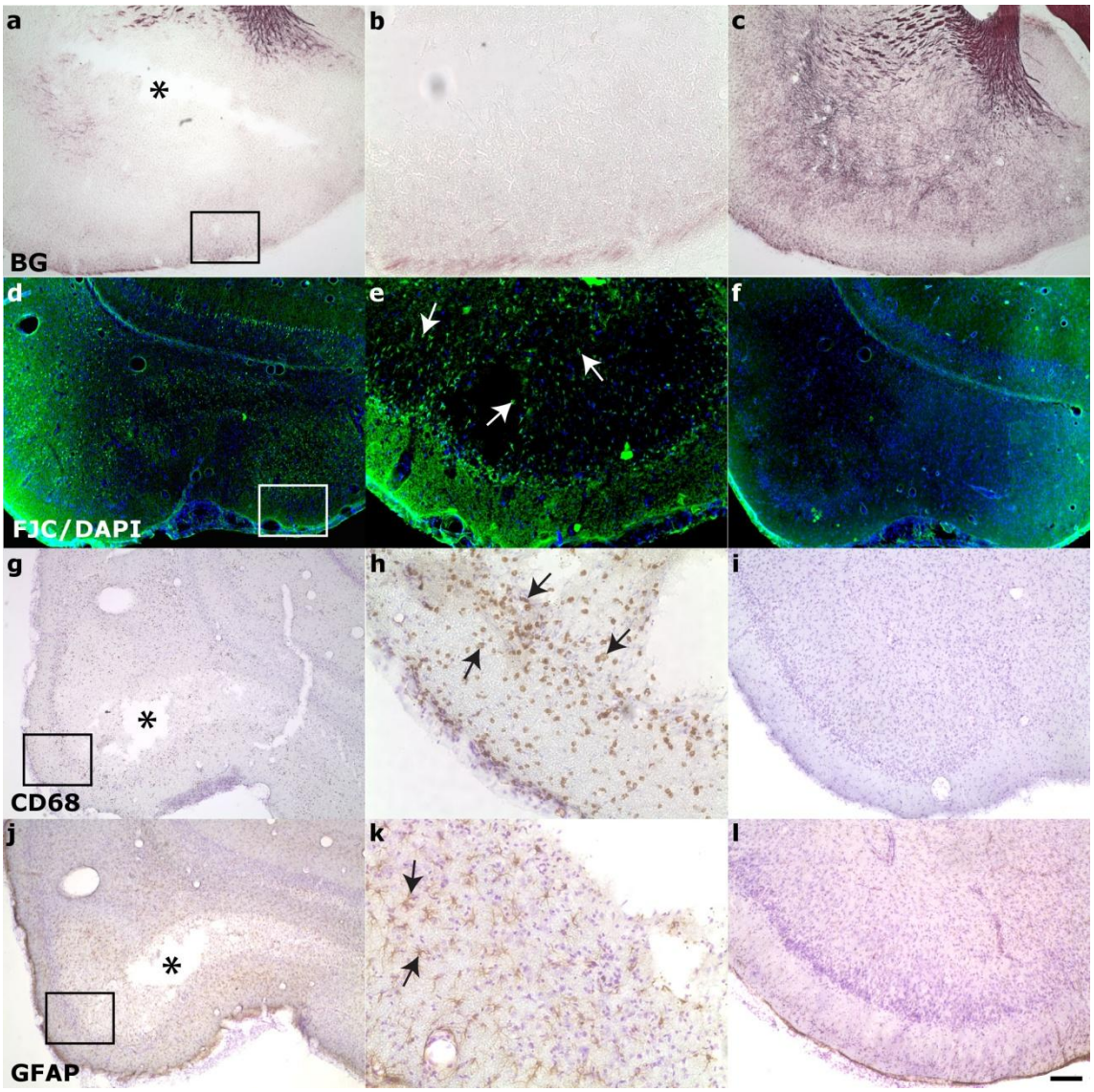

Figure 3-6. Characterization of parahippocampal damage 24 hours post-SE. Hyperintense regions observed in the parahippocampal gyrus during in vivo T2-weighted imaging corresponded to A-C) myelin degradation, D-F) neuronal degeneration, G-I) macrophage activation, J-L) astrocytosis, and A,G,J) cavitation. Asterisks denote cavitation. Compare injured (left column:low magnification, middle column:high magnification) to uninjured (right column). BG = Black-gold II; FJC/DAPI = Flouro-jade C with 4',6-diamidino-2-phenylindole nuclear counterstain; GFAP = Glial fibrillary acidic protein; CD68 = Cluster of Differentiation 68; CV = Cresyl violet. Scale bar is 50µm for b,e,h,k; 200µm for all other images.

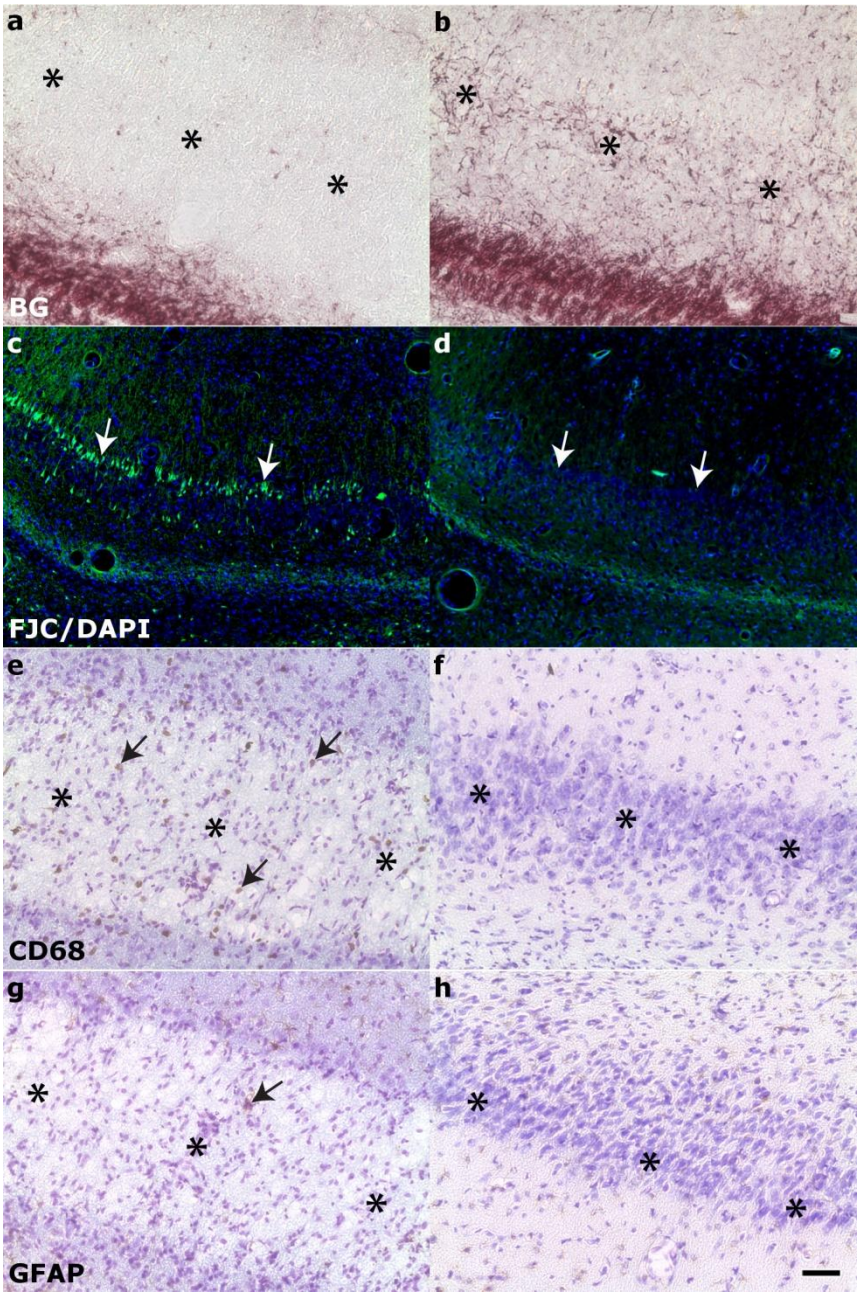

Figure 3-7. Damage to the ventral subiculum was seen in 6/17 rats 24 hours post-SE. Affected (left column) is compared to unaffected hippocampi (right column). Injury in the ventral subiculum resulted in considerable A-B) myelin degradation, asterisks, and C-D) ongoing neuronal degeneration of the pyramidal cell layer, white arrows. E-H) Cresyl violet staining reveals significant cell layer degradation, asterisks. E-F) activated microglia, black arrows, were also seen in the ventral subiculum, while G-H) total activated astrocytes were minimal, black arrows. BG = Black-gold II; FJC/DAPI = Flouro-jade C with 4',6-diamidino-2-phenylindole nuclear counterstain; GFAP = Glial fibrillary acidic protein, CD68 = Cluster of Differentiation 68; CV = Cresyl violet. Scale bar is 50µm.

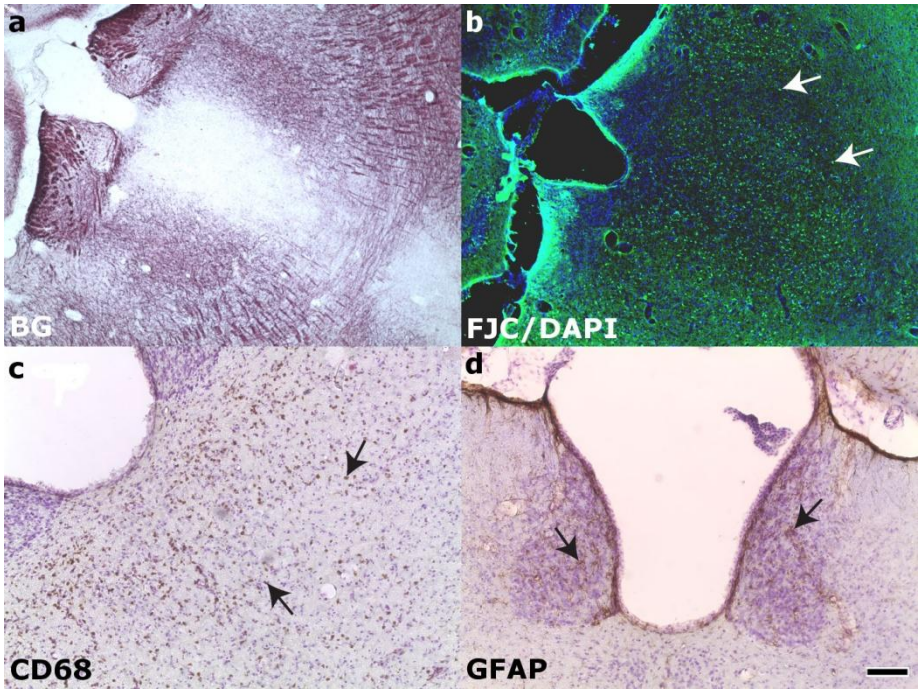

Figure 3-8. Characterization of thalamic injury 24 hours post-SE. A) myelin staining did not show notable fiber degradation. B) ongoing neuronal degeneration and C) macrophage activation within middle thalamic nuclei. D) Activated astrocytes, arrows, were not seen in middle thalamic nuclei, but were present in middle habenular nuclei. BG = Black-gold II; FJC/DAPI = Flouro-jade C with 4',6-diamidino-2-phenylindole nuclear counterstain; GFAP = Glial fibrillary acidic protein, CD68 = Cluster of Differentiation 68; CV = Cresyl violet. Scale bar is 50µm.

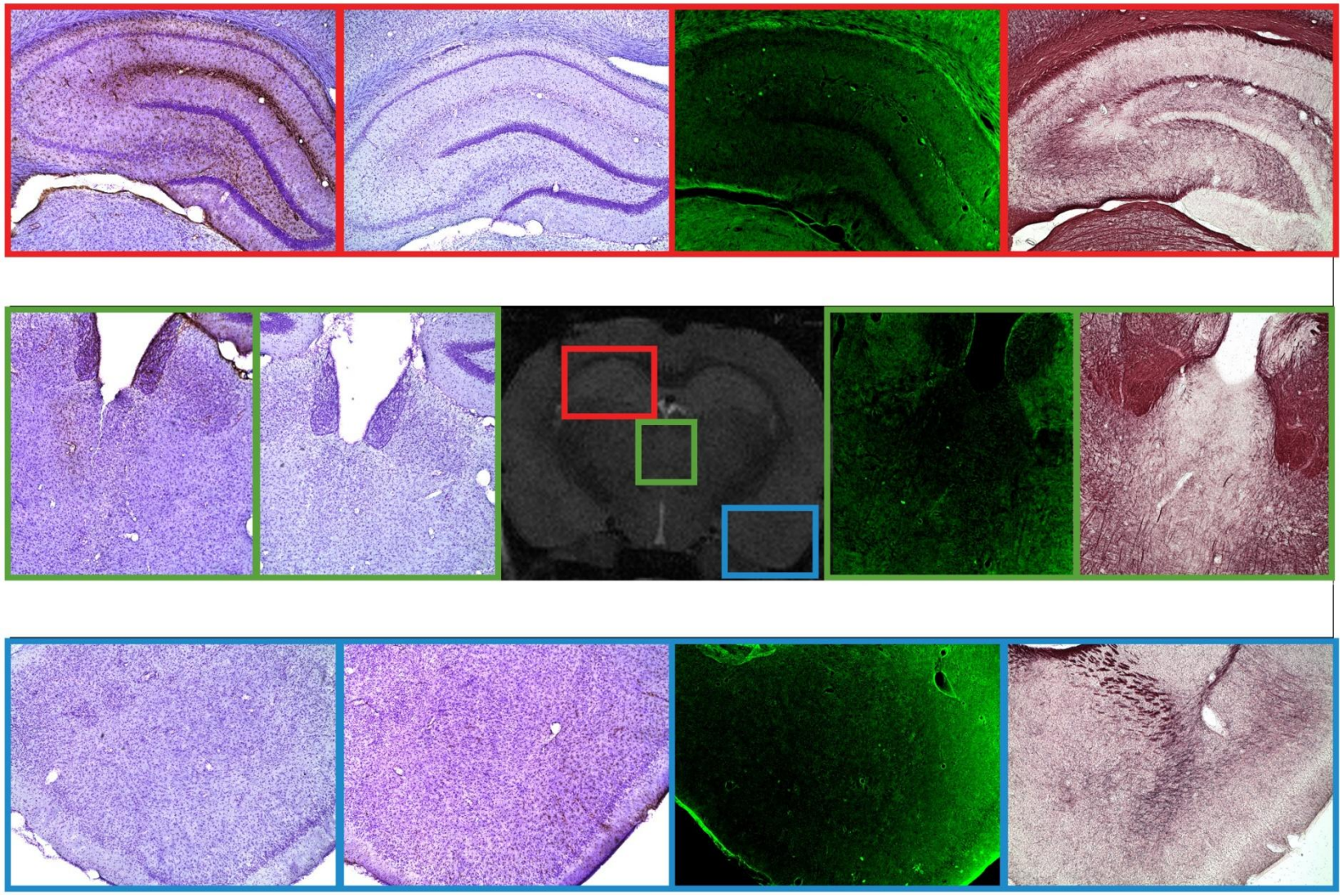

Figure 3-9. T2-weighted MR image with corresponding histology of a spontaneously seizing animal 60 days post-SE. Each row displays histological staining for GFAP, CD68, FJC, and BG (from left to right, see Figures 3-5 to 3-8 for abbreviations). Colored boxes correspond to colored regions outlined on the MR image.

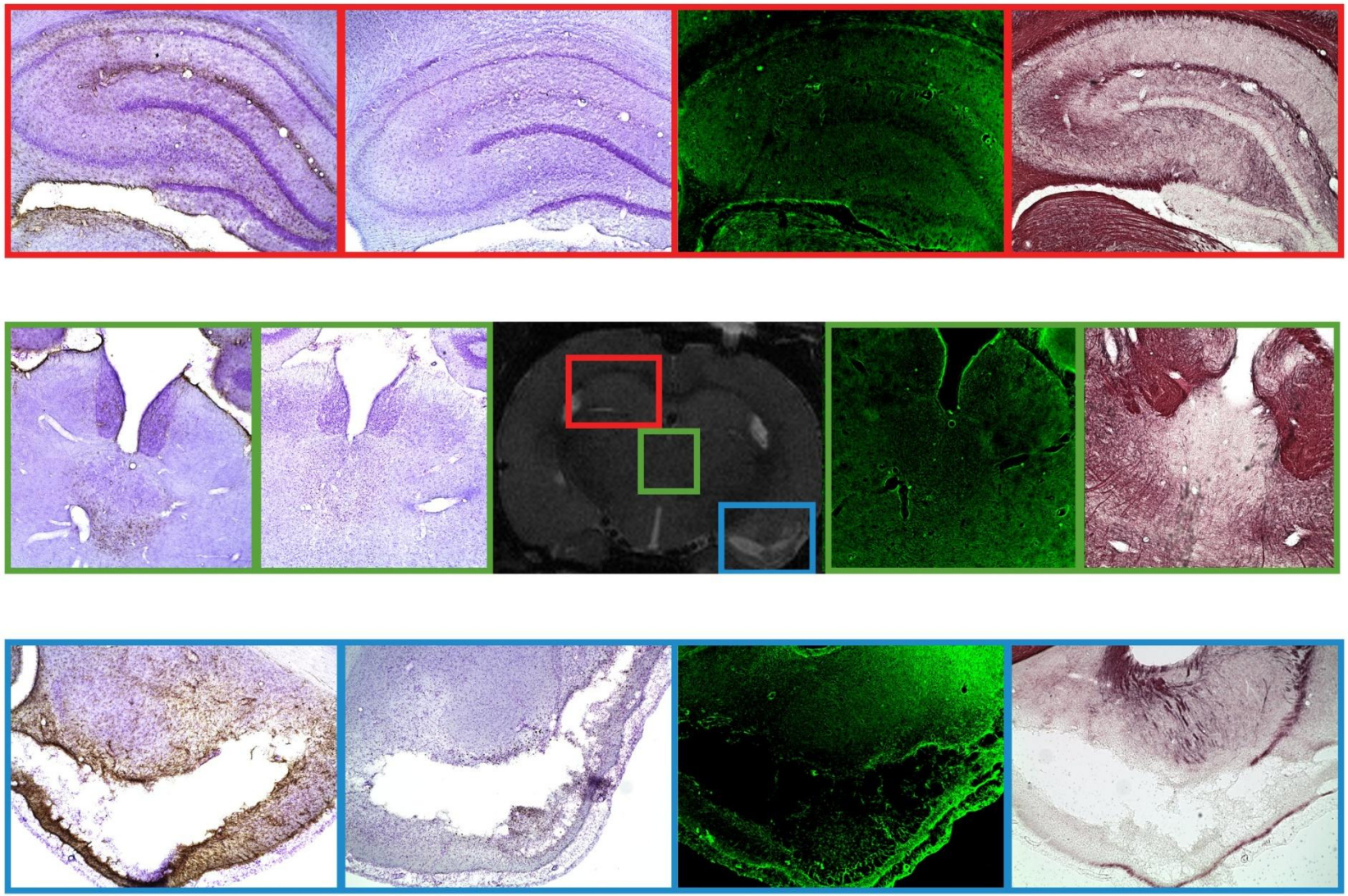

Figure 3-10. T2-weighted MR image and corresponding histology of another spontaneously seizing animal 60 days post-SE. Each row displays histological staining for GFAP, CD68, FJC, and BG (from left to right, see Figures 3-5 to 3-8 for abbreviations). Colored boxes correspond to colored regions outlined on the MR image.

CHAPTER 4
CONVECTION-ENHANCED DELIVERY OF THERAPEUTIC AGENT CARRIERS

Introduction

Chapters 2 and 3 describe CED distributions of Gd-albumin in normal and injured hippocampi. These studies emphasize the importance of local tissue structure on infusate distribution, specifically the presence of dense cell layers, fissures, white matter bundles, and edema. However, they likely reveal "best-case scenario" distributions because albumin is a non-binding, low-reactivity protein tracer. As mentioned in the Chapter 3 subsection "Other Factors Affecting Final Infusate Distribution", variability in CED distribution is also introduced by physico-chemical properties (size, shape, viscosity, solubility, binding, concentration, rate of efflux, etc.) of the infusate. The initial Gd-albumin studies described in Chapters 1 and 2 can be used as a guide for predicting the distribution of therapeutic agents with more complex properties, such as viral vectors or neural stem cells (NSCs). As described further in this chapter, the use of viral vectors and NSCs to deliver therapeutic agents are novel strategies that have shown promise experimentally (see "Gene Therapy for Epilepsy" and "Stem Cell Therapy for Epilepsy", below). These systems also exhibit interesting migratory properties of which CED studies are lacking. Further work analyzing the effect of other variables, such as cellular interaction and chemotaxis, will allow for more accurate prediction of

---

Excerpts from this chapter are reprinted from Njie eG, Kantorovich S, Astary GW, Green C, Zheng T, Semple-Rowland SL, Steindler DA, Sarntinoranont M, Streit WJ, Borchelt DR (2012) A Preclinical Assessment of Neural Stem Cells as Delivery Vehicles for Anti-Amyloid Therapeutics. PLoS ONE 7: e34097. doi:10.1371/journal.pone.0034097.

This work was completed with the help of Drs. eMalick Njie and Garrett Astary. Dr. Njie provided the NSCs used in this study, helped with surgical procedures, and performed the quantification of transplant dimensions. Dr. Astary loaded the infusion pump for the surgeries and performed the image segmentation.

distribution. Therefore, as a follow-up to initial CED investigations, proof-of-principle studies using viral and NSC drug carriers were undertaken to elucidate whether these agents share the spatial and temporal properties of small molecule infusate distributions.

Gene Therapy for Epilepsy

Gene therapy is often proposed as a solution for correcting or supplementing defective genes responsible for disease development. The generation of viral vectors, which can be engineered to induce specific and stable gene transfer, offers an attractive strategy for epilepsy treatment. Thus far, therapeutic strategies have focused on modulating the signaling of neurotransmitters and neuroactive peptides that may have anticonvulsant or neuroprotective effects. Raol et al. (2006) showed the incidence of developing chronic seizures was significantly lower in pilocarpine-treated animals that overexpressed the $GABA_A$ receptor α1 subunit. Due to reports of reduced numbers of GABAergic neuropeptides in experimental epilepsy (Gant et al., 2009), gene therapy has also been designed to restore galanin (McCown, 2006; Kanter-Schlifke et al., 2007; Loscher et al., 2008), neuropeptide Y (McCown, 2006; Noe et al., 2007; Noe et al., 2008), and somatostatin (Zafar et al., 2012). Neuroprotective effects have also been demonstrated with the overexpression of the glucose transporter-1 and the apoptosis inhibitor Bcl-2 (McLaughlin et al., 2000).

Experimental evidence shows gene therapy is a promising utility for epilepsy therapy, with several caveats. Vector systems differ in important aspects and the choice of system should be based on a combination of safety and effectiveness of the vector in a particular strategy. The adeno-associated virus (AAV) vector system has several advantages over other systems such as lentiviruses or retroviruses. Lentiviruses, a

subclass of retroviruses 80-100nm in diameter, exhibit insertional mutagenesis. Overall they seem to be less mutagenic than parent retroviruses (Modlich and Baum, 2009), because they generally integrate into gene regions less likely to disturb regulation and expression of host genes. Retroviruses integrate in promoter regions and CpG islands that may influence the acitivity of the host promoter or give rise to new full-length transcripts (Wu et al., 2003). AAV, on the other hand, exhibits low immunogenicity similar to lentivirus, but does not integrate into the genome.

AAV is a small (20 nm) replication-defective, nonpathogenic human parvovirus that requires co-infection with a helper virus to replicate (Mandel et al., 2006). It is possible to concentrate and purify AAV vectors to very high titers, resulting in widespread and stable transduction with low toxicity. Eleven strains of AAV have been identified, and much effort has been put into modifying the tropism of the vector through capsid manipulation and its specificity through promoter design. AAV serotypes are distinct from each other in their capsid regions, allowing binding and entry into different cell types. Tissue tropisms of AAV vectors likely arise due to the cumulative effects of viral binding to multiple cell surface receptors, cellular uptake, intracellular processing, nuclear delivery of vector genomes, uncoating, and second-strand DNA conversion (Wu et al., 2006). AAV2 shows moderate efficiency in the CNS, but AAV1 and 5 have been shown to exhibit higher tranduction frequencies (Davidson et al., 2000; Burger et al., 2004). AAV8 and AAV9 (Cearley and Wolfe, 2006; Klein et al., 2006; Klein et al., 2007) are also capable of achieving high levels of neuronal expression, but AAV4 appears to transduce ependyma and astrocytes in the subventricular zone (Davidson et al., 2000). The differential cellular interactions of AAV serotypes introduce another variable to CED

distributions. In this study, distributions of AAV1, 5, 8, and 9 were chosen to evaluate after CED due to their increased efficiency and neuronal tropism.

Stem Cell Therapy for Temporal Lobe Epilepsy

The need for alternative therapeutic approaches for the evolution of TLE has also resulted in intervention strategies involving the grafting of neural stem cells. Due to its focal nature, TLE is one of the neurological disorders that could benefit from transplantation of cells. This strategy has the potential to curb epileptogenesis, ease chronic seizures, and benefit learning and memory impairments (Shetty and Hattiangady, 2007).

Although this field is still in its infancy, there have been sundry approaches to replace lost neurons or glia, produce more GABA-ergic cells, or deliver neuroprotective factors via stem cells. Replacement of degenerated neurons in the injured hippocampus via grafting of fetal hippocampal cells has shown promise for restraining epileptogenic changes and controlling seizures (Shetty et al., 2005; Rao et al., 2007). Grafting of cells engineered to produce GABA and fetal GABA-ergic cells into the epileptic foci have been shown to transiently reduce seizures in a variety of animal models (Gernert et al., 2002; Thompson, 2005; Castillo et al., 2006). Transplantation of GABA-producing cells in the dentate gyrus was associated with increased GABA levels, enhanced local electrical seizure threshold, and delayed onset of behavioral seizures in the kindling model of epilepsy (Thompson, 2005). In the kainic acid model of TLE in rats, grafts containing fetal neural precursors from CA3 were effective in increasing GABAergic function (Shetty and Turner, 2000), and grafts of striatal precursor cells decreased the frequency of spontaneous seizures (Hattiangady et al., 2008). Limited repair of the adult

hippocampus is also possible with grafts of neural stem cells with more restricted neural or glial fates (Shetty et al., 2008).

In general, stem cell-based approaches focus on developing strategies to activate NSCs to produce new neurons, facilitate differentiation into GABA-ergic neurons, and to suppress established seizures. However, it would also be interesting to develop methods for testing whether NSCs could prevent chronic epilepsy. Chu et al. (2004) transplanted human NSCs intravenously after a pilocarpine injection and found a positive result in the suppression of the formation of spontaneous seizures. Embryonic stem (ES) cell derived neuronal precursors engineered to release adenosine protected against developing generalized seizures in a kindling model of TLE (Li et al., 2007) and suppression of spontaneous seizures in mice (Li et al., 2008).

To be successful, grafts of stem cells must not only survive, but also migrate correctly to the appropriate sites to establish appropriate synaptic connections. Spatial dynamics of implanted cells have been described after grafting (Hoehn et al., 2002), but are solely attributed to pronounced migration towards chemotactic signals. This chapter describes the pre-migrational mobility of NSCs.

Proof-of-Principle Studies for Viral Vector and Stem Cell CED Delivery

Although much progress has been made in developing viral vector and NSC-based therapies for epilepsy, translation of either of these techniques requires control, or at the very least, understanding of their interstitial mobility so risks of aberrant migration could be weighed against potential benefits. One of the major hurdles in development today is being able to control dispersion of these carriers. The effect of the initial distribution of both AAV and NSCs has often been overlooked because these other factors (migration, cellular uptake) are assumed to play a larger role in the final

distribution. However, enhancing initial distribution with CED can affect final outcome. This has been shown through increase of viral spread and transduction efficiency in the striatum (Bankiewicz et al., 2000). CED delivery of AAV has not been studied in the hippocampus; and transduction efficiency varies markedly from one region to another (McCown et al., 1996). No CED studies of NSC delivery exist; in fact, NSC distribution outside of migration has not been studied. Therefore, this chapter presents preliminary data to 1) illustrate the utility of CED in delivering NSCs and viral vectors in the hippocampus, 2) reveal the effect of initial CED distribution on NSC spread, and 3) describe the effect of vector tropism and size on hippocampal CED distribution.

Methods

Animals

NSC experiments were performed on 8-14 month C67/B6 non-transgenic mice. Both host mice and NSC donor mice were congenic on the C57BL/6J background, eliminating problems with graft rejection. AAV experiments were performed on male Sprague-Dawley rats weighing 225-250 g.

Vector Construction

Standard cloning techniques were used to construct recombinant AAV-based plasmids. GFP was subcloned in an expression cassette that had the cytomegalovirus immediate early enhancer and the chicken beta-actin promoter (construct pTRUF11, UF vector core). This was subcloned at the UF vector core into the rAAV backbone flanked by rAAV2 inverted terminal repeats and pseudotyped with serotype 1, 5, 8, and 9 capsid proteins (titers of 1.68×10^{13} vg/mL, 9.02×10^{12} vg/mL, 6.47×10^{12} vg/mL, 6.56×10^{12} vg/mL, respectively).

Lentivirus plasmids containing CaMKII-Channelrhodopsin-2/GFP were obtained from Karl Deisseroth (Stanford University) and packaged by Dr. Phil Barish.

Transduction and Isolation of NSCs

GFP-expressing NSCs were provided by eMalick Njie. The NSCs were isolated by removing the subependymal zone of neonatal B6 mice, processing with trypsin/ethylenediaminetetraacetic acid, and dissociating into a single cell suspension. Cells were maintained in culture flasks, and then transduced with self-inactivating Lentiviruses containing plankton copepod green fluorescent protein (courtesy of Dr. Sue Semple-Rowland). Cells were then enriched with fluorescence activated cell sorting (FACS). Prior to transplantation, monolayers were detached from flasks, washed, and diluted to 5 x 10^4 cells/µL. Concentration was determined with two reference cell counts on a hemacytometer.

Surgical Procedures and CED Infusions for NSC Experiments

Mice were deeply anesthetized with 1-5% isoflurane and then securely mounted with ear bars and a nose bar to a stereotaxic apparatus (Kopf Instruments, Tujunga, CA). The anesthesia mixture was delivered through an inlet within the nose bar enclosure for the duration of the surgery. The top of the head was shaved and sterilized with alternating swipes of betadine antiseptic and 70% ethanol. A sterile scalpel was used to make a small incision into the skin above the skull. The skin was reflected in order to expose Bregma and a burr holes were drilled to allow cells to be injected bilaterally to the thalamus (n=7; [-2.0mm AP, +/- 1.5mm ML, -4mm DV]), striatum (n=3; [+1.18mm AP, +/-1.5mm ML, -4mm DV]), and three depths within the hippocampus [-2.00mm AP, +/-2.0mm ML, -1.5mm DV, -2.1mm DV, and -2.8mm DV]. Hippocampal DV coordinates correspond to the superior aspect (n=5), dorsoventral center (n=5), and

inferior aspect (n=7) of the septal hippocampus, respectively. Approximately 5 x 10^5 cells (9.8 µL) were infused into each region. Per experiment, 4-6 confluent T75 flasks were harvested and concentrated at 5 x 10^4 cells/µL in order to reliably have enough volume for transplantation and for void volume in the infusion system. In general, the infusion parameters used here are established protocols in other studies (Park et al., 2006; Yamasaki et al., 2007; Tang et al., 2008). The cell numbers and volumes used here are similar to intracranial surgeries by Park et al. (2006), in which mouse brains were infused with 3 x 10^5 NSCs in 8 µL.

All infusions were delivered via CED at 1 µL/min using the same infusion system mentioned in Chapters 2 and 3. Following injection, the needle was left in place for 3 minutes to minimize backflow before being slowly withdrawn.

Surgical Procedures and CED Infusions for Viral Vector Experiments

Surgical procedures to expose bregma and lambda on the skull were performed as described in Chapters 2 and 3. Once exposed, burr holes were drilled over the left hippocampus for the injection of viral vectors (n=4; at [-3.80 mm AP, -2.50 mm ML, -3.10 DV]). Injections were performed at 0.3 µL/min with a 10 mL Hamilton syringe (33 gauge, point style 4) attached to an infusion pump. The needle was kept in place for 5 additional minutes after cessation of injection to allow for distribution of the vector before retraction. Volumes of injection were adjusted per serotype (2.0-5.19 µL) to equalize the number of vector genomes (vg) delivered to be 3.36 x 10^{10} vg.

Perfusion and Immunochemistry

Tissue harvesting was performed within 15 minutes of NSC injection to visualize immediate pre-migrational distribution. To harvest tissues, mice were deeply anesthetized and euthanized by isoflurane overdose followed by immediate

exsanguination and perfusion with cold 1x PBS. Whole brains were quickly dissected out and submerged in cold 4% paraformaldehyde fixative overnight. Fixed brains were then cryoprotected in 30% sucrose and sectioned at 20 µm intervals with a cryostat. Sections were stored in anti-freeze media at -20°C until staining with 4',6-diamidino-2-phenylindole (DAPI, Invitrogen, Carlsbad, CA). Immunostained cells and tissue sections were photographed with an Olympus DP71 camera mounted on an Olympus BX60 microscope.

Tissues from viral vector-injected animals were harvested one month post-infusion. Perfusion, brain extraction, and tissue sectioning was performed as described in Chapter 3. No staining was performed on these sections.

Quantification of NSC Transplant Dimensions

NSC transplant dimensions were quantified using a method adapted from Mazel et al. (1998). An index of anisotropy, designated A, was determined by dividing the distance of engraftment (x) along the transverse (i.e. mediolateral) axis by the distance of engraftment (y) along the vertical (i.e. dorsoventral) axis. With this method, spherical engraftments would result in A values close to 1, while anisotropical engraftments would result in larger or smaller values of A. For each infusion, one to two 20 µm sections containing engraftments were analyzed with AxioVision LE software (Zeiss, Jena, Germany). Images of samples with equal pixel/micrometer value were used to determine the distance of x and y. An unpaired, two-tailed Student's t-test using Microsoft Excel was used to compare A from different sites of infusion. A p-value of <0.05 was considered statistically significant.

Image Segmentation and 3D Reconstruction of NSC Engraftments

A semi-automatic image segmentation routine was implemented in MATLAB® (The MathWorks, Inc., Natick, MA USA) that distinguished regions of GFP expression from control regions of the brain by means of a threshold unique to each histological section. RGB images of the histological sections were imported into MATLAB®; however, only the green channel of the images was used for image segmentation. The average background signal was determined by averaging the signal intensity in GFP-free regions of interest for each section. Similarly, the standard deviation of noise was determined by evaluating the noise behavior in tissue-free regions in images. Thresholds were calculated by adding six times the standard deviation of noise to the control signal intensity for each section. The image segmentations were refined in ITK-SNAP (Yushkevich et al., 2006), an open source medical image segmentation tool. Refinements included removing regions of auto-fluorescence (false-positives) from the image segmentation as well as segmentation of annotations such as scale bars. Three-dimensional reconstructions were generated by first aligning the histological sections prior to image segmentation and finally generating a mesh from the 3D image segmentation using ITK-SNAP's built in mesh generation tool.

Results

Distribution of Viral Vectors in the Hippocampus

Four neuronal serotypes of AAV-GFP and a lentivirus vector were infused into the dorsal hippocampus (Figure 4-2, 4-3). A summary of these results can be found in Table 4-1. AAV1-GFP (Figure 4-2A, 4-3) transduced cells in the dentate granule cell layer, hilus, CA1, CA2, and medial CA3 throughout approximately 2800 µm of the hippocampal septo-temporal axis. A portion of cells in Layer VI of the overlying cortex

were also transduced and projections in the lateral posterior thalamic nucleus were visible throughout ~800 µm in the anterior-posterior direction. Contralateral projections of transduced cells were visible in all subregions of the hippocampus proper.

AAV5-GFP (Figure 4-2B, 4-3) transduced cells were visible mostly in the CA2, with less transduction in the CA3 and CA1 through approximately 2400 µm of the septo-temporal axis. Hilar cells were also transduced, but almost no granule cells expressed GFP. Interestingly, contralateral projections of transduced cells were visible in all subregions of the hippocampus proper and in the inner molecular layer of the dentate gyrus, the target of hilar mossy cells.

AAV8-GFP (Figure 4-2C, 4-3) transduced cells in the CA3, CA3, and CA1, with minimal transduction in the hilus and dentate granule cells. Transduction was visible through approximatel 2400 µm along the septo-temporal axis. Commissural projections were visualized in the contralateral CA1 and CA2.

AAV9-GFP (Figure 4-2D, 4-3) transduced cells mainly in the CA1, CA2, and Layer V1 of the overlying cortex. CA3 cells expressed GFP in the septal hippocampus, but GFP in CA3 was not visible ~4.5 mm behind bregma through the temporal hippocampus. Projections from transduced cells could be visualized in the contralateral CA1, CA2, and in lateral posterior thalamic nuclei for ~1000 µm in the anterior-posterior direction. AAV9-GFP expression was noticeably the most widespread and exhibited the highest intensity of GFP expression.

The lentivector (Figure 4-2E) transduced pyramidal cells in the CA1 and granule cells of the dentate gyrus. While AAV transduction occurred throughout the septo-

temporal axis, GFP expression from lentivirus was only visualized along 600 μm of the septo-temporal axis.

Distribution of Transplanted NSCs in the Hippocampus

NSCs were bilaterally infused into the hippocampus and host mice sacrificed within fifteen minutes of surgery to visualize pre-migrational distribution via CED. Across various depths of infusion into the hippocampus, well-defined ellipsoid distributions of GFP fluorescence were consistently observed in the transverse plane (Figure 4-4A-B, E-F). GFP fluorescence was found distributed largely in three structures: the corpus callosum, the velum interpositum and the hippocampal fissure. Specifically, NSCs that were infused into the superior aspect of the septal hippocampus yielded GFP fluorescence distributions throughout the corpus callosum (Figure 4-4A; n=5). Cells that initially colonized white matter tracts moved laterally within this structure but did not migrate into adjacent gray matter (Figure 4-4A). NSCs targeted to the inferior aspect of the septal hippocampus produced GFP fluorescence distributed mediolaterally along the velum interpositum (Figure 4-4B; n=7). The velum interpositum is a soft tissue partition between the diencephalon and the telencephalon rather than a cavity or space (Tubbs et al., 2008). Functionally, the velum interpositum forms the roof of the 3rd ventricle and connects the choroid plexus of this ventricle to that of the lateral ventricle. The distribution of GFP fluorescence in this region extended hundreds of micrometers from the 3rd ventricle to above the dorsal lateral geniculate nucleus. NSCs targeted to the dorso-ventral center commonly distributed in the hippocampal fissure, corpus callosum, and velum interpositum (Figure 4-4E). In some instances, GFP fluorescence was not only at the position the cells were targeted, but also in areas hundreds of micrometers away (Figure 4-4E-F).

Distribution of Transplanted NSCs in the Thalamus and Striatum

NSCs were also infused into the thalamus and striatum to determine whether engraftment patterns in the hippocampus are unique. NSCs that were infused into the thalamus (Figure 4-4C; n=7) and striatum (Figure 4-4D; n=3) produced spherical distributions of GFP fluorescence that were indicative of isotropic transport. 3D reconstruction of serial sections of a representative corpus callosum infusion illustrates the sheet-like spread of GFP fluorescence across the wide, flat bundle of corpus colossal fibers (Figure 4-5A). In contrast, thalamic infusion reconstruction shows a globular spread of GFP fluorescence (Figure 4-5B). These patterns of distribution were consistent with the cells having been distributed along structure-specific pathways at the time of injection (Figure 4-5C).

Discussion

Viral Vector Distribution

Comparisons of five viral vector infusions into the septal rat hippocampus revealed primarily neuronal expression patterns that differed across serotype and vector. Intensity of GFP expression was higher with AAV1 and 9 than AAV5 or 8. AAV9 resulted in the widespread expression in CA1 and CA2, but AAV1 and 8 resulted in better expression in CA3. AAV1 and 9 resulted in GFP fluorescence in the thalamus, though AAV9 showed the most widespread expression. Viral genomes were equalized across all AAV serotypes by varying infusion volume, which cannot be discounted as an influence on distribution. However, the largest volume infused was of AAV 8, which resulted in the second-to-worst transduction efficiency. Alternatively, the second-to-least volume infused was of AAV1, which resulted in the next best transduction efficiency. Another study in which viral genomes are equal across serotypes is needed to

determine the effect of volume on AAV distribution. Despite this limitation, these results are similar to that of other comparative studies. Previous comparisons have shown that transgene expression was greater with AAV1 and AAV8 than AAV5, but no difference between AAV1 or 8 (Klein et al., 2006). Another study demonstrated that AAV1 and AAV5 are of similar efficiency (Burger et al., 2004). A study examining transgene expression after systemic injection in mice revealed that AAV9 > AAV1, 8 > AAV5 (Zincarelli et al., 2008).

It is important to note results pertaining to serotype tropism should be interpreted cautiously due to inter-study variations in vector titers, doses, and promoters. The preliminary studies described in this chapter are distributions from one animal per vector and do not represent quantifiable comparisons. They do, however, provide a practical illustration of the targeting strategies presented by viral vector choice. On one hand, AAV infusions result in widespread and efficient gene expression that can be modulated by serotype. The disadvantage of AAV is the small (4-5 kb) cloning capacity of the vector. This constrains the choice of genetic regulatory elements, which allow for modulation of gene expression. Alternatively, lentiviruses do not have significant limitations on gene size. With a cloning capacity of up to 8kb, lentivectors have the ability to induce long-term stable expression and low immunogenicity (McGrew et al., 2004). However, lentivectors can range from 80-100 nm in size, while AAV particles are approximately 25 nm. In contrast to AAV vectors, the lentivirus infusion resulted in a very focal pattern of expression of <1 mm, which may be due to larger particle sizes relative to AAV.

As mentioned in Chapters 2 and 3, infusion site presents a considerable influence on distribution. Infusion site could be visualized through a higher density and intensity of GFP expression. Infusion with AAV5 was approximately 1 mm lateral as compared to the other infusions, a potential explanation for the difference in transduction for this animal. The widespread expression from AAV9 in CA1 may be due to a more dorsal infusion site as compared to the other serotypes. As described in Chapter 1, preferential distribution in the septal hippocampus is dependent upon location of the cannula tip along the dorsoventral axis. Further studies with more animals are needed to distinguish this influence from serotype cellular interactions.

NSC Distribution

To characterize NSC distribution patterns, transplants were analyzed immediately after infusion into areas of diverse anisotropic properties. The main finding of this study revealed areas of low fluid resistance (namely corpus callosum, hippocampal fissure, velum interpositum) were a prevailing influence on the distribution of NSCs. Anisotropic distribution patterns were most prominent in the hippocampus, but absent in other regions such as the thalamus and striatum. Interestingly, the ectopic engraftment pattern of NSCs is long-term, as demonstrated by the fact that NSCs engrafted in the corpus callosum under identical conditions do not redistribute into gray matter after a month (Njie et al., 2012). In fact, NSCs deposited into various hippocampal and cortical sites paradoxically distribute mainly in the corpus callosum and to a lesser extent, the hippocampal fissure (Olstorn et al., 2007; Blurton-Jones et al., 2009; Radojevic and Kapfhammer, 2009). Similar distribution characteristics have been reported in epilepsy models as well. Hattiangady et al. (2008) grafted striatal precursor cells 4 days post kainate-induced SE and analyzed 9-12 months later. The grafts were targeted to CA3 of

the septal hippocampus, but were later found to be in the velum interpositum as well as the targeted region.

Engraftment patterns in short and long-term studies may be an artifact of injection parameters, such as the rate, volume of cells, or infusion site. This is unlikely, due to the range of parameters used in various studies. Furthermore, infusion site was varied in this study to include three different depths within the hippocampus. All three depths resulted in NSC spread to areas of least resistance. Alternative explanations for the ectopic engraftments in the long term may be due to cell viability. It is possible that NSCs distributed throughout the hippocampus, but only those within low resistance spaces remained viable at the time of observation. Regardless, these results raise fundamental questions regarding how engrafted NSCs are ultimately distributed after transplantation. Cell migration is clearly one determinant of graft distribution. Indeed, subventricular zone NSCs transplanted into the lateral ventricle follow migrational cues in the rostral migrational stream (Zheng et al., 2006). In this study, NSC infusions showed neuroarchitecture may play an underappreciated role in distribution of engraftments. Host mice harvested only minutes after surgery had remarkably similar distributions of NSCs in paths of least resistance to reports of long-term distributions. This pattern of distribution is similar to anisotropic distributions observed in the work described in Chapters 2, 3, and previously with other small molecule infusions (Vorisek and Sykova, 1997; Mazel et al., 1998; Astary et al., 2010), although to an exaggerated extent due to the greater size constraints for NSCs.

Conclusions

Gene and stem cell transfer have the capability to induce expression of neuroprotective compounds, anticonvulsant agents, or supply supportive replacement

cells for temporal lobe epilepsy. A combination therapy of gene and stem cell therapy may even be potential strategy in which GABA-ergic cell transplants supplement viral vector delivery of anti-convulsants. Unfortunately, there are still many hurdles for stem cell treatments for intractable epilepsy. Cells must first be capable of exhibiting enduring survival and maintaining neurotransmitter release on a long term basis in the epileptic brain (Zaman et al., 2000). Second, fetal precursor cells have not been shown generate specific types of neurons or glial cells needed to replace damaged cell types. Embryonic stem cells can be used to generate neural or glial precursors, but risk of tumor formation is high because they are pluripotent and mitotically active. As stem cell therapies grow in popularity, these challenges are among the studies being undertaken.

Chapter 4 describes proof-of-concept applications for CED in epilepsy using carrier vehicles commonly proposed as novel therapeutic strategies. CED delivery of these carriers resulted in distributions along paths of least resistance and exhibited a dependence on infusion site, akin to infusions of Gd-albumin. Distributions of NSCs, particularly, were influenced by hippocampal-specific anatomical constraints that resulted in previously uncharacterized anisotropic transport. These results reiterate the significance of biostructural factors in targeting strategies of delivery approaches, in addition to the influence of serotype and chemotaxis.

Table 4-1. Features of gene expression vectors

Viruses	Packaging capacity	Inflammatory Response	Advantage	Disadvantage
Retrovirus	8 kb	Low	Large cloning capacity; stable transgene expression	Does not infect non-dividing cells. Insertional mutagenesis
Lentivirus	8-10 kb	Low	Infects diving and non-diving cells with 30% efficiency, large cloning capacity	Insertional mutagenesis
Adenovirus	8 kb	High	Infects all cell types with 100% efficiency; does not integrate with host	High inflammatory response
AAV	4.7 kb	Very Low	Infects all cell types; non-pathogenic, does not integrate with host	Small packaging capacity

Table 4-2. Results of hippocampal viral vector infusions

Viral vector	Volume Infused	Length of A/P Transduction	Length of M/L Transduction	Hippocampal subregions tranduced
AAV1	3.73 µL	2800 µm	2739 µm	CA1-CA3, some DGC and hilar
AAV5	2.00 µL	2400 µm	1557 µm	CA1-CA3, some hilar
AAV8	5.19 µL	2400 µm	3789 µm	CA1-CA3, some hilar
AAV9	5.09 µL	3200 µm	4036 µm	CA1-CA3
Lentivirus	3.6 µL	600 µm	900 µm	CA1, DGC

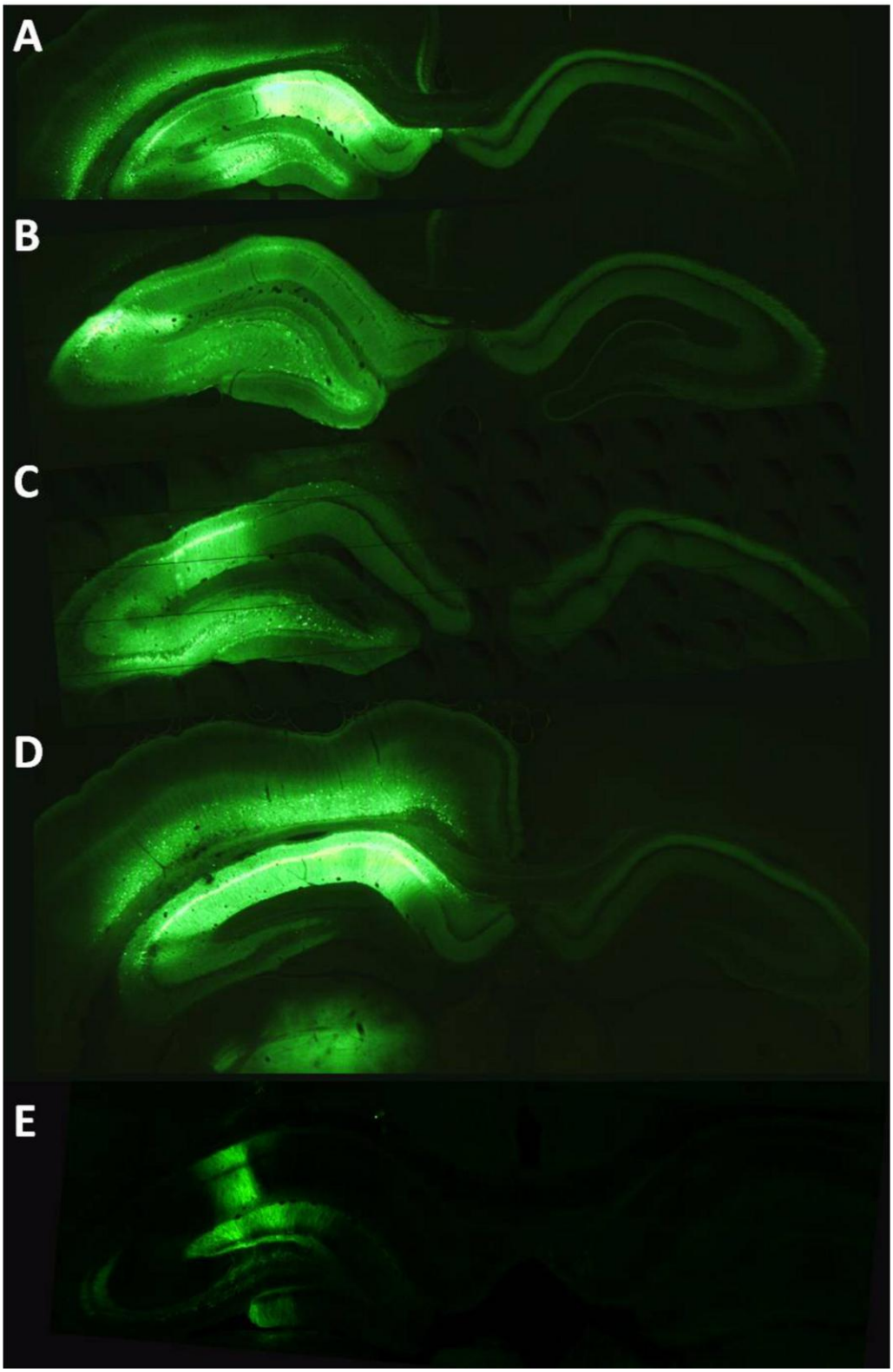

Figure 4-2. Infusions of viral vectors into the left rat septal hippocampus. A) AAV1-GFP, B) AAV5-GFP, C) AAV8-GFP, D) AAV9-GFP, E) Lentivirus-CaMKII-ChR2/GFP. Right side shows contralateral projections of transduced cells.

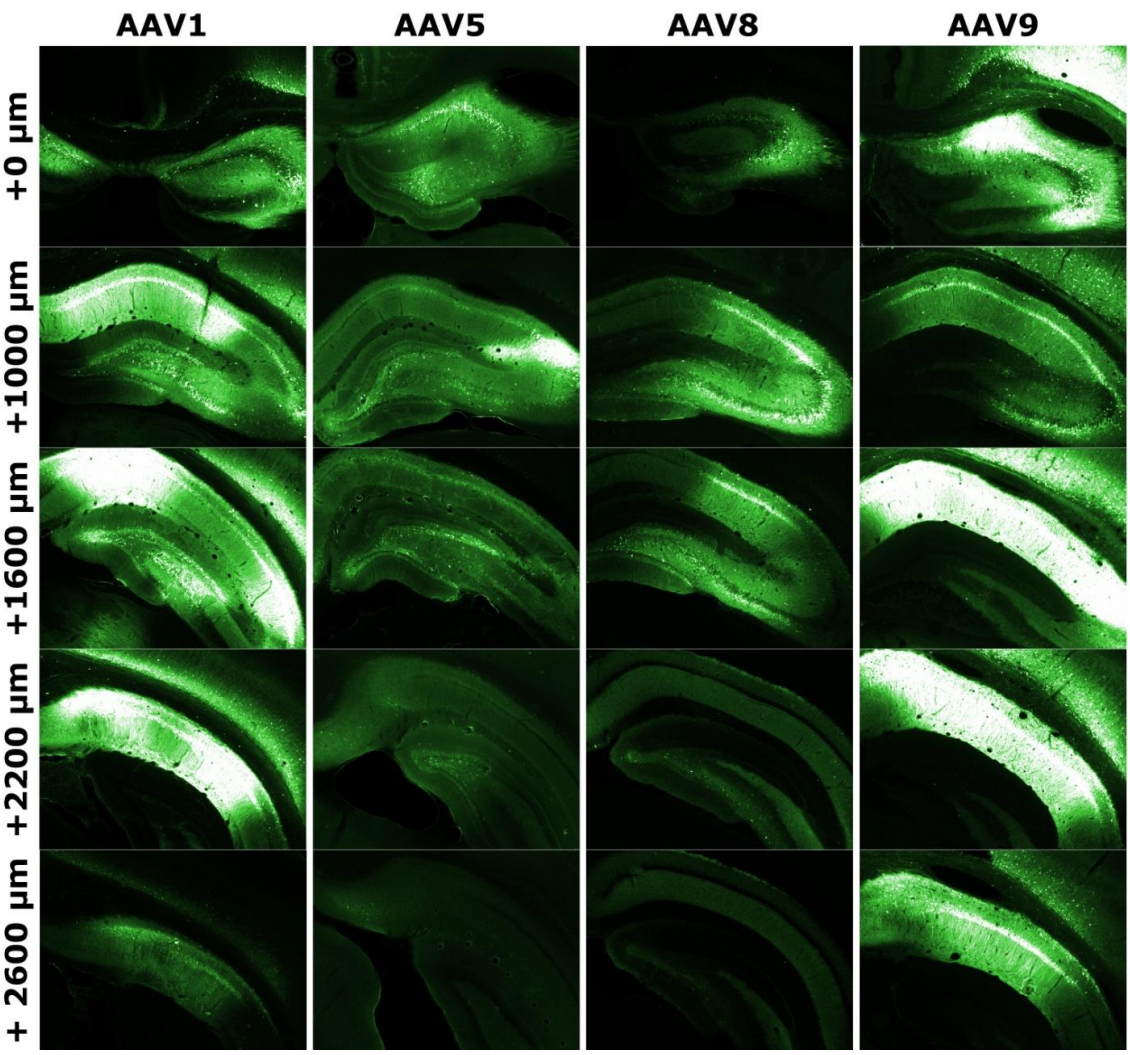

Figure 4-3. Infusions of four AAV serotypes exhibit specific distribution patterns throughout the hippocampal septo-temporal axis. Each column shows the GFP expression per AAV serotype at specific coronal sections along the septo-temporal plane. Each row depicts a coronal section posterior to the first row by the distance indicated on the y-axis.

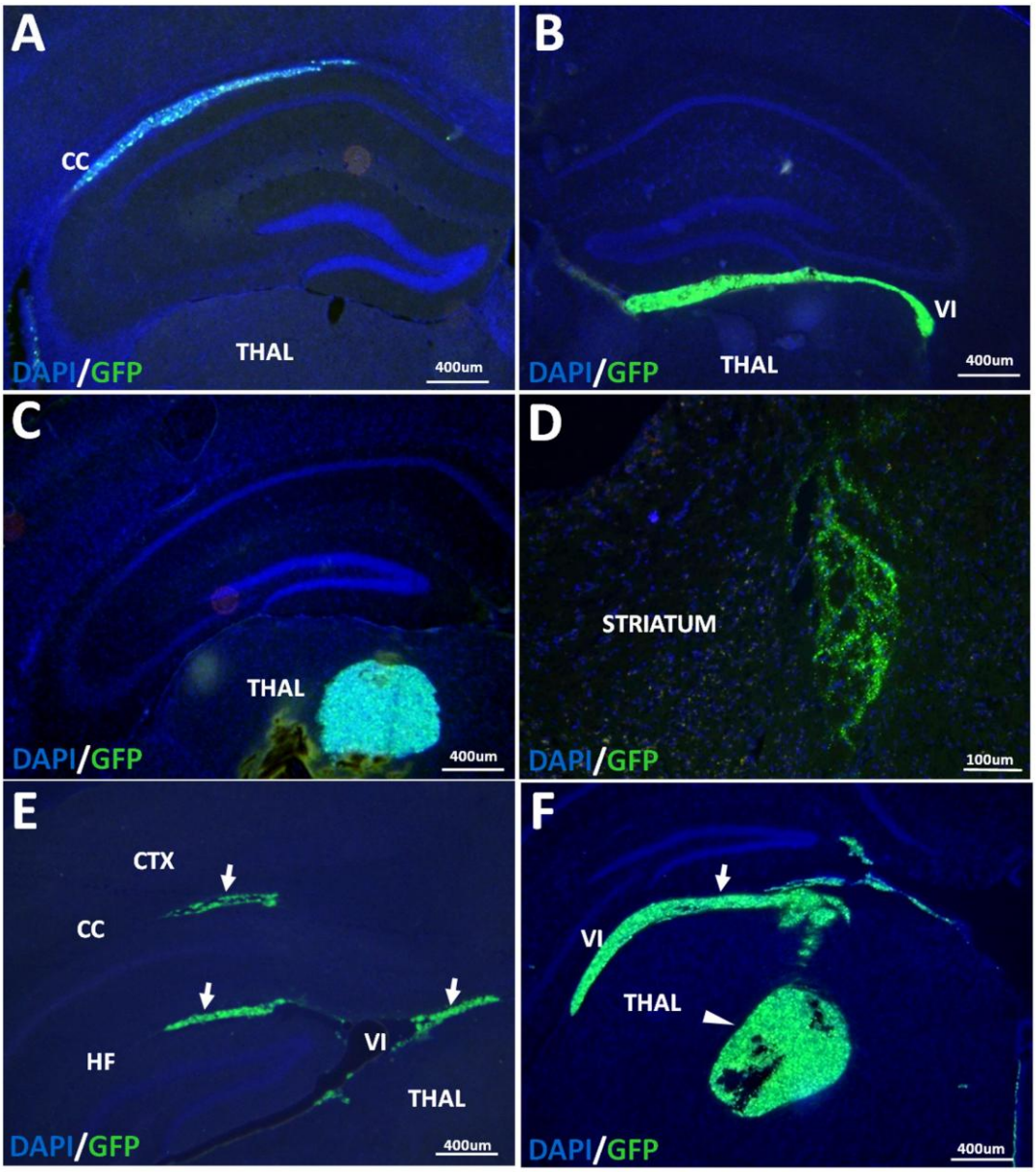

Figure 4-4. Short-term engraftments of NSCs expressing GFP demonstrate the hippocampus specifically features anisotropic transport. NSCs infused into the septal hippocampus distributed anisotropically along A) the corpus callosum (CC) when deposited in the superior aspect of the septal hippocampus, and B) the velum interpositum (VI) when deposited in the inferior aspect of the hippocampus. In contrast, engraftments into C) the thalamus (THAL) and D) the striatum resulted in isotropic distributions that did not spread preferentially along the transverse plane. E) When injected into the dorsoventral center of the hippocampus, 38.5% of infusions resulted in transport along “paths of least resistance” to sites distal of target such as the hippocampal fissure (HF), the CC, and the VI. F) Backflow in thalamic infusions resulted in anisotropic transport along the VI.

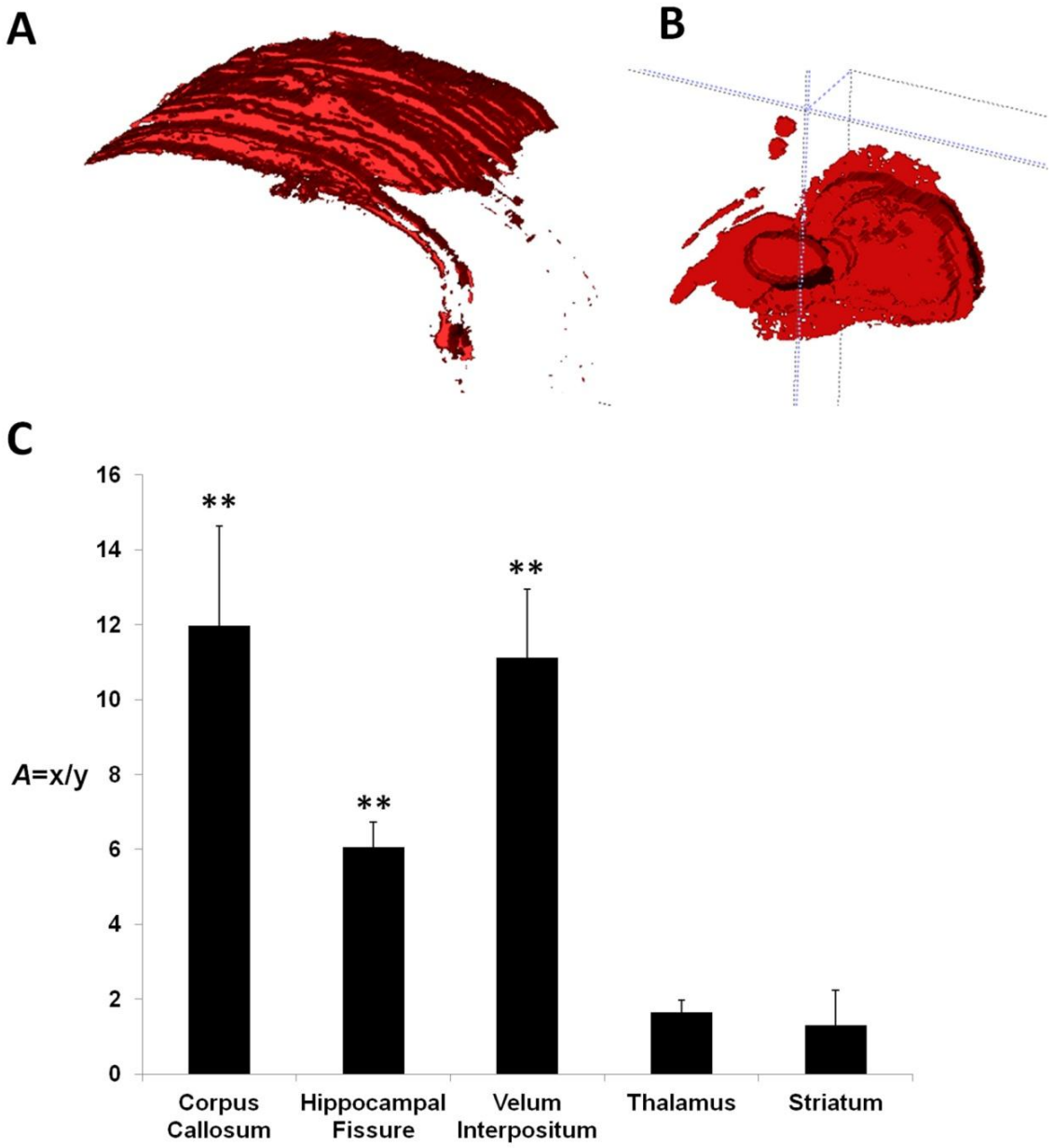

Figure 4-5. Geometric analyses of NSC infusions. A-B) 3-dimensional reconstructions of serial histological sections shows engraftments form A) a sheet-like spread in the corpus callosum, and B) a globular spread in the thalamus. C) Anisotropy (A) was quantified by dividing the spread along the transverse plane (x) by the spread along the vertical plane (y). Compared to the thalamus, A is 7.3 times larger in the corpus callosum, 3.7 times larger in the hippocampal fissure, and 6.8 times larger in the velum interpositum (**, $p<0.01$, comparison to the thalamus).

CHAPTER 5
CONCLUSIONS AND FUTURE WORK

Conclusions

TLE is a devastating disease that affects people of all ages, races, and socioeconomic backgrounds. Even with an advanced understanding of underlying mechanisms, the current treatment approach has not changed in decades. Systemic administration of AEDs is the main approach to treating seizures, even though one third of patients are resistant to current pharmacotherapies. Furthermore, treatment occurs only at chronic time points; there are currently no drugs available that prevent the development of epilepsy after an initial insult, such as SE. Thus, the National Institute of Health has listed several important benchmarks for epilepsy research, including 1) identifying approaches to prevent epilepsy or its progression, 2) developing and optimizing new strategies for targeted therapies, and 3) developing animal models for the progression of epilepsy. The work presented herein addresses these NIH benchmarks through the development of CED for targeted, prophylactic treatment of TLE.

Identifying Approaches to Prevent Epilepsy or Its Progression

CED provides a targeting strategy applicable at any stage of epilepsy progression that is amenable to delivery of various therapeutic agents--far more than systemic administration is capable of transmitting to the brain. As discussed in Chapter 1, CED results in widespread distributions that are capable of reaching clinically-relevant volumes without the risk of systemic side effects. In this work, CED was applied to the infusion of NSCs and several viral vectors into the rat hippocampus as a proof-of-principle approach to delivering therapeutic compounds at a local level (Chapter 4). We

found NSCs distributed according to previously uncharacterized anisotropic conduits (corpus callosum, hippocampal fissure, velum interpositum), which had a significant impact on the final residence of the transplanted cells. Moreover, the distribution of NSCs shared spatio-temporal similarities with small molecule distributions (Chapter 2), validating the use of surrogate markers to enable real-time monitoring and prediction of the distributed agents. Because NSCs are many orders of magnitude larger than most tracers, we suspect size was a major factor in this transport pattern. This was also observed when viral vectors were tested. Lentivirus (80-100 nm) expression in the hippocampus was markedly reduced as compared AAV (25 nm) expression. Within CED distributions of different AAV serotypes, AAV9 was found to have the most widespread transduction efficiency, followed by AAV1 and 8, and lastly, AAV 5. The variability in transduction distribution was likely due to both capsid interaction and infusion site. No adverse effects were observed from the infusion of NSCs or viral vectors in animal behavior, as assessed by daily handling, or cellular structure, as analyzed through DAPI staining. CED of these therapeutic carriers is a possible approach for the direct application of anti-epileptic drugs, viral-mediated gene transfer of inhibitory peptides, or cell-based therapies. A combination therapy of gene and stem cell therapy may be another potential strategy in which GABA-ergic cell transplants supplement viral vector delivery of anti-convulsants.

Developing and Optimizing New Strategies for Targeted Therapies

Apart from molecular and enzymatic targeting strategies, physical targeting strategies are commonly overlooked and underappreciated in drug delivery. Unfortunately, the failure of several CED clinical trials (Sampson et al., 2007a; Sampson et al., 2010) has prompted researchers to look more closely at the influence of

neurostructure on infusate distribution. Properties of CED have been well established in homogenous gray and white matter, but only one study (Heiss et al., 2005) has examined CED in the hippocampus, a structure commonly affected in TLE. Therefore, to develop and optimize CED targeting for epilepsy treatment, infusions of Gd-albumin were performed in normal (Chapter 2) and injured (Chapter 3) rat hippocampi at two time points. We found hippocampal distributions to be influenced by the site and size of the target structure, density of cellular elements, presence and orientation of pial surfaces, and potentially, orientation of local axonal projections. We also found that distribution volumes varied with the extent of brain injury, with diffuse limbic system edema increasing the distribution volumes up to twice the volume measured in normal animals. Differences in distributions of injured animals are likely due to decreases in the size of extracellular channels, potentially resulting from ongoing neuronal degeneration and accumulation of neuroinflammatory markers in the interstitium. These changes, in addition to swelling of cellular elements and glia, affect diffusion parameters within the hippocampus and influence the spread of infusate. This is supported by the fact that the volume of infusate distributions 60 days post-SE returned to control ranges, accordant with the abatement of these markers. The effect of varying the infusion site and integrity of structure on distribution volume supports the hypothesis that anisotropic hippocampal neuroarchitecture plays a prominent role in the distribution of infusate. These results not only demonstrate a strategy for targeting and tracking therapies to the hippocampus, but they also provide guidance for the planning of infusion therapy in heterogenous tissue.

Developing Animal Models for the Progression of Epilepsy

The idea of preventative treatment for TLE was initiated in an article by Dr. Murray Falconer (Falconer, 1974). Dr. Falconer, and many others since, believes the latent period may offer a therapeutic window for the prevention of epileptogenesis. Experimental evidence suggests there is a cascade of morphologic and biological changes after an initial insult that are potential targets for the administration of neuroprotective or anti-ictal substances. SE models are ideal for studying the progression of epilepsy because they exhibit a latent period similar to the human condition. Preventative studies are currently performed on kindling, pilocarpine, or kainate models. However, these models are poor approximations of structural rearrangements that occur in humans. Kindling models produce little to no damage, while chemical models result in sizable injury with a high mortality rate. Moreover, chemical models act on specific receptors, which present a confound to pharmacological research and drug design.

In the electrical SE model presented here, we investigated the neuropathological changes occurring within 24 hours of SE (Chapter 3). This model is often considered to have the greatest parallels to human TLE, and thus was developed as a testing paradigm for CED infusions. At 24 hours post-SE, diffuse limbic injury was observed in the hippocampus (specifically CA3 and CA1), amygdala, piriform cortex, entorhinal cortex, middle thalamic and lateral thalamic nuclei, and lateral septum. Additionally, previous work (Parekh et al., 2010) has determined the presence of parahippocampal edema in this model is predictive of the development of spontaneous seizures. These early structural changes present a target for prophylactic treatment that resolve by the time spontaneous seizures begin, when animals exhibit varying amounts of neuronal

loss and gliosis, similar to human hippocampal injury. We found the extent of injury was a significant variable for infusate distribution volumes. This finding underscores the importance of using appropriate models for drug delivery.

Future Work

This dissertation discusses CED for the infusion of therapeutic agents for epilepsy treatment. Future work will focus on three extensions of these studies. Firstly, a larger CED study will be undertaken at chronic time points. Since there are millions of people in the world suffering from chronic epilepsy today, it is important to quantify distributions using more animals at this treatment time point. Preliminary data from two animals suggests distribution volumes at 60 days post-SE are not significantly different from controls, implying that control Gd-albumin distributions can reliably predict infusion patterns in chronic brain injury. We suspected ongoing neurodegeneration, cell loss, and Wallerian degeneration would create pooling within the enlarged ECS and decrease infusate volumes in the brain. Preliminary studies do not seem to support this hypothesis, but more animals are needed to make that conclusion.

Secondly, one important dimension not measured in the studies described is the distribution of concentration. Quantifying volume distributions is particularly relevant for infusions of toxic or lytic agents that should be controlled carefully. It is also important to know which structures are being targeted. However, the increase or decrease of distribution volumes in the brain implies differences in concentration across animals. Acquiring concentration measurements with MR are a future goal of these studies. Concentration can currently be determined with autoradiography studies post-mortem, but quantifying concentration maps using MR in addition to volumetric analyses will allow for true co-registration of infusate concentration and spatial spread *in vivo*.

Finally, a third, and natural extension of these studies is to use CED to deliver therapeutic agents. Work is currently being done to deliver light-activated protein channels into the hippocampus to evoke cell-type specific activity with light. These proteins can be virally transduced into any cell type with gene therapy, and then used to modulate cell firing. This approach can be used to explore the causal function of individual neuron types in epileptic circuitry and characterize the underlying cellular dysfunction in the hippocampus.

Future studies also include using CED to deliver nanoparticles encapsulating or conjugating potential drugs. Depending on their molecular weight and stability, nanoparticles can release drugs over hours and days to several months (Yasukawa et al., 2005). In general, nanoparticles are considered optimal for drug delivery to the brain as their mean size allows traveling through physical restrictions presented by the brain interstitial space. Nanoparticle encapsulation of the compound MRZ 2/576 resulted in an increased duration of its antiepileptic activity (Friese et al., 2000). Efforts have also been made to prepare and optimize nano-sized carrier systems for phenytoin (Thakur and Gupta, 2006), carbamazepine (Douroumis and Fahr, 2007), clonazepam (Jeong et al., 1998; Ryu et al., 2000), diazepam (Abdelbary and Fahmy, 2009), and valproic acid (Darius et al., 2000). Although experimental progress has been made in development of nano-carriers for AED release, pharmacokinetic data on the use of nanoparticles to deliver these drugs are very limited. Future work will focus on using CED to deliver and study *in vivo* pharmacodynamics.

LIST OF REFERENCES

Abdelbary G, Fahmy RH (2009) Diazepam-loaded solid lipid nanoparticles: design and characterization. AAPS PharmSciTech 10:211-219.

Abujudeh HH, Kaewlai R, Kagan A, Chibnik LB, Nazarian RM, High WA, Kay J (2009) Nephrogenic systemic fibrosis after gadopentetate dimeglumine exposure: case series of 36 patients. Radiology 253:81-89.

Agyare EK, Curran GL, Ramakrishnan M, Yu CC, Poduslo JF, Kandimalla KK (2008) Development of a smart nano-vehicle to target cerebrovascular amyloid deposits and brain parenchymal plaques observed in Alzheimer's disease and cerebral amyloid angiopathy. Pharm Res 25:2674-2684.

Amaral DG, Lavenex P (2007) Hippocampal Neuroanatomy. In: The Hippocampus Book, pp 37-94. New York: Oxford University Press.

Andersen P, Bliss TV, Lomo T, Olsen LI, Skrede KK (1969) Lamellar organization of hippocampal excitatory pathways. Acta Physiol Scand 76:4A-5A.

Astary GW, Kantorovich S, Carney PR, Mareci TH, Sarntinoranont M (2010) Regional convection-enhanced delivery of gadolinium-labeled albumin in the rat hippocampus in vivo. J Neurosci Methods 187:129-137.

Babb TL, Brown W.J. (1987) Pathological findings in epilepsy. In: Surgical Treatment of the Epilepsies (J. Enfel J, ed), pp 511-540. New York: Raven Press.

Baker GA, Jacoby A, Buck D, Stalgis C, Monnet D (1997) Quality of life of people with epilepsy: a European study. Epilepsia 38:353-362.

Bakhshi S, North RB (1995) Implantable pumps for drug delivery to the brain. J Neurooncol 26:133-139.

Bankiewicz KS, Eberling JL, Kohutnicka M, Jagust W, Pivirotto P, Bringas J, Cunningham J, Budinger TF, Harvey-White J (2000) Convection-enhanced delivery of AAV vector in parkinsonian monkeys; in vivo detection of gene expression and restoration of dopaminergic function using pro-drug approach. Exp Neurol 164:2-14.

Barcia JA, Gallego JM (2009) Intraventricular and intracerebral delivery of anti-epileptic drugs in the kindling model. Neurotherapeutics 6:337-343.

Basser PJ, Jones DK (2002) Diffusion-tensor MRI: theory, experimental design and data analysis - a technical review. NMR Biomed 15:456-467.

Ben-Ari Y, Crepel V, Represa A (2008) Seizures beget seizures in temporal lobe epilepsies: the boomerang effects of newly formed aberrant kainatergic synapses. Epilepsy Curr 8:68-72.

Beniczky S, Jose Miranda M, Alving J, Heber Povlsen J, Wolf P (2010) Effectiveness of the ketogenic diet in a broad range of seizure types and EEG features for severe childhood epilepsies. Acta Neurologica Scandinavica 121:58-62.

Berg AT, Vickrey BG, Langfitt JT, Sperling MR, Walczak TS, Shinnar S, Bazil CW, Pacia SV, Spencer SS (2003) The multicenter study of epilepsy surgery: recruitment and selection for surgery. Epilepsia 44:1425-1433.

Bernasconi N, Duchesne S, Janke A, Lerch J, Collins DL, Bernasconi A (2004) Whole-brain voxel-based statistical analysis of gray matter and white matter in temporal lobe epilepsy. Neuroimage 23:717-723.

Bertram EH (1997) Functional anatomy of spontaneous seizures in a rat model of limbic epilepsy. Epilepsia 38:95-105.

Bertram EH (2009) Temporal lobe epilepsy: where do the seizures really begin? Epilepsy Behav 14 Suppl 1:32-37.

Bertram EH, Cornett JF (1994) The evolution of a rat model of chronic spontaneous limbic seizures. Brain Res 661:157-162.

Bertram EH, Lothman EW, Lenn NJ (1990) The hippocampus in experimental chronic epilepsy: a morphometric analysis. Ann Neurol 27:43-48.

Bland M (1995) Methods based on rank order. In: An Introduction to Medical Statistics, pp 205-225. Oxford: Oxford University Press.

Blasberg RG, Patlak C, Fenstermacher JD (1975) Intrathecal chemotherapy: brain tissue profiles after ventriculocisternal perfusion. J Pharmacol Exp Ther 195:73-83.

Blumcke I, Thom M, Wiestler OD (2002) Ammon's horn sclerosis: a maldevelopmental disorder associated with temporal lobe epilepsy. Brain Pathol 12:199-211.

Blumcke I, Suter B, Behle K, Kuhn R, Schramm J, Elger CE, Wiestler OD (2000) Loss of hilar mossy cells in Ammon's horn sclerosis. Epilepsia 41 Suppl 6:S174-180.

Blumcke I, Zuschratter W, Schewe JC, Suter B, Lie AA, Riederer BM, Meyer B, Schramm J, Elger CE, Wiestler OD (1999) Cellular pathology of hilar neurons in Ammon's horn sclerosis. J Comp Neurol 414:437-453.

Blurton-Jones M, Kitazawa M, Martinez-Coria H, Castello NA, Muller FJ, Loring JF, Yamasaki TR, Poon WW, Green KN, LaFerla FM (2009) Neural stem cells improve cognition via BDNF in a transgenic model of Alzheimer disease. Proc Natl Acad Sci U S A 106:13594-13599.

Bobo RH, Laske DW, Akbasak A, Morrison PF, Dedrick RL, Oldfield EH (1994) Convection-enhanced delivery of macromolecules in the brain. Proc Natl Acad Sci U S A 91:2076-2080.

Bodor N, Kaminski JJ (1987) Prodrugs and site-specific chemical delivery systems. Annual Reports in Medicinal Chemistry 22:303-313.

Bondareff W, Pysh JJ (1968) Distribution of the extracellular space during postnatal maturation of rat cerebral cortex. Anat Rec 160:773-780.

Borowicz KK, Luszczki JJ, Duda AM, Czuczwar SJ (2003) Effect of topiramate on the anticonvulsant activity of conventional antiepileptic drugs in two models of experimental epilepsy. Epilepsia 44:640-646.

Bradbury MW (1985) The blood-brain barrier. Transport across the cerebral endothelium. Circ Res 57:213-222.

Brandt C, Potschka H, Loscher W, Ebert U (2003) N-methyl-D-aspartate receptor blockade after status epilepticus protects against limbic brain damage but not against epilepsy in the kainate model of temporal lobe epilepsy. Neuroscience 118:727-740.

Brightman MW (1965) The distribution within the brain of ferritin injected into cerebrospinal fluid compartments. II. Parenchymal distribution. Am J Anat 117:193-219.

Brodie MJ, Dichter MA (1996) Antiepileptic drugs. N Engl J Med 334:168-175.

Browne TR, Holmes GL (2001) Epilepsy. N Engl J Med 344:1145-1151.

Bruton C (1988) The neuropathology of temporal lobe epilepsy. In: Institute of Psychiatry Maudsley Monographs 31. Oxford, UK: Oxford University Press.

Burger C, Gorbatyuk OS, Velardo MJ, Peden CS, Williams P, Zolotukhin S, Reier PJ, Mandel RJ, Muzyczka N (2004) Recombinant AAV Viral Vectors Pseudotyped with Viral Capsids from Serotypes 1, 2, and 5 Display Differential Efficiency and Cell Tropism after Delivery to Different Regions of the Central Nervous System. Mol Ther 10:302-317.

Burtea C, Laurent S, Vander Elst L, Muller RN (2008) Contrast agents: magnetic resonance. Handb Exp Pharmacol:135-165.

Caravan P, Ellison JJ, McMurry TJ, Lauffer RB (1999) Gadolinium(III) Chelates as MRI Contrast Agents: Structure, Dynamics, and Applications. Chem Rev 99:2293-2352.

Castillo CG, Mendoza S, Freed WJ, Giordano M (2006) Intranigral transplants of immortalized GABAergic cells decrease the expression of kainic acid-induced seizures in the rat. Behav Brain Res 171:109-115.

Cavalheiro E (1995) The pilocarpine model of epilepsy. The Italian Journal of Neurological Sciences 16:33-37.

Cearley CN, Wolfe JH (2006) Transduction characteristics of adeno-associated virus vectors expressing cap serotypes 7, 8, 9, and Rh10 in the mouse brain. Mol Ther 13:528-537.

Charous SJ, Kempster G, Manders E, Ristanovic R (2001) The effect of vagal nerve stimulation on voice. Laryngoscope 111:2028-2031.

Chen MY, Lonser RR, Morrison PF, Governale LS, Oldfield EH (1999) Variables affecting convection-enhanced delivery to the striatum: a systematic examination of rate of infusion, cannula size, infusate concentration, and tissue-cannula sealing time. J Neurosurg 90:315-320.

Chen MY, Hoffer A, Morrison PF, Hamilton JF, Hughes J, Schlageter KS, Lee J, Kelly BR, Oldfield EH (2005) Surface properties, more than size, limiting convective distribution of virus-sized particles and viruses in the central nervous system. J Neurosurg 103:311-319.

Chen X, Astary GW, Sepulveda H, Mareci TH, Sarntinoranont M (2008) Quantitative assessment of macromolecular concentration during direct infusion into an agarose hydrogel phantom using contrast-enhanced MRI. Magn Reson Imaging 26:1433-1441.

Chu K, Kim M, Jung KH, Jeon D, Lee ST, Kim J, Jeong SW, Kim SU, Lee SK, Shin HS (2004) Human neural stem cell transplantation reduces spontaneous recurrent seizures following pilocarpine-induced status epilepticus in adult rats. Brain Research 1023:213-221.

Coloma MJ, Lee HJ, Kurihara A, Landaw EM, Boado RJ, Morrison SL, Pardridge WM (2000) Transport across the primate blood-brain barrier of a genetically engineered chimeric monoclonal antibody to the human insulin receptor. Pharm Res 17:266-274.

Commission on Classification and Terminology of the International League Against Epilepsy (1981) Proposal for revised clinical and electroencephalographic classification of epileptic seizures. Epilepsia 22:489-501.

Commission on Classification and Terminology of the International League Against Epilepsy (1989) Proposal for revised classification of epilepsies and epileptic syndromes. Epilepsia 30:389-399.

Commission on Epidemiology and Prognosis of the International League Against Epilepsy (1993) Guidelines for epidemiologic studies on epilepsy. . Epilepsia 34:592-596.

Corsellis JA, Goldberg GJ, Norton AR (1968) "Limbic encephalitis" and its association with carcinoma. Brain 91:481-496.

Cragg B (1979) Brain extracellular space fixed for electron microscopy. Neurosci Lett 15:301-306.

Cundy KC, Annamalai T, Bu L, De Vera J, Estrela J, Luo W, Shirsat P, Torneros A, Yao F, Zou J, Barrett RW, Gallop MA (2004) XP13512 [(+/-)-1-([(alpha-isobutanoyloxyethoxy)carbonyl] aminomethyl)-1-cyclohexane acetic acid], a novel gabapentin prodrug: II. Improved oral bioavailability, dose proportionality, and colonic absorption compared with gabapentin in rats and monkeys. J Pharmacol Exp Ther 311:324-333.

Darius J, Meyer FP, Sabel BA, Schroeder U (2000) Influence of nanoparticles on the brain-to-serum distribution and the metabolism of valproic acid in mice. J Pharm Pharmacol 52:1043-1047.

Davidson BL, Stein CS, Heth JA, Martins I, Kotin RM, Derksen TA, Zabner J, Ghodsi A, Chiorini JA (2000) Recombinant adeno-associated virus type 2, 4, and 5 vectors: transduction of variant cell types and regions in the mammalian central nervous system. Proc Natl Acad Sci U S A 97:3428-3432.

de Lanerolle NC, Lee TS (2005) New facets of the neuropathology and molecular profile of human temporal lobe epilepsy. Epilepsy Behav 7:190-203.

de Lanerolle NC, Kim JH, Williamson A, Spencer SS, Zaveri HP, Eid T, Spencer DD (2003) A retrospective analysis of hippocampal pathology in human temporal lobe epilepsy: evidence for distinctive patient subcategories. Epilepsia 44:677-687.

DeGiorgio CM et al. (2000) Prospective long-term study of vagus nerve stimulation for the treatment of refractory seizures. Epilepsia 41:1195-1200.

Demeule M, Regina A, Che C, Poirier J, Nguyen T, Gabathuler R, Castaigne JP, Beliveau R (2008) Identification and design of peptides as a new drug delivery system for the brain. J Pharmacol Exp Ther 324:1064-1072.

deToledo-Morrell L, Stoub TR, Wang C (2007) Hippocampal atrophy and disconnection in incipient and mild Alzheimer's disease. Prog Brain Res 163:741-753.

Dickson DW, Davies P, Bevona C, Van Hoeven KH, Factor SM, Grober E, Aronson MK, Crystal HA (1994) Hippocampal sclerosis: a common pathological feature of dementia in very old (> or = 80 years of age) humans. Acta Neuropathol 88:212-221.

Dietzel I, Heinemann U, Lux HD (1989) Relations between slow extracellular potential changes, glial potassium buffering, and electrolyte and cellular volume changes during neuronal hyperactivity in cat brain. Glia 2:25-44.

Dietzel I, Heinemann U, Hofmeier G, Lux HD (1980) Transient changes in the size of the extracellular space in the sensorimotor cortex of cats in relation to stimulus-induced changes in potassium concentration. Exp Brain Res 40:432-439.

Ding D, Kanaly CW, Cummings TJ, Ii JE, Raghavan R, Sampson JH (2009) Long-term safety of combined intracerebral delivery of free gadolinium and targeted chemotherapeutic agent PRX321. Neurol Res.

Dolorfo CL, Amaral DG (1998) Entorhinal cortex of the rat: topographic organization of the cells of origin of the perforant path projection to the dentate gyrus. J Comp Neurol 398:25-48.

Doolittle ND, Abrey LE, Ferrari N, Hall WA, Laws ER, McLendon RE, Muldoon LL, Peereboom D, Peterson DR, Reynolds CP, Senter P, Neuwelt EA (2002) Targeted delivery in primary and metastatic brain tumors: summary report of the seventh annual meeting of the Blood-Brain Barrier Disruption Consortium. Clin Cancer Res 8:1702-1709.

Douroumis D, Fahr A (2007) Stable carbamazepine colloidal systems using the cosolvent technique. Eur J Pharm Sci 30:367-374.

Du F, Schwarcz R, Tamminga CA (1995) Entorhinal cortex in temporal lobe epilepsy. Am J Psychiatry 152:826.

Du F, Whetsell WO, Jr., Abou-Khalil B, Blumenkopf B, Lothman EW, Schwarcz R (1993) Preferential neuronal loss in layer III of the entorhinal cortex in patients with temporal lobe epilepsy. Epilepsy Res 16:223-233.

Duyckaerts C, Panchal M, Delatour B, Potier MC (2009) [Morphologic and molecular neuropathology of Alzheimer's disease.]. Ann Pharm Fr 67:127-135.

Engel J, Jr. (2001a) A proposed diagnostic scheme for people with epileptic seizures and with epilepsy: report of the ILAE Task Force on Classification and Terminology. Epilepsia 42:796-803.

Engel J, Jr. (2001b) Intractable epilepsy: definition and neurobiology. Epilepsia 42 Suppl 6:3.

Esclassan F, Coutureau E, Di Scala G, Marchand AR (2009) Differential contribution of dorsal and ventral hippocampus to trace and delay fear conditioning. Hippocampus 19:33-44.

Fa Z, Zhang R, Li P, Zhang J, Zhang P, Zhu S, Wu Q, Huang F, Liu Y, Yang L, Chang H, Wen Z, Gao D, Zeng Y, Jiang X (2011) Effects of temporarily disrupting BBB on activity-induced manganese-dependent functional MRI. Brain Imaging Behav 5:181-188.

Fabene P, Marzola P, Sbarbati A, Bentivoglio M (2003) Magnetic resonance imaging of changes elicited by status epilepticus in the rat brain: diffusion-weighted and T2-weighted images, regional blood volume maps, and direct correlation with tissue and cell damage. Neuroimage 18:375-389.

Falconer MA (1974) Mesial temporal (Ammon's horn) sclerosis as a common cause of epilepsy. Aetiology, treatment, and prevention. Lancet 2:767-770.

Fechner J, Schwilden H, Schuttler J (2008) Pharmacokinetics and pharmacodynamics of GPI 15715 or fospropofol (Aquavan injection) - a water-soluble propofol prodrug. Handb Exp Pharmacol:253-266.

Fenstermacher J, Kaye T (1988) Drug "diffusion" within the brain. Ann N Y Acad Sci 531:29-39.

Fiandaca MS, Varenika V, Eberling J, McKnight T, Bringas J, Pivirotto P, Beyer J, Hadaczek P, Bowers W, Park J, Federoff H, Forsayeth J, Bankiewicz KS (2009) Real-time MR imaging of adeno-associated viral vector delivery to the primate brain. Neuroimage 47 Suppl 2:T27-35.

Foley CP, Nishimura N, Neeves KB, Schaffer CB, Olbricht WL (2009) Flexible microfluidic devices supported by biodegradable insertion scaffolds for convection-enhanced neural drug delivery. Biomed Microdevices 11:915-924.

French JA, Williamson PD, Thadani VM, Darcey TM, Mattson RH, Spencer SS, Spencer DD (1993) Characteristics of medial temporal lobe epilepsy: I. Results of history and physical examination. Ann Neurol 34:774-780.

Fricke R, Cowan WM (1978) An autoradiographic study of the commissural and ipsilateral hippocampo-dentate projections in the adult rat. J Comp Neurol 181:253-269.

Friedman A (2011) Blood-brain barrier dysfunction, status epilepticus, seizures, and epilepsy: a puzzle of a chicken and egg? Epilepsia 52 Suppl 8:19-20.

Friese A, Seiller E, Quack G, Lorenz B, Kreuter J (2000) Increase of the duration of the anticonvulsive activity of a novel NMDA receptor antagonist using poly(butylcyanoacrylate) nanoparticles as a parenteral controlled release system. Eur J Pharm Biopharm 49:103-109.

Gabathuler R (2010) Approaches to transport therapeutic drugs across the blood-brain barrier to treat brain diseases. Neurobiol Dis 37:48-57.

Gant JC, Thibault O, Blalock EM, Yang J, Bachstetter A, Kotick J, Schauwecker PE, Hauser KF, Smith GM, Mervis R, Li Y, Barnes GN (2009) Decreased number of interneurons and increased seizures in neuropilin 2 deficient mice: implications for autism and epilepsy. Epilepsia 50:629-645.

Gasior M, White NA, Rogawski MA (2007) Prolonged attenuation of amygdala-kindled seizure measures in rats by convection-enhanced delivery of the N-type calcium channel antagonists omega-conotoxin GVIA and omega-conotoxin MVIIA. J Pharmacol Exp Ther 323:458-468.

Gernert M, Thompson KW, Loscher W, Tobin AJ (2002) Genetically engineered GABA-producing cells demonstrate anticonvulsant effects and long-term transgene expression when transplanted into the central piriform cortex of rats. Exp Neurol 176:183-192.

Geyelin HR (1921) Fasting as a method for treating epilepsy. Med Record 99:1037-1039.

Gibbons JD (1993) Nonparametric measures of association. Thousand Oaks, CA: Sage Publication.

Gill SS, Patel NK, Hotton GR, O'Sullivan K, McCarter R, Bunnage M, Brooks DJ, Svendsen CN, Heywood P (2003) Direct brain infusion of glial cell line-derived neurotrophic factor in Parkinson disease. Nat Med 9:589-595.

Goldstein GW, Betz AL (1986) The blood-brain barrier. Sci Am 255:74-83.

Goodman JH (1998) Experimental models of status epilepticus. In: Neuropharmacological Methods in Epilepsy Research (Peterson SL, Albertson T.E., ed), pp 95-125. Boca Raton: CRC Press.

Gorter JA, Goncalves Pereira PM, van Vliet EA, Aronica E, Lopes da Silva FH, Lucassen PJ (2003) Neuronal cell death in a rat model for mesial temporal lobe epilepsy is induced by the initial status epilepticus and not by later repeated spontaneous seizures. Epilepsia 44:647-658.

Gowers WR (1881) Epilepsy and other chronic convulsive diseases; their causes, symptoms and treatment. London: J&A Churchill.

Groothuis DR, Vavra MW, Schlageter KE, Kang EW, Itskovich AC, Hertzler S, Allen CV, Lipton HL (2007) Efflux of drugs and solutes from brain: the interactive roles of diffusional transcapillary transport, bulk flow and capillary transporters. J Cereb Blood Flow Metab 27:43-56.

Guarnieri M, Carson BS, Khan A, Penno M, Jallo GI (2005) Flexible versus rigid catheters for chronic administration of exogenous agents into central nervous system tissues. J Neurosci Methods 144:147-152.

Haberman RP, Samulski RJ, McCown TJ (2003) Attenuation of seizures and neuronal death by adeno-associated virus vector galanin expression and secretion. Nat Med 9:1076-1080.

Haluska M, Anthony ML (2004) Osmotic blood-brain barrier modification for the treatment of malignant brain tumors. Clin J Oncol Nurs 8:263-267.

Handforth A, Treiman DM (1994) A new, non-pharmacologic model of convulsive status epilepticus induced by electrical stimulation: behavioral/electroencephalographic observations and response to phenytoin and phenobarbital. Epilepsy Res 19:15-25.

Harbaugh RE, Saunders RL, Reeder RF (1988) Use of implantable pumps for central nervous system drug infusions to treat neurological disease. Neurosurgery 23:693-698.

Haring JH, Davis JN (1985) Differential distribution of locus coeruleus projections to the hippocampal formation: anatomical and biochemical evidence. Brain Res 325:366-369.

Hattiangady B, Rao MS, Shetty AK (2008) Grafting of striatal precursor cells into hippocampus shortly after status epilepticus restrains chronic temporal lobe epilepsy. Exp Neurol 212:468-481.

Hauser WA (1997) Incidence and prevalence. Philadelphia: Lippincott-Raven.

Hauser WA, Lee JR (2002) Do seizures beget seizures? Progress in Brain Research 135:215-219.

Heiss JD, Walbridge S, Morrison P, Hampton RR, Sato S, Vortmeyer A, Butman JA, O'Malley J, Vidwan P, Dedrick RL, Oldfield EH (2005) Local distribution and toxicity of prolonged hippocampal infusion of muscimol. J Neurosurg 103:1035-1045.

Hellier JL, Patrylo PR, Buckmaster PS, Dudek FE (1998) Recurrent spontaneous motor seizures after repeated low-dose systemic treatment with kainate: assessment of a rat model of temporal lobe epilepsy. Epilepsy Res 31:73-84.

Hoehn M, Kustermann E, Blunk J, Wiedermann D, Trapp T, Wecker S, Focking M, Arnold H, Hescheler J, Fleischmann BK, Schwindt W, Buhrle C (2002) Monitoring of implanted stem cell migration in vivo: a highly resolved in vivo magnetic resonance imaging investigation of experimental stroke in rat. Proc Natl Acad Sci U S A 99:16267-16272.

Hrabetova S (2005) Extracellular diffusion is fast and isotropic in the stratum radiatum of hippocampal CA1 region in rat brain slices. Hippocampus 15:441-450.

Hrabetova S, Nicholson C (2000) Dextran decreases extracellular tortuosity in thick-slice ischemia model. J Cereb Blood Flow Metab 20:1306-1310.

Hrabetova S, Nicholson C (2007) Biophysical Properties of Brain Extracellular Space Explored with Ion-Selective Microelectrodes, Integrative Optical Imaging and Related Techniques. In: Electrochemical Methods for Neuroscience (Michael AC, Borland LM, eds). Boca Raton (FL).

Hsu YH, Lee WT, Chang C (2007) Multiparametric MRI evaluation of kainic acid-induced neuronal activation in rat hippocampus. Brain 130:3124-3134.

Hudson LP, Munoz DG, Miller L, McLachlan RS, Girvin JP, Blume WT (1993) Amygdaloid sclerosis in temporal lobe epilepsy. Ann Neurol 33:622-631.

Hughes GA (2005) Nanostructure-mediated drug delivery. Nanomedicine 1:22-30.

Humphrey T (1967) The development of the human hippocampal fissure. J Anat 101:655-676.

Huttunen KM, Raunio H, Rautio J (2011) Prodrugs--from serendipity to rational design. Pharmacol Rev 63:750-771.

Hwang DW, Son S, Jang J, Youn H, Lee S, Lee D, Lee YS, Jeong JM, Kim WJ, Lee DS (2011) A brain-targeted rabies virus glycoprotein-disulfide linked PEI nanocarrier for delivery of neurogenic microRNA. Biomaterials.

Ishizuka N, Weber J, Amaral DG (1990) Organization of intrahippocampal projections originating from CA3 pyramidal cells in the rat. J Comp Neurol 295:580-623.

Ivanchenko O, Ivanchenko V (2011) Designing and testing of backflow-free catheters. J Biomech Eng 133:061003.

Jagannathan J, Walbridge S, Butman JA, Oldfield EH, Lonser RR (2008) Effect of ependymal and pial surfaces on convection-enhanced delivery. J Neurosurg 109:547-552.

Jeong YI, Cheon JB, Kim SH, Nah JW, Lee YM, Sung YK, Akaike T, Cho CS (1998) Clonazepam release from core-shell type nanoparticles in vitro. J Control Release 51:169-178.

Jung MW, Wiener SI, McNaughton BL (1994) Comparison of spatial firing characteristics of units in dorsal and ventral hippocampus of the rat. J Neurosci 14:7347-7356.

Kanter-Schlifke I, Toft Sorensen A, Ledri M, Kuteeva E, Hokfelt T, Kokaia M (2007) Galanin gene transfer curtails generalized seizures in kindled rats without altering hippocampal synaptic plasticity. Neuroscience 150:984-992.

Karkan D, Pfeifer C, Vitalis TZ, Arthur G, Ujiie M, Chen Q, Tsai S, Koliatis G, Gabathuler R, Jefferies WA (2008) A unique carrier for delivery of therapeutic compounds beyond the blood-brain barrier. PLoS One 3:e2469.

Kikuchi T, Saito R, Sugiyama S, Yamashita Y, Kumabe T, Krauze M, Bankiewicz K, Tominaga T (2008) Convection-enhanced delivery of polyethylene glycol-coated liposomal doxorubicin: characterization and efficacy in rat intracranial glioma models. J Neurosurg 109:867-873.

Kim JA, Chung JI, Yoon PH, Kim DI, Chung TS, Kim EJ, Jeong EK (2001) Transient MR signal changes in patients with generalized tonicoclonic seizure or status epilepticus: periictal diffusion-weighted imaging. American journal of neuroradiology 22:1149-1160.

Kim JH, Mareci TH, Sarntinoranont M (2010) A voxelized model of direct infusion into the corpus callosum and hippocampus of the rat brain: model development and parameter analysis. Med Biol Eng Comput 48:203-214.

Kim JH, Astary GW, Chen X, Mareci TH, Sarntinoranont M (2009) Voxelized model of interstitial transport in the rat spinal cord following direct infusion into white matter. J Biomech Eng 131:071007.

Klein RL, Dayton RD, Tatom JB, Henderson KM, Henning PP (2007) AAV8, 9, Rh10, Rh43 Vector Gene Transfer in the Rat Brain: Effects of Serotype, Promoter and Purification Method. Mol Ther 16:89-96.

Klein RL, Dayton RD, Leidenheimer NJ, Jansen K, Golde TE, Zweig RM (2006) Efficient neuronal gene transfer with AAV8 leads to neurotoxic levels of tau or green fluorescent proteins. Mol Ther 13:517-527.

Krauze MT, Forsayeth J, Park JW, Bankiewicz KS (2006) Real-time imaging and quantification of brain delivery of liposomes. Pharm Res 23:2493-2504.

Krauze MT, Saito R, Noble C, Tamas M, Bringas J, Park JW, Berger MS, Bankiewicz K (2005) Reflux-free cannula for convection-enhanced high-speed delivery of therapeutic agents. J Neurosurg 103:923-929.

Krauze MT, Vandenberg SR, Yamashita Y, Saito R, Forsayeth J, Noble C, Park J, Bankiewicz KS (2008) Safety of real-time convection-enhanced delivery of liposomes to primate brain: a long-term retrospective. Exp Neurol 210:638-644.

Krettek JE, Price JL (1977) Projections from the amygdaloid complex and adjacent olfactory structures to the entorhinal cortex and to the subiculum in the rat and cat. J Comp Neurol 172:723-752.

Kuzniecky R, de la Sayette V, Ethier R, Melanson D, Andermann F, Berkovic S, Robitaille Y, Olivier A, Peters T, Feindel W (1987) Magnetic resonance imaging in temporal lobe epilepsy: pathological correlations. Ann Neurol 22:341-347.

Lambert DM (2000) Rationale and applications of lipids as prodrug carriers. Eur J Pharm Sci 11 Suppl 2:S15-27.

Lauffer RB, Vincent AC, Padmanabhan S, Villringer A, Saini S, Elmaleh DR, Brady TJ (1987) Hepatobiliary MR contrast agents: 5-substituted iron-EHPG derivatives. Magn Reson Med 4:582-590.

Lee SJ, Sun J, Flint JJ, Guo S, Xie HK, King MA, Sarntinoranont M (2011) Optically based-indentation technique for acute rat brain tissue slices and thin biomaterials. J Biomed Mater Res B Appl Biomater 97:84-95.

Lewis DV (2005) Losing neurons: selective vulnerability and mesial temporal sclerosis. Epilepsia 46 Suppl 7:39-44.

Li T, Ren G, Lusardi T, Wilz A, Lan JQ, Iwasato T, Itohara S, Simon RP, Boison D (2008) Adenosine kinase is a target for the prediction and prevention of epileptogenesis in mice. J Clin Invest 118:571-582.

Li T, Steinbeck JA, Lusardi T, Koch P, Lan JQ, Wilz A, Segschneider M, Simon RP, Brustle O, Boison D (2007) Suppression of kindling epileptogenesis by adenosine releasing stem cell-derived brain implants. Brain 130:1276-1288.

Li XG, Somogyi P, Ylinen A, Buzsaki G (1994) The hippocampal CA3 network: an in vivo intracellular labeling study. J Comp Neurol 339:181-208.

Liu KC, Bhardwaj A (2007) Use of prophylactic anticonvulsants in neurologic critical care: a critical appraisal. Neurocrit Care 7:175-184.

Lonser RR, Walbridge S, Garmestani K, Butman JA, Walters HA, Vortmeyer AO, Morrison PF, Brechbiel MW, Oldfield EH (2002) Successful and safe perfusion of the primate brainstem: in vivo magnetic resonance imaging of macromolecular distribution during infusion. J Neurosurg 97:905-913.

Loscher W (1997) Animal models of intractable epilepsy. Prog Neurobiol 53:239-258.

Loscher W (2011) Critical review of current animal models of seizures and epilepsy used in the discovery and development of new antiepileptic drugs. Seizure 20:359-368.

Loscher W, Schmidt D (2002) New horizons in the development of antiepileptic drugs. Epilepsy Res 50:3-16.

Loscher W, Gernert M, Heinemann U (2008) Cell and gene therapies in epilepsy--promising avenues or blind alleys? Trends Neurosci 31:62-73.

Lothman EW, Bertram EH, Bekenstein JW, Perlin JB (1989) Self-sustaining limbic status epilepticus induced by 'continuous' hippocampal stimulation: electrographic and behavioral characteristics. Epilepsy Res 3:107-119.

Lothman EW, Bertram EH, Kapur J, Stringer JL (1990) Recurrent spontaneous hippocampal seizures in the rat as a chronic sequela to limbic status epilepticus. Epilepsy Res 6:110-118.

Luo D, Woodrow-Mumford K, Belcheva N, Saltzman WM (1999) Controlled DNA delivery systems. Pharm Res 16:1300-1308.

MacKay JA, Deen DF, Szoka FC, Jr. (2005) Distribution in brain of liposomes after convection enhanced delivery; modulation by particle charge, particle diameter, and presence of steric coating. Brain Res 1035:139-153.

Maier M, Ron MA, Barker GJ, Tofts PS (1995) Proton magnetic resonance spectroscopy: an in vivo method of estimating hippocampal neuronal depletion in schizophrenia. Psychol Med 25:1201-1209.

Mandel RJ, Manfredsson FP, Foust KD, Rising A, Reimsnider S, Nash K, Burger C (2006) Recombinant adeno-associated viral vectors as therapeutic agents to treat neurological disorders. Mol Ther 13:463-483.

Manford M, Hart YM, Sander JW, Shorvon SD (1992) The National General Practice Study of Epilepsy. The syndromic classification of the International League Against Epilepsy applied to epilepsy in a general population. Arch Neurol 49:801-808.

Marchi N, Teng Q, Ghosh C, Fan Q, Nguyen MT, Desai NK, Bawa H, Rasmussen P, Masaryk TK, Janigro D (2010) Blood-brain barrier damage, but not parenchymal white blood cells, is a hallmark of seizure activity. Brain Res 1353:176-186.

Marchi N, Angelov L, Masaryk T, Fazio V, Granata T, Hernandez N, Hallene K, Diglaw T, Franic L, Najm I, Janigro D (2007) Seizure-promoting effect of blood-brain barrier disruption. Epilepsia 48:732-742.

Mardor Y, Last D, Daniels D, Shneor R, Maier SE, Nass D, Ram Z (2009) Convection-enhanced drug delivery of interleukin-4 Pseudomonas exotoxin (PRX321): increased distribution and magnetic resonance monitoring. J Pharmacol Exp Ther 330:520-525.

Margerison JH, Corsellis JA (1966) Epilepsy and the temporal lobes. A clinical, electroencephalographic and neuropathological study of the brain in epilepsy, with particular reference to the temporal lobes. Brain 89:499-530.

Marks WJ, Jr., Ostrem JL, Verhagen L, Starr PA, Larson PS, Bakay RA, Taylor R, Cahn-Weiner DA, Stoessl AJ, Olanow CW, Bartus RT (2008) Safety and tolerability of intraputaminal delivery of CERE-120 (adeno-associated virus serotype 2-neurturin) to patients with idiopathic Parkinson's disease: an open-label, phase I trial. Lancet Neurol 7:400-408.

Mathern GW, Pretorius JK, Babb TL (1995a) Quantified patterns of mossy fiber sprouting and neuron densities in hippocampal and lesional seizures. J Neurosurg 82:211-219.

Mathern GW, Babb TL, Pretorius JK, Leite JP (1995b) Reactive synaptogenesis and neuron densities for neuropeptide Y, somatostatin, and glutamate decarboxylase immunoreactivity in the epileptogenic human fascia dentata. J Neurosci 15:3990-4004.

Mathern GW, Babb TL, Leite JP, Pretorius K, Yeoman KM, Kuhlman PA (1996) The pathogenic and progressive features of chronic human hippocampal epilepsy. Epilepsy Res 26:151-161.

Mazel T, Simonova Z, Sykova E (1998) Diffusion heterogeneity and anisotropy in rat hippocampus. Neuroreport 9:1299-1304.

McBain CJ, Traynelis SF, Dingledine R (1990) Regional variation of extracellular space in the hippocampus. Science 249:674-677.

McCown TJ (2006) Adeno-associated virus-mediated expression and constitutive secretion of galanin suppresses limbic seizure activity in vivo. Mol Ther 14:63-68.

McCown TJ, Xiao X, Li J, Breese GR, Samulski RJ (1996) Differential and persistent expression patterns of CNS gene transfer by an adeno-associated virus (AAV) vector. Brain Res 713:99-107.

McGrew MJ, Sherman A, Ellard FM, Lillico SG, Gilhooley HJ, Kingsman AJ, Mitrophanous KA, Sang H (2004) Efficient production of germline transgenic chickens using lentiviral vectors. EMBO Rep 5:728-733.

McLaughlin J, Roozendaal B, Dumas T, Gupta A, Ajilore O, Hsieh J, Ho D, Lawrence M, McGaugh JL, Sapolsky R (2000) Sparing of neuronal function postseizure with gene therapy. Proc Natl Acad Sci U S A 97:12804-12809.

Meierkord H, Wieshmann U, Niehaus L, Lehmann R (1997) Structural consequences of status epilepticus demonstrated with serial magnetic resonance imaging. Acta Neurologica Scandinavica 96:127-132.

Mirski MA, Ferrendelli JA (1986) Anterior thalamic mediation of generalized pentylenetetrazol seizures. Brain Res 399:212-223.

Misra A, Ganesh S, Shahiwala A, Shah SP (2003) Drug delivery to the central nervous system: a review. J Pharm Pharm Sci 6:252-273.

Modlich U, Baum C (2009) Preventing and exploiting the oncogenic potential of integrating gene vectors. J Clin Invest 119:755-758.

Morrison PF, Chen MY, Chadwick RS, Lonser RR, Oldfield EH (1999) Focal delivery during direct infusion to brain: role of flow rate, catheter diameter, and tissue mechanics. Am J Physiol 277:R1218-1229.

Moser E, Moser MB, Andersen P (1993) Spatial learning impairment parallels the magnitude of dorsal hippocampal lesions, but is hardly present following ventral lesions. J Neurosci 13:3916-3925.

Nair S SD, Pardalos PD, Lasemidis L, Sackellares JC, Carney PR (2005) Dynamical Responses to Hippocampal Stimulation in a Rodent Model of Chronic Limbic Epilepsy. Epilepsia 46 Suppl:332.

Nairismagi J, Pitkanen A, Kettunen MI, Kauppinen RA, Kubova H (2006) Status epilepticus in 12-day-old rats leads to temporal lobe neurodegeneration and volume reduction: a histologic and MRI study. Epilepsia 47:479-488.

Nakasu Y, Nakasu S, Morikawa S, Uemura S, Inubushi T, Handa J (1995) Diffusion-weighted MR in experimental sustained seizures elicited with kainic acid. American journal of neuroradiology 16:1185-1192.

Nelson MD, Saykin AJ, Flashman LA, Riordan HJ (1998) Hippocampal volume reduction in schizophrenia as assessed by magnetic resonance imaging: a meta-analytic study. Arch Gen Psychiatry 55:433-440.

Neuwelt EA (2004) Mechanisms of disease: the blood-brain barrier. Neurosurgery 54:131-140; discussion 141-132.

Nicholson C, Sykova E (1998) Extracellular space structure revealed by diffusion analysis. Trends Neurosci 21:207-215.

Nicoletti JN, Shah SK, McCloskey DP, Goodman JH, Elkady A, Atassi H, Hylton D, Rudge JS, Scharfman HE, Croll SD (2008) Vascular endothelial growth factor is up-regulated after status epilepticus and protects against seizure-induced neuronal loss in hippocampus. Neuroscience 151:232-241.

Nitsch C, Klatzo I (1983) Regional patterns of blood-brain barrier breakdown during epileptiform seizures induced by various convulsive agents. J Neurol Sci 59:305-322.

Njie eG, Kantorovich S, Astary GW, Green C, Zheng T, Semple-Rowland SL, Steindler DA, Sarntinoranont M, Streit WJ, Borchelt DR (2012) A Preclinical Assessment of Neural Stem Cells as Delivery Vehicles for Anti-Amyloid Therapeutics. PLoS One 7: e34097. doi:10.1371/journal.pone.0034097.

Noe F, Nissinen J, Pitkanen A, Gobbi M, Sperk G, During M, Vezzani A (2007) Gene therapy in epilepsy: the focus on NPY. Peptides 28:377-383.

Noe F, Pool AH, Nissinen J, Gobbi M, Bland R, Rizzi M, Balducci C, Ferraguti F, Sperk G, During MJ, Pitkanen A, Vezzani A (2008) Neuropeptide Y gene therapy decreases chronic spontaneous seizures in a rat model of temporal lobe epilepsy. Brain 131:1506-1515.

Ohm TG (2007) The dentate gyrus in Alzheimer's disease. Prog Brain Res 163:723-740.

Olstorn H, Moe MC, Roste GK, Bueters T, Langmoen IA (2007) Transplantation of stem cells from the adult human brain to the adult rat brain. Neurosurgery 60:1089-1098; discussion 1098-1089.

Ommaya AK (1963) Subcutaneous Reservoir and Pump for Sterile Access to Ventricular Cerebrospinal Fluid. Lancet 2:983-984.

Oommen J, Kraus AC, Fisher RS (2007) Intraventricular administration of gabapentin in the rat increases flurothyl seizure threshold. Neurosci Lett 417:308-311.

Pardridge WM (1988) Recent advances in blood-brain barrier transport. Annu Rev Pharmacol Toxicol 28:25-39.

Pardridge WM (1997) Drug delivery to the brain. J Cereb Blood Flow Metab 17:713-731.

Pardridge WM (2003a) Blood-brain barrier genomics and the use of endogenous transporters to cause drug penetration into the brain. Curr Opin Drug Discov Devel 6:683-691.

Pardridge WM (2003b) Molecular biology of the blood-brain barrier. Methods Mol Med 89:385-399.

Pardridge WM (2005) The blood-brain barrier: bottleneck in brain drug development. NeuroRx 2:3-14.

Pardridge WM (2007) Drug targeting to the brain. Pharm Res 24:1733-1744.

Parekh MB, Carney PR, Sepulveda H, Norman W, King M, Mareci TH (2010) Early MR diffusion and relaxation changes in the parahippocampal gyrus precede the onset of spontaneous seizures in an animal model of chronic limbic epilepsy. Exp Neurol 224:258-270.

Park KI, Himes BT, Stieg PE, Tessler A, Fischer I, Snyder EY (2006) Neural stem cells may be uniquely suited for combined gene therapy and cell replacement: Evidence from engraftment of Neurotrophin-3-expressing stem cells in hypoxic-ischemic brain injury. Exp Neurol 199:179-190.

Paxinos GW, C. (1998) The rat brain in stereotaxic coordinates, 4th Edition. San Diego: Academic Press.

Perez-Pinzon MA, Tao L, Nicholson C (1995) Extracellular potassium, volume fraction, and tortuosity in rat hippocampal CA1, CA3, and cortical slices during ischemia. J Neurophysiol 74:565-573.

Peura L, Malmioja K, Laine K, Leppanen J, Gynther M, Isotalo A, Rautio J (2011) Large amino acid transporter 1 (LAT1) prodrugs of valproic acid: new prodrug design ideas for central nervous system delivery. Mol Pharm 8:1857-1866.

Pitkanen A (2002a) Efficacy of current antiepileptics to prevent neurodegeneration in epilepsy models. Epilepsy Res 50:141-160.

Pitkanen A (2002b) Drug-mediated neuroprotection and antiepileptogenesis: animal data. Neurology 59:S27-33.

Pitkanen A, Sutula TP (2002) Is epilepsy a progressive disorder? Prospects for new therapeutic approaches in temporal-lobe epilepsy. Lancet Neurol 1:173-181.

Racine RJ (1972) Modification of seizure activity by electrical stimulation. II. Motor seizure. Electroencephalogr Clin Neurophysiol 32:281-294.

Radojevic V, Kapfhammer JP (2009) Directed fiber outgrowth from transplanted embryonic cortex-derived neurospheres in the adult mouse brain. Neural Plast 2009:852492.

Raghavan R, Brady ML, Rodriguez-Ponce MI, Hartlep A, Pedain C, Sampson JH (2006) Convection-enhanced delivery of therapeutics for brain disease, and its optimization. Neurosurg Focus 20:E12.

Rao MS, Hattiangady B, Rai KS, Shetty AK (2007) Strategies for promoting anti-seizure effects of hippocampal fetal cells grafted into the hippocampus of rats exhibiting chronic temporal lobe epilepsy. Neurobiol Dis 27:117-132.

Raol YH, Lund IV, Bandyopadhyay S, Zhang G, Roberts DS, Wolfe JH, Russek SJ, Brooks-Kayal AR (2006) Enhancing GABA(A) receptor alpha 1 subunit levels in hippocampal dentate gyrus inhibits epilepsy development in an animal model of temporal lobe epilepsy. J Neurosci 26:11342-11346.

Rapoport SI (2000) Osmotic opening of the blood-brain barrier: principles, mechanism, and therapeutic applications. Cell Mol Neurobiol 20:217-230.

Rautio J, Kumpulainen H, Heimbach T, Oliyai R, Oh D, Jarvinen T, Savolainen J (2008) Prodrugs: design and clinical applications. Nat Rev Drug Discov 7:255-270.

Richichi C, Lin EJ, Stefanin D, Colella D, Ravizza T, Grignaschi G, Veglianese P, Sperk G, During MJ, Vezzani A (2004) Anticonvulsant and antiepileptogenic effects mediated by adeno-associated virus vector neuropeptide Y expression in the rat hippocampus. J Neurosci 24:3051-3059.

Rogawski MA (2009) Convection-enhanced delivery in the treatment of epilepsy. Neurotherapeutics 6:344-351.

Rubenstein JE (2008) Use of the ketogenic diet in neonates and infants. Epilepsia 49:30-32.

Ryu J, Jeong YI, Kim IS, Lee JH, Nah JW, Kim SH (2000) Clonazepam release from core-shell type nanoparticles of poly(epsilon-caprolactone)/poly(ethylene glycol)/poly(epsilon-caprolactone) triblock copolymers. Int J Pharm 200:231-242.

Saito R, Krauze MT, Noble CO, Tamas M, Drummond DC, Kirpotin DB, Berger MS, Park JW, Bankiewicz KS (2006) Tissue affinity of the infusate affects the distribution volume during convection-enhanced delivery into rodent brains: implications for local drug delivery. J Neurosci Methods 154:225-232.

Saltzman WM, Olbricht WL (2002) Building drug delivery into tissue engineering. Nat Rev Drug Discov 1:177-186.

Sampson JH, Brady ML, Petry NA, Croteau D, Friedman AH, Friedman HS, Wong T, Bigner DD, Pastan I, Puri RK (2007a) Intracerebral infusate distribution by convection-enhanced delivery in humans with malignant gliomas: descriptive effects of target anatomy and catheter positioning. Neurosurgery 60:89.

Sampson JH, Archer G, Pedain C, Wembacher-Schröder E, Westphal M, Kunwar S, Vogelbaum MA, Coan A, Herndon JE, Raghavan R (2010) Poor drug distribution as a possible explanation for the results of the PRECISE trial. J Neurosurg 113:301-309.

Sampson JH, Brady M, Raghavan R, Mehta AI, Friedman AH, Reardon DA, Petry NA, Barboriak DP, Wong TZ, Zalutsky MR, Lally-Goss D, Bigner DD (2011) Colocalization of gadolinium-diethylene triamine pentaacetic acid with high-molecular-weight molecules after intracerebral convection-enhanced delivery in humans. Neurosurgery 69:668-676.

Sampson JH, Raghavan R, Brady ML, Provenzale JM, Herndon JE, 2nd, Croteau D, Friedman AH, Reardon DA, Coleman RE, Wong T, Bigner DD, Pastan I, Rodriguez-Ponce MI, Tanner P, Puri R, Pedain C (2007b) Clinical utility of a patient-specific algorithm for simulating intracerebral drug infusions. Neuro Oncol 9:343-353.

Sanchez JC, Mareci TH, Norman WM, Principe JC, Ditto WL, Carney PR (2006) Evolving into epilepsy: Multiscale electrophysiological analysis and imaging in an animal model. Exp Neurol 198:31-47.

Sander JW (1993) Some aspects of prognosis in the epilepsies: a review. Epilepsia 34:1007-1016.

Sarntinoranont M, Chen X, Zhao J, Mareci TH (2006) Computational model of interstitial transport in the spinal cord using diffusion tensor imaging. Ann Biomed Eng 34:1304-1321.

Schmidt D, Loscher W (2009) New developments in antiepileptic drug resistance: an integrative view. Epilepsy Curr 9:47-52.

Schmued L, Bowyer J, Cozart M, Heard D, Binienda Z, Paule M (2008) Introducing Black-Gold II, a highly soluble gold phosphate complex with several unique advantages for the histochemical localization of myelin. Brain Res 1229:210-217.

Schmued LC, Stowers CC, Scallet AC, Xu L (2005) Fluoro-Jade C results in ultra high resolution and contrast labeling of degenerating neurons. Brain Res 1035:24-31.

Serralta A, Barcia JA, Ortiz P, Duran C, Hernandez ME, Alos M (2006) Effect of intracerebroventricular continuous infusion of valproic acid versus single i.p. and i.c.v. injections in the amygdala kindling epilepsy model. Epilepsy Res 70:15-26.

Shetty AK, Turner DA (2000) Fetal hippocampal grafts containing CA3 cells restore host hippocampal glutamate decarboxylase-positive interneuron numbers in a rat model of temporal lobe epilepsy. J Neurosci 20:8788-8801.

Shetty AK, Hattiangady B (2007) Concise review: prospects of stem cell therapy for temporal lobe epilepsy. Stem Cells 25:2396-2407.

Shetty AK, Zaman V, Hattiangady B (2005) Repair of the injured adult hippocampus through graft-mediated modulation of the plasticity of the dentate gyrus in a rat model of temporal lobe epilepsy. J Neurosci 25:8391-8401.

Shetty AK, Rao MS, Hattiangady B (2008) Behavior of hippocampal stem/progenitor cells following grafting into the injured aged hippocampus. J Neurosci Res 86:3062-3074.

Siegal T, Rubinstein R, Bokstein F, Schwartz A, Lossos A, Shalom E, Chisin R, Gomori JM (2000) In vivo assessment of the window of barrier opening after osmotic blood-brain barrier disruption in humans. J Neurosurg 92:599-605.

Simonova Z, Svoboda J, Orkand P, Bernard CC, Lassmann H, Sykova E (1996) Changes of extracellular space volume and tortuosity in the spinal cord of Lewis rats with experimental autoimmune encephalomyelitis. Physiol Res 45:11-22.

Sirven JI, Sperling M, Naritoku D, Schachter S, Labar D, Holmes M, Wilensky A, Cibula J, Labiner DM, Bergen D, Ristanovic R, Harvey J, Dasheiff R, Morris GL, O'Donovan CA, Ojemann L, Scales D, Nadkarni M, Richards B, Sanchez JD (2000) Vagus nerve stimulation therapy for epilepsy in older adults. Neurology 54:1179-1182.

Sloviter RS (1999) Status epilepticus-induced neuronal injury and network reorganization. Epilepsia 40 Suppl 1:S34-39; discussion S40-31.

Song DK, Lonser RR (2008) Convection-enhanced delivery for the treatment of pediatric neurologic disorders. J Child Neurol 23:1231-1237.

Spencer BJ, Verma IM (2007) Targeted delivery of proteins across the blood-brain barrier. Proc Natl Acad Sci U S A 104:7594-7599.

Stein AG, Eder HG, Blum DE, Drachev A, Fisher RS (2000) An automated drug delivery system for focal epilepsy. Epilepsy Res 39:103-114.

Sutula T (2002) Antiepileptic drugs to prevent neural degeneration associated with epilepsy: assessing the prospects for neuroprotection. Epilepsy Res 50:125-129.

Sykova E (1983) Extracellular K+ accumulation in the central nervous system. Prog Biophys Mol Biol 42:135-189.

Sykova E (1997a) The Extracellular Space in the CNS: Its Regulation, Volume and Geometry in Normal and Pathological Neuronal Function. The Neuroscientist 3:28-41.

Sykova E (1997b) The extracellular space in the CNS: its regulation, volume and geometry in normal and pathological neuronal function. In, pp 28-41: WILLIAMS & WILKINS.

Sykova E, Nicholson C (2008) Diffusion in brain extracellular space. Physiol Rev 88:1277-1340.

Sykova E, Mazel T, Simonova Z (1998) Diffusion constraints and neuron-glia interaction during aging. Exp Gerontol 33:837-851.

Sykova E, Svoboda J, Polak J, Chvatal A (1994) Extracellular volume fraction and diffusion characteristics during progressive ischemia and terminal anoxia in the spinal cord of the rat. J Cereb Blood Flow Metab 14:301-311.

Sykova E, Vargova L, Prokopova S, Simonova Z (1999a) Glial swelling and astrogliosis produce diffusion barriers in the rat spinal cord. Glia 25:56-70.

Sykova E, Roitbak T, Mazel T, Simonova Z, Harvey AR (1999b) Astrocytes, oligodendroglia, extracellular space volume and geometry in rat fetal brain grafts. Neuroscience 91:783-798.

Tang J, Xu H, Fan X, Li D, Rancourt D, Zhou G, Li Z, Yang L (2008) Embryonic stem cell-derived neural precursor cells improve memory dysfunction in Abeta(1-40) injured rats. Neurosci Res 62:86-96.

Tao L, Nicholson C (1996) Diffusion of albumins in rat cortical slices and relevance to volume transmission. Neuroscience 75:839-847.

Tate DF, Bigler ED (2000) Fornix and hippocampal atrophy in traumatic brain injury. Learn Mem 7:442-446.

Thakur R, Gupta RB (2006) Formation of phenytoin nanoparticles using rapid expansion of supercritical solution with solid cosolvent (RESS-SC) process. Int J Pharm 308:190-199.

Theodore WH, Fisher RS (2004) Brain stimulation for epilepsy. Lancet Neurol 3:111-118.

Thom M, Zhou J, Martinian L, Sisodiya S (2005) Quantitative post-mortem study of the hippocampus in chronic epilepsy: seizures do not inevitably cause neuronal loss. Brain 128:1344-1357.

Thomas LB, Steindler DA (1995) Glial boundaries and scars: programs for normal development and wound healing in the brain. Neuroscientist 1:142-154.

Thompson KW (2005) Genetically engineered cells with regulatable GABA production can affect afterdischarges and behavioral seizures after transplantation into the dentate gyrus. Neuroscience 133:1029-1037.

Thorne RG, Nicholson C (2006) In vivo diffusion analysis with quantum dots and dextrans predicts the width of brain extracellular space. Proc Natl Acad Sci U S A 103:5567-5572.

Trojnar MK, Wierzchowska-Cioch E, Krzyzanowski M, Jargiello M, Czuczwar SJ (2004) New generation of valproic acid. Pol J Pharmacol 56:283-288.

Tubbs RS, Louis RG, Jr., Wartmann CT, Loukas M, Shoja MM, Apaydin N, Oakes WJ (2008) The velum interpositum revisited and redefined. Surg Radiol Anat 30:131-135.

Van Harreveld A (1972) The extracellular space in the vertebrate central nervous system. In: The Structure and Function of Nervous Tissue (Bourne GH, ed), pp 447-511. New York: Academic Press.

Van Harreveld A, J C, SK M (1965) A study of extracellular space in central nervous tissue by freeze-substitution. J Cell Biol 25:117-137.

van Vliet EA, da Costa Araujo S, Redeker S, van Schaik R, Aronica E, Gorter JA (2007) Blood-brain barrier leakage may lead to progression of temporal lobe epilepsy. Brain 130:521-534.

Verney C, Baulac M, Berger B, Alvarez C, Vigny A, Helle KB (1985) Morphological evidence for a dopaminergic terminal field in the hippocampal formation of young and adult rat. Neuroscience 14:1039-1052.

Voges J, Reszka R, Gossmann A, Dittmar C, Richter R, Garlip G, Kracht L, Coenen HH, Sturm V, Wienhard K, Heiss WD, Jacobs AH (2003) Imaging-guided convection-enhanced delivery and gene therapy of glioblastoma. Ann Neurol 54:479-487.

Vonck K, Van Laere K, Dedeurwaerdere S, Caemaert J, De Reuck J, Boon P (2001) The mechanism of action of vagus nerve stimulation for refractory epilepsy: the current status. J Clin Neurophysiol 18:394-401.

Vorisek I, Sykova E (1997) Evolution of anisotropic diffusion in the developing rat corpus callosum. J Neurophysiol 78:912-919.

Vorisek I, Hajek M, Tintera J, Nicolay K, Sykova E (2002) Water ADC, extracellular space volume, and tortuosity in the rat cortex after traumatic injury. Magn Reson Med 48:994-1003.

Wall CJ, Kendall EJ, Obenaus A (2000) Rapid alterations in diffusion-weighted images with anatomic correlates in a rodent model of status epilepticus. AJNR Am J Neuroradiol 21:1841-1852.

White H, Johnson M, Wolf H, Kupferberg H (1995) The early identification of anticonvulsant activity: role of the maximal electroshock and subcutaneous pentylenetetrazol seizure models. The Italian Journal of Neurological Sciences 16:73-77.

Wiebe S, Blume WT, Girvin JP, Eliasziw M (2001) A randomized, controlled trial of surgery for temporal-lobe epilepsy. N Engl J Med 345:311-318.

Wieshmann UC, Clark CA, Symms MR, Barker GJ, Birnie KD, Shorvon SD (1999) Water diffusion in the human hippocampus in epilepsy. Magn Reson Imaging 17:29-36.

Willmore LJ (2005) Antiepileptic drugs and neuroprotection: current status and future roles. Epilepsy Behav 7 Suppl 3:S25-28.

Wu X, Li Y, Crise B, Burgess SM (2003) Transcription start regions in the human genome are favored targets for MLV integration. Science 300:1749-1751.

Wu Z, Asokan A, Samulski RJ (2006) Adeno-associated virus serotypes: vector toolkit for human gene therapy. Mol Ther 14:316-327.

Yamasaki TR, Blurton-Jones M, Morrissette DA, Kitazawa M, Oddo S, LaFerla FM (2007) Neural stem cells improve memory in an inducible mouse model of neuronal loss. J Neurosci 27:11925-11933.

Yasuhara T, Hara K, Maki M, Xu L, Yu G, Ali MM, Masuda T, Yu SJ, Bae EK, Hayashi T, Matsukawa N, Kaneko Y, Kuzmin-Nichols N, Ellovitch S, Cruz EL, Klasko SK, Sanberg CD, Sanberg PR, Borlongan CV (2010) Mannitol facilitates neurotrophic factor up-regulation and behavioural recovery in neonatal hypoxic-ischaemic rats with human umbilical cord blood grafts. J Cell Mol Med 14:914-921.

Yasukawa T, Ogura Y, Sakurai E, Tabata Y, Kimura H (2005) Intraocular sustained drug delivery using implantable polymeric devices. Adv Drug Deliv Rev 57:2033-2046.

Yushkevich PA, Piven J, Hazlett HC, Smith RG, Ho S, Gee JC, Gerig G (2006) User-guided 3D active contour segmentation of anatomical structures: significantly improved efficiency and reliability. Neuroimage 31:1116-1128.

Zafar R, King MA, Carney PR (2012) Adeno associated viral vector-mediated expression of somatostatin in rat hippocampus suppresses seizure development. Neurosci Lett 509:87-91.

Zaman V, Turner DA, Shetty AK (2000) Survival of grafted fetal neural cells in kainic acid lesioned CA3 region of adult hippocampus depends upon cell specificity. Exp Neurol 161:535-561.

Zhang Y, Pardridge WM (2005) Delivery of beta-galactosidase to mouse brain via the blood-brain barrier transferrin receptor. J Pharmacol Exp Ther 313:1075-1081.

Zheng T, Marshall GP, 2nd, Laywell ED, Steindler DA (2006) Neurogenic astrocytes transplanted into the adult mouse lateral ventricle contribute to olfactory neurogenesis, and reveal a novel intrinsic subependymal neuron. Neuroscience 142:175-185.

Zincarelli C, Soltys S, Rengo G, Rabinowitz JE (2008) Analysis of AAV serotypes 1-9 mediated gene expression and tropism in mice after systemic injection. Mol Ther 16:1073-1080.

BIOGRAPHICAL SKETCH

Svetlana Kantorovich was born in Vinnitsa, Ukraine where she lived with her parents, twin sister, and older brother before moving to St. Louis, MO at the age of four. After completing high school in St. Louis, she attended Washington University in St. Louis to pursue her undergraduate degree. She graduated with honors in 2007 with a Bachelor of Arts in Biology and a minor in psychology. In the fall of 2007, Svetlana began graduate school in the Interdisciplinary Program in Biomedical Sciences (IDP) at the University of Florida with a concentration in Neuroscience. She joined the laboratory of Dr. Paul R. Carney in 2008 where she began characterizing the effect of normal and pathological tissue structure on infusate distribution profiles following convection-enhanced delivery for epilepsy. Her work culminated in a Ph.D. from the University of Florida in the spring of 2012. Following graduation, Svetlana plans to widen her knowledge and skill sets through the continuation of training in the field of biomedical sciences.